

**STUDIES ON THE EFFECTS OF LIGHTNING
GENERATED ELECTRIC FIELD UPON SOME
PARAMETERS OF LOWER ATMOSPHERE**

**THESIS SUBMITTED FOR THE DEGREE OF
DOCTOR OF PHILOSOPHY (SCIENCE)
OF
JADAVPUR UNIVERSITY**

**BY
ABHIJIT GHOSH**



**DEPARTMENT OF PHYSICS
JADAVPUR UNIVERSITY
KOLKATA 700 032
INDIA**

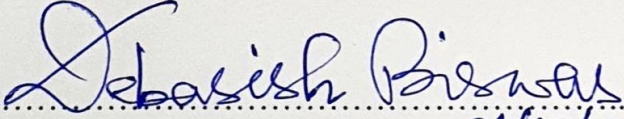
2022



FACULTY OF SCIENCE : DEPARTMENT OF PHYSICS

CERTIFICATE FROM THE SUPERVISOR

This is to certify that the thesis entitled “**Studies on the Effects of Lightning Generated Electric Field upon Some Parameters of Lower Atmosphere**” submitted by **Sri Abhijit Ghosh** who got his name registered on April 25, 2014 bearing Index No. **80/14/Phys./23** of **2014** for the award of Ph. D. (Science) degree of Jadavpur University, is absolutely based upon his own work under the supervision of **Prof. Debasish Biswas** and that neither this thesis nor any part of it has been submitted for either any degree/diploma or any other academic award anywhere before.


(DEBASISH BISWAS) 21/12/2022



DR. DEBASISH BISWAS
Professor of Physics
Jadavpur University
Kolkata - 700032, India

Professor
Department of Physics
Jadavpur University
Kolkata – 700032, India

DECLARATION

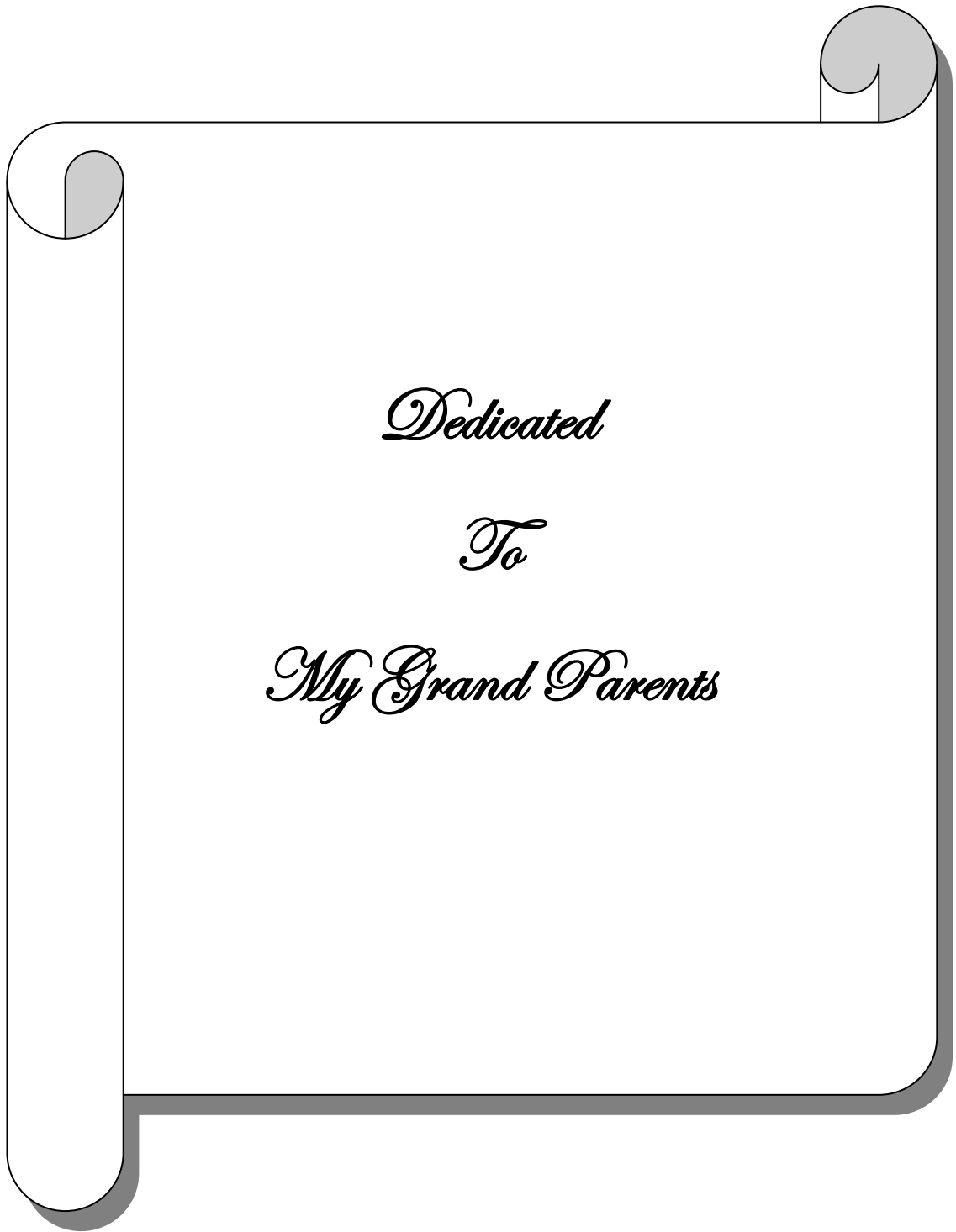
I declare that the work described in the thesis entitled, "Studies on The Effects of Lightning Generated Electric Field upon Some Parameters of Lower Atmosphere" is the result of investigation carried out by me under the supervision Prof. Debasish Biswas, Department of Physics, Jadavpur University, Jadavpur, Kolkata- 700032, India and that it has not been submitted elsewhere for the award of any degree or diploma. I declare that this written document represents my ideas in my own words and I have adhered to all principles of academic honesty and integrity and have not misrepresented or fabricated or falsified any idea/data/fact/source in my submission.

In keeping with the general practice in reporting scientific observations, due acknowledgement and citation has been made whenever the work described based on the findings of other investigators. Any omission that might have occurred by oversight or error of judgment is regretted.

Date: 21.12.2022

(ABHIJIT GHOSH)

Index No.: 80/14/Phys./23



Dedicated

To

My Grand Parents

Acknowledgement

Looking over the past few years, I have a great desire to express my deepest gratitude to those I have encountered along my Ph.D. journey. This thesis would not have been completed without the encouragement and support of some institution and of many individuals. It is a pleasure for me to acknowledge those who have supported and inspired me including my well-wishers, family members, friends and co-workers all through the course of my work.

Firstly, I would like to express my heart-felt appreciation and highest gratitude from the core of my heart to my supervisor Prof. Debasish Biswas, Department of Physics, Jadavpur University, Kolkata for providing me the opportunity to work with him. It is an honour to work closely with him. Thanks for his continuous guidance, immense professional support, constructive discussions, valuable suggestions and encouragement throughout the progress of the work. Under his unique guidance, I successfully overcame many difficulties and learned a lot. During these years I had the chance of learning from the passion, dedication and seriousness he puts in his research. He also influenced me in different ways with his strong perception of life. He helped me a lot in finalizing this project within limited time frame. I will remain grateful throughout my life for his immense support.


I express my indebtedness to Late Syam Sundar De, Professor, Institute of Radio Physics & Electronics, University of Calcutta, who was my joint supervisor till death for suggesting me the problems which are included in this thesis. His valuable suggestions in the different topics of research, and criticism throughout the progress of my researches supported me a lot. He provided me with his laboratory facility and allowed me to use all facilities for the smooth functioning of my research activities. It

was an enlightening experience to work under him. I would like to express my sincere gratitude to him.

I would like to thank other respected Professors of the Department of Physics of Jadavpur University for valuable discussions time to time when required. I am also thankful to the coworkers of the research group for their active support and co-operation. Help and co-operation from the different staff members of the S. K. Mitra Centre for Researches in Space Environment, Centre of Advanced Study in Radio Physics and Electronics, University of Calcutta are duly acknowledged.

Thanks are also due to my wife Mrs. Riya Ghosh for her inspirations and mental support. Co-operation from my daughter, son and colleagues are duly acknowledged. I am indebted to my parents for their blessing towards carrying out my research activities.

December, 2022
Department of Physics
Jadavpur University


.....
(Abhijit Ghosh) 21.12.2022

ABSTRACT

The investigations presented in this thesis are concerned about the studies on responses of different geophysical and extra terrestrial events like thunderstorm, lightning, solar eclipse, solar flare, earthquake on various atmospheric electricity parameters like, Potential Gradient (PG), Point Discharge Current (PDC), current density, conductivity of air, low frequency (LF) sferics signals as well as very low frequency (VLF) transmitted signals etc. Investigations of important characteristics of lightning generated electric field upon some parameters of the lower atmosphere are carried out and the results are examined. In fair weather condition, electric field at a point on the Earth's surface depends on the major thunderstorm activities of the globe and on the local environmental factors.

At the onset, a general background about the contents of the thesis is narrated. Also, the scope of investigations and main objective of the thesis are summarised. Then an overview of the rudimentary concepts, measurement setup and measuring techniques used in this work regarding the description of antenna systems are presented.

The atmospheric electric Potential Gradient (PG) on ground surface is measured at Kolkata during monsoon and winter for 90 fair weather days and the results are plotted and compared with the results obtained from other ground-based stations of northern and southern hemispheres and critically analyzed thereafter. Considerable fluctuation in the magnitudes of PG is observed at day time and night time. The atmospheric electric field values are seen to be higher from the daily average. Also the measured field recorded a few hours difference in phase with the observation made by other researchers at different tropical and temperate latitudes. The high value of PG is interpreted as a consequence of the poor value of conductivity of air over Kolkata

which is due to the presence of excessive pollutant particles such as aerosol, aiten nuclei, CO₂ from fossil fuel etc. Analysing the diurnal and seasonal variation of PG, inter-relationship between global thunderstorm activities and PG is established.

Point Discharge Current (PDC) plays an important role to transfer charges from the atmosphere to the Earth. This current is found to be proportional to the vertical electric PG of the atmosphere measured from the earth surface. The variations of electric field, current density, conductivity and air-temperature over the surface of the Earth are much dependent on global thunderstorm and lightning activities, solar radiations and the relative abundance of the aerosol content in the lower ionosphere. The correlations of PG and PDC are depicted using the recorded data under different situations and calculating correlation coefficients the results of which are concluded in the thesis.

Along with the analysis of PG, PDC and air conductivity, the characteristic of Schumann Resonance (SR) spectra from Kolkata are investigated from the recorded data. Various aspects of SR phenomena as well as their observation and measurement techniques are presented in the thesis in details. The variations of amplitude and frequency using the recorded data from Kolkata, for the period January 2000 to December 2000 during the terrestrial and extraterrestrial events like thunderstorm, lightning, earthquake, solar proton event were analysed. The variations of global thunderstorm activity as inferred from monthly intensity fluctuations of global SR signals over Kolkata and Modra (Lat. 48.61° N) have been presented and the observed difference is interpreted. From the analysis of SR records a logical relation of SR parameter with surface air temperature of Earth and upper tropospheric water vapour (UTWV) is established. Analysing the intensity and peak frequency of SR mode the level of lightning is estimated.

SR behaves as a sensitive global tropical thermometer on diurnal and seasonal time scales. Warmer and cooler periods of the entire tropical belt are due to the enhanced and suppressed magnetic field amplitudes of SR. There is a good correlation between tropospheric water content and SR. Some related parameters of SR could be used to monitor global lightning activities. The field could be explored using long term data. After developing a model, climate can be forecasted using SR data.

Schumann Resonance variation is related to El Niño and La Niña phenomena. Both electric and magnetic components of the SR intensity vary with the spatial shifts of the thunderstorm region under El Niño and La Niña conditions. The SR is also linked to the natural climate oscillation known as El Niño Southern Oscillation (ENSO) that changes the Earth's climate in three to seven years. Variation in SR parameters is best utilized in monitoring the natural ENSO phenomena by the measurement of surface temperature and upper tropospheric water vapour. The details of all are presented in this thesis.

Very recently, few relations between the thermospheric / ionospheric wave number-4 (WN-4) structure and the global tropical lightning characteristics are identified through SR. All these are detected from the 4th chimney (4th lightning centre) with different magnitude and intensity. Further information about the fourth chimney is yet to be explored.

The enhancement of the amplitude and frequency of the fourth mode of SR spectra during the occurrence of earthquake was detected. It includes the impact of SR in the study of precursors of earthquake through Lithosphere-Ionosphere-Atmosphere coupling. The results of the analyses of SR spectra have been presented in the thesis. From the observational records over Kolkata, the precursors and some specific

characteristics of few earthquakes are investigated, the outcomes of those are presented here.

In the middle of the thesis, some typical variations of maximum temperature, relative humidity, air pressure, wind speed and rainfall during a large earthquake are presented. During the occurrences, abrupt increase in greenhouse gases (like CO₂, CH₄, H₂ etc.) and enhancement of radon emanations are found which introduced anomaly in the fluid expulsion from seismically active faults and produced air ionization before a large earthquake. In the next chapter, a model calculation is set up to estimate the changes in the electron concentration and the electron temperature in the ionospheric regions through energy balance equation, continuity equation and ionization balance equation. In the following part of the thesis, the statistical analyses are pictured on the three sub-ionospheric VLF transmitted signals from the recorded data at Kolkata investigated during the occurrence of several earthquakes having $M \geq 5.0$. These all are considered as the precursor of earthquake.

Results of observations from various experimental set-ups in connection with the stated phenomena are analysed and in some cases results are interpreted graphically and compared with earlier works. The thesis contains the outcomes of the results of investigations during the past ten years of research activities of the author.

Further works on most of the topics of the stated areas are envisaged. It is contemplated that some more will be attempted in the near future. The results of investigations presented in the thesis will be of some use to different experimental groups.

LIST OF PUBLICATIONS

Included in the thesis:

1. Responses of Meteorological Parameters during August 24, 2016 Myanmar Earthquake, *Indian Journal of Radio & Space Physics*, Vol **49**, March-June 2020, pp. 5-12, **Abhijit Ghosh**, Pranab Hazra, S. S. De, Gautam Guha and Debasish Biswas
2. Studies on Schumann Resonance Phenomena and Some Recent Advancements, *Geomagnetism and Aeronomy*, 2019, Vol. **59**, No. 8, pp. 980–994, **Abhijit Ghosh**, Debasish Biswas, Pranab Hazra, Gautam Guha, and S. S. De
3. Studies on the seasonal variation of atmospheric electricity parameters at a tropical station in Kolkata, *J. Atmos. Sol.-Terr. Phys.*, **105**, 2013, pp. 135-141, S. S. De, Suman Paul, S Barui, Pinaki Pal, B Bandyopadhyay, D Kala and **Abhijit Ghosh**
4. Irregularities in the plasma of ionosphere in presence of precursory signals from earthquake, **Abhijit Ghosh**, Debasish Biswas and S. S. De – Communicated.
5. Statistical analyses on three subionospheric transmitted signals recorded at Kolkata during 18 earthquakes, **Abhijit Ghosh**, Debasish Biswas, Pranab Hazra, Gautam Guha, and S. S. De – Communicated.

Not included in the thesis:

1. Thermal Anomalies Around the Time of Nepal Earthquakes M 7.8 April 25, 2015 And M 7.3 May 12, 2015, *International Journal of Geotechnical Earthquake Engineering*, **8**, (2017), pp. 58-73, Pranab Hazra, Syam Sundar De, Suman Paul, Goutam Guha, **Abhijit Ghosh**

2. Characteristic Feature Studies of Integrated Field Intensity of Sferics at North-East India, *Indian J. Radio Space Phys.*, **42**, 2013, 397-403, S Barui, S. S. De, D K Haldar, Suman Paul, G Guha, P Hazra and **Abhijit Ghosh**
3. Point Discharge Current during a Solar Eclipse, *Earth Moon Planets*, **111**, 2013, pp. 79 -87. S. S. De, Suman Paul, S Barui, P Hazra, D Kala, D K Haldar, **Abhijit Ghosh** and G Guha
4. El Nino Southern Oscillation (ENSO) and its Effects on Indian Monsoon Investigated Through Changes in Atmospheric Electrical Parameters, Gautam Guha, Suman Paul, Pronab Hazra, **Abhijit Ghosh**, Debasish Biswas and S. S. De – Communicated.

Seminar/Conference publications:

1. *1st National Conference on Severe Weather (NCSW-2019)* held at the Bose Institute, Kolkata during March 17th - 20th, 2019. The paper entitled “Studies on Schumann Resonance Phenomena and its Present Scenario” was presented by **Abhijit Ghosh**, Debasish Biswas and S. S. De
2. *41st COSPAR Scientific Assembly*, Istanbul, Turkey. Paper had been accepted for a poster presentation entitled “On the Influence of Aerosols in Measurement of Electric Field from Earth Surface Using a Field-Mill”, COSPAR Assembly presentation number was C0.2-0054-16, by **Abhijit Ghosh**, S. S. De

C O N T E N T S

	PAGE
CERTIFICATE FROM THE SUPERVISOR	
ACKNOWLEDGEMENTS	i-ii
ABSTRACT	iii-vi
LIST OF PUBLICATIONS	vii-viii
SEMINER/CONFERENCE PUBLICATIONS	viii
ABBREVIATIONS	xii-xiii
Chapter 1 Introduction	1-63
1.1 General Background	1
1.2 Scope of Investigation	46
1.3 Main objectives	48
1.4 References	50
Chapter 2 Rudimentary concepts, Experimental setup and measuring techniques	64-82
2.1 Rudimentary concepts	64
2.2 Experimental setup & measuring techniques	73
2.2.1 Experimental Arrangement for measuring Potential Gradient (PG)	73
2.2.2 Measurement of Point Discharge Current (PDC)	76
2.2.3 Measurement of Conductivity	77
2.2.4 Recording of VLF transmitted signals	78
2.2.5 Measurement of Schumann Resonance (SR) parameters	78
2.2.5.1 Square-loop Antennas	79
2.2.5.2 Ball Antenna	80
2.2.5.3 Induction Coil Magnetometer	81
2.3 References	82

Chapter 3	A Study on the Seasonal Variation of Atmospheric Vertical Potential Gradient at a Tropical Station in Kolkata	83-101
	3.1 Introduction	83
	3.2 Experimental arrangement	86
	3.3 Observations and Interpretations	86
	3.4 Conclusion	98
	3.5 References	99
Chapter 4	Measurement of Schumann Resonance Spectra over Kolkata and Some of its Recent Observed Characteristics	102-128
	4.1 Introduction	102
	4.2 Measurement of SR parameters	104
	4.3 Experimental evidences of SR	105
	4.4 Different aspects of SR	109
	4.5 Results of some observations of SR from Kolkata	112
	4.6 Recent scenario about Schumann Resonance	123
	4.7 Conclusion	126
	4.8 References	127
Chapter 5	Responses of meteorological parameters during August 24, 2016 Myanmar earthquake	129-142
	5.1 Introduction	129
	5.2 Observations and Analyses	131
	5.3 Conclusion	140
	5.4 References	141
Chapter 6	Precursor of earthquake mathematical analysis and experimental observations	143-157
	6.1 Irregularities in the plasma of ionosphere in presence of precursory signals from earthquake.	143
	6.1.1 Introduction	143

6.1.2 Mathematical Formulation	144
6.1.3 Results and discussions	146
6.2 Statistical analyses on three sub-ionospheric transmitted signals recorded at Kolkata during 18 earthquakes	147
6.2.1 Introduction	147
6.2.2 Measurement of the VLF transmitted signals	148
6.2.3 Analyses of recorded data	148
6.2.4 Results and consequences	155
6.3 References	156
Chapter 7 Summary and Conclusions	158-163
7.1 Summary	158
7.2 Conclusions	161
7.3 Further scope	163

ABBREVIATIONS

UV	:	Ultraviolet
ppm	:	Parts per million
EUV	:	Extreme ultra violet
NO	:	Nitric oxide
SPE	:	Solar proton events
PCA	:	Polar Cap Absorption
Db	:	Decibel
MHz	:	Mega hertz
kV	:	Kilo volt
AGW	:	Atmospheric Gravity Waves
TID	:	Traveling Ionospheric Disturbance
HF	:	High frequency
ULF	:	Ultra low frequency
LF	:	Low frequency
VLF	:	Very low frequency
ELF	:	Extremely low frequency
SR	:	Schumann Resonances
R_C	:	Columnar resistance
IMF	:	Interplanetary magnetic field
R_e	:	Radius of the Earth
HP	:	High Power

TRIP	:	Thunderstorm Research International Programme
DUNDEE	:	Down Under Doppler and Electricity Experiment
STEPS	:	Severe Thunderstorm Electrification and Precipitation Study
CG	:	Cloud to ground
IC	:	Intra cloud
GEC	:	Global Electric Circuit
V_I	:	Ionospheric potential
AC	:	Alternating current
DC	:	Direct Current
IFIS	:	Integrated Field Intensity of Sferics
ARNFS	:	Atmospheric Radio Noise Field Strength
IFIA	:	Integrated Field Intensity of the Atmospherics
TLE	:	Transient luminous event
FDTD	:	Finite Difference Time Domain
UTWV	:	Upper tropospheric water vapor
ENSO	:	El Niño Southern Oscillation
EA	:	Electromagnetic Anomalies
J_C	:	Conduction current density
PG	:	Potential Gradient
PDC	:	Point discharge current
E	:	Electric field

CHAPTER 1

Introduction

1.1 General Background

The atmosphere of Earth is a layer of gases surrounding the Earth that is retained by Earth's gravity. The atmosphere protects life on Earth by absorbing ultraviolet (UV) solar radiation, warming the surface through heat retention (greenhouse effect), and reducing temperature extremes between day and night (the diurnal temperature variation) etc. Atmospheric stratification describes the structure of the atmosphere, dividing it into distinct layers, each with specific characteristics such as temperature or composition. The atmosphere becomes rarer with increasing altitude, with no definite boundary between the atmosphere and space.

Atmosphere contains roughly (by volume) 78.09% N₂, 20.95% O₂, 0.93% Ar, 0.039% CO₂, and small amounts of other gases. It also contains a variable amount of water vapor on an average around 1%. The average temperature of the atmosphere at the surface of Earth is about 14 °C or 15 °C. Though air pressure and density decrease in the atmosphere as height increases, temperature has a more complicated profile with altitude. Because the general pattern of this profile is constant and recognizable through means such as balloon soundings, temperature provides a useful metric to distinguish between atmospheric layers. In this way, Earth's atmosphere can be divided into five main layers [1.1]. These are:

(i) Troposphere: The troposphere begins at the surface of the Earth and extends to space between 9 km at the poles and 17 km at the equator, with little variation due to weather. This layer is mostly heated by transfer of energy from the surface, so on average the lowest part of this layer is warmest and temperature decreases with altitude.

The troposphere contains roughly 80% of the mass of the atmosphere. The tropo-pause is the boundary between the troposphere and stratosphere. Atmospheric circulation is the large-scale movement of air through the troposphere, and the means (with ocean circulation) by which heat is distributed around the Earth. The large-scale structure of the atmospheric circulation varies from year to year, but the basic structure remains fairly constant as it is determined by the Earth's rotation rate and the difference in solar radiation between the equator and the poles.

(ii) Stratosphere: The stratosphere extends from the tropo-pause to about 50 km. Temperature increases with height due to increased absorption of ultraviolet radiation by the ozone layer, which restricts turbulence and mixing. While the temperature may be $-60\text{ }^{\circ}\text{C}$ at the tropo-pause, the top of the stratosphere is much warmer, and may be near freezing. The strato-pause, which is the boundary between the stratosphere and mesosphere, typically is at 50 to 55 km.

(iii) Ozonosphere: The ozone (O_3) layer is contained within the stratosphere. In this layer ozone concentrations are about 2 to 8 parts per million (ppm), which is much higher than in the lower atmosphere but still very small compared to the main components of the atmosphere. It is mainly located in the lower region of the stratosphere from about 20–40 km, though the thickness varies seasonally and geographically. About 90% of the O_3 in the atmosphere is contained in the stratosphere. Air pollution is due to the introduction of chemicals, particulate matter, or biological materials that cause harm or discomfort to organisms into the atmosphere. Stratospheric ozone depletion is believed to be caused by air pollution (chiefly from chlorofluorocarbons).

(iv) Mesosphere: The mesosphere extends from the strato-pause to 80–85 km. It is the layer where most meteors burn up upon entering the atmosphere. Temperature

decreases with height in this layer. The meso-pause, the temperature minimum that marks the top of the mesosphere, is the coldest place on Earth and has an average temperature around $-85\text{ }^{\circ}\text{C}$. At The meso-pause, temperatures may drop to $-100\text{ }^{\circ}\text{C}$. Due to the cold temperature of the mesosphere, water vapor is frozen, forming ice clouds. A type of lightning referred to as either sprites or elves, form several kilometres above thunderclouds in the troposphere.

(v) Thermosphere: Temperature increases with height in the thermosphere from the meso-pause up to the thermo-pause; then is constant with height. Unlike in the stratosphere, where the inversion is caused by absorption of radiation by ozone, in the thermosphere the inversion is a result of the extremely low density of molecules. The temperature of this layer can rise to $1,500\text{ }^{\circ}\text{C}$, though the gas molecules are so far apart that temperature in the usual sense is not well defined. The International Space Station orbits in this layer, between 320 and 380 km. Because of the relative infrequency of molecular collisions, air above the meso-pause is poorly mixed compared to air below. While the composition from the troposphere to the mesosphere is fairly constant, above a certain point, air is poorly mixed and becomes compositionally stratified. The point dividing these two regions is known as the turbo-pause. The region below is the homosphere, and the region above is the heterosphere. The top of the thermosphere is the bottom of the exosphere, called the exo-base. Its height varies with solar activity and ranges from about 500–10,000 km.

(vi) Exosphere: The outermost layer of Earth's atmosphere extends from the exo-base upward. It is mainly composed of H_2 and He. The particles are so far apart that they can travel hundreds of kilometres without colliding with one another. Since the particles rarely collide, the atmosphere no longer behaves like a fluid. These free-moving

particles follow ballistic trajectories and may migrate into and out of the magnetosphere or the solar wind.

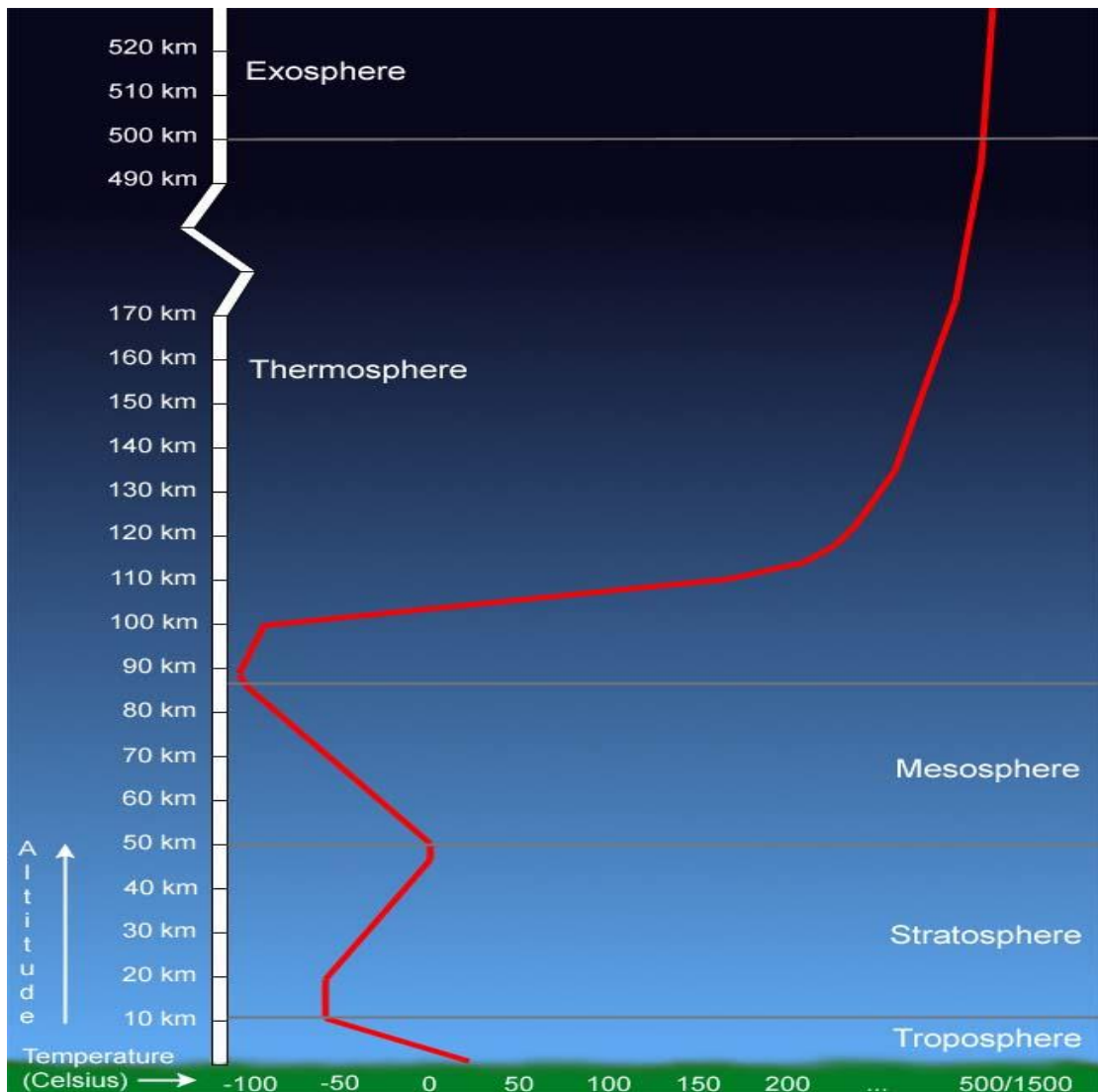


Fig. 1.1: Temperature of atmospheric layers with altitude [1.2].

(vii) Ionosphere: The ionosphere is a part of the atmosphere that is ionized by solar radiation (mainly due to EUV and UV), stretches from 50 to 1,000 km and typically overlaps both the exosphere and the thermosphere. It forms the inner edge of the magnetosphere and is coupled to both the magnetosphere and neutral atmosphere. The study of ionosphere is must as it has great practical importance because of its interaction with radio waves.

Among the various layers of ionosphere the E-layer (heights from 90 km to about 130 km) behaves as a surface from which signals can be reflected to distant stations. The present work is mainly focused on the non-linear phenomena that happen in this layer of the ionosphere. It is responsible for auroras also [1.3]. The ionospheric layers are classified as:

(a) D-layer: The D-layer is the innermost layer, 60 km to 90 km above the surface of the Earth. Ionization here is due to Lyman series-alpha hydrogen radiation at a wavelength of 121.5 nm ionizing nitric oxide (NO). In addition, with high solar activity hard X-rays (wavelength < 1 nm) may ionize N_2 and O_2 . During the night cosmic rays produce a residual amount of ionization. Recombination is high in the D-layer, the net ionization effect is low, but loss of wave energy is great due to frequent collisions of the electrons (about ten collisions every msec). As a result high-frequency (HF) radio waves are not reflected by the D layer but suffer loss of energy therein. This is the main reason for absorption of HF radio waves, particularly at 10 MHz and below, with progressively smaller absorption as the frequency gets higher. The absorption is small at night and the greatest at about midday. The layer reduces greatly after sunset; a small part remains due to galactic cosmic rays.

During solar proton events (SPE), ionization can reach unusually high levels in the D-region over high and polar latitudes. Such very rare events are known as Polar Cap Absorption (PCA) events, because the increased ionization significantly enhances the absorption of radio signals passing through the region. In fact, absorption levels can increase by many tens of dB during intense events, which is enough to absorb most (if not all) transpolar HF radio signal transmissions. Such events typically last less than 24 to 48 hours.

(b) E-layer: The E-layer is the middle layer, 90 km to 120 km above the surface of the Earth. Ionization is due to soft X-ray (1-10 nm) and for ultraviolet (UV) solar radiation ionization of molecular oxygen (O_2). Normally, at oblique incidence, this layer can only reflect radio waves having frequencies lower than about 10 MHz and may contribute a bit to absorption on frequencies above. However, during intense sporadic Events, the E_s -layer can reflect frequencies up to 50 MHz and higher. The vertical structure of the E-layer is primarily determined by the competing effects of ionization and recombination. At night the E-layer rapidly disappears because the primary source of ionization is no longer present. After sunset an increase in the height of the E-layer maximum increases the range to which radio waves can travel by reflection from the layer. This region is also known as the Kennelly-Heaviside layer or simply the Heaviside layer.

(c) E_s -layer: The E_s -layer (sporadic E-layer) is characterized by small, thin clouds of intense ionization, which can support reflection of radio waves; rarely up to 225 MHz. Sporadic-E events may last for just a few minutes to several hours. Sporadic E propagation makes radio amateurs very excited, as propagation paths that are generally unreachable can open up. There are multiple causes of sporadic-E that are still being pursued by researchers. This propagation occurs most frequently during the summer months when high signal levels may be reached.

(d) F-layer: The F-layer or region, also known as the Appleton layer extends from about 200 km to more than 500 km above the surface of Earth. It is the densest point of the ionosphere, which implies signals penetrating this layer will escape into space. Beyond this layer is the topside ionosphere. Here extreme ultraviolet (10–100 nm) solar radiation ionizes atomic oxygen. The F-layer consists of one layer at night, but during the day, a deformation often forms in the profile that is labeled F_1 . The F_2 -layer remains

by day and night responsible for most sky-wave propagation of radio waves, facilitating high frequency (short wave) radio communications over long distances.

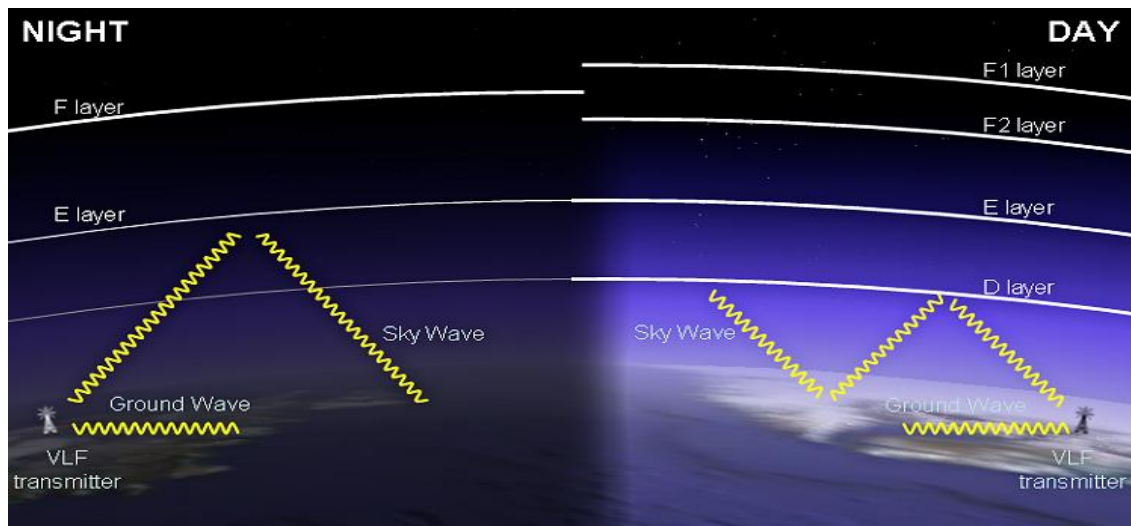


Fig. 1.2: Ionospheric layers in day and night time [1.2].

Homosphere and Heterosphere: The homosphere and heterosphere are defined by whether the atmospheric gases are well mixed. In the homosphere the chemical composition of the atmosphere does not depend on molecular weight because the gases are mixed by turbulence. The homosphere includes the troposphere, stratosphere, and mesosphere. Above the turbo-pause at about 100 km (essentially corresponding to the meso-pause), the composition varies with altitude. This is because the distance that particles can move without colliding with one another is large compared with the size of motions that cause mixing. This allows the gases to stratify by molecular weight, with the heavier ones such as O_2 and N_2 present only near the bottom of the heterosphere. The upper part of the heterosphere is composed almost completely of H_2 , the lightest element. [1.1–1.3].

Auroras: A magnetic field surrounds the Earth. The Earth's 'magnet' is deep in the core. The field lines go into and out of the Earth around the Earth's magnetic poles.

Where the lines are closest together the field is strongest. Where they are furthest apart it is the weakest.

The Sun also has an atmosphere and a magnetic field that extend into space. The Sun's atmosphere is made of H_2 , which itself is made of subatomic particles: protons and electrons. These particles are constantly boiling off the Sun and streaming outward at very high speeds. Together, the Sun's magnetic field and particles are called the 'solar wind'. The aurora happens when the energetic electrically charged particles (mostly electrons) accelerate along the magnetic field lines into the upper atmosphere, where they collide with gas atoms, causing the atoms to give off light.

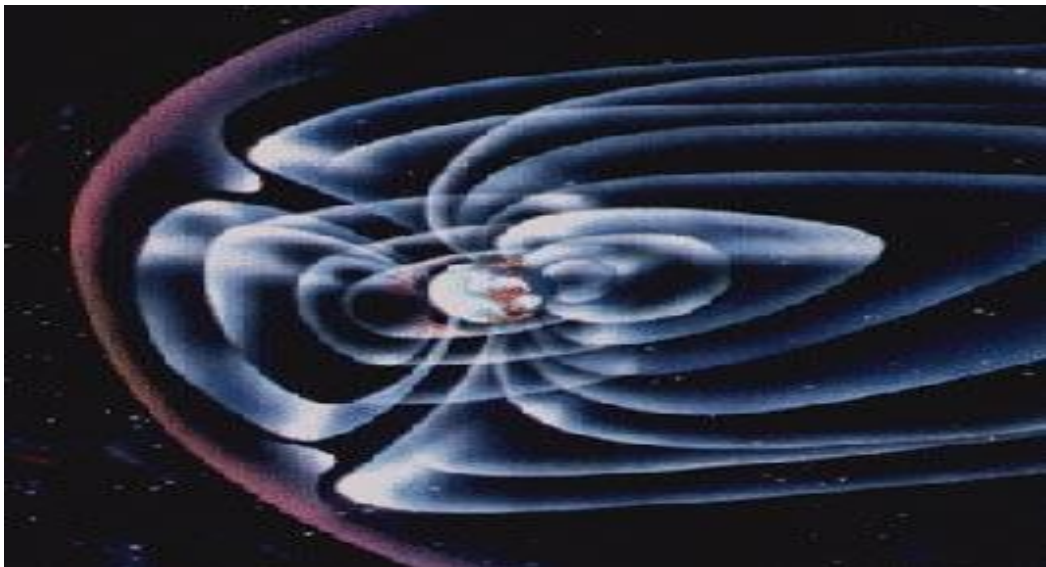


Fig. 1.3: Typical diagram of Earth's magnetosphere showing magneto-tail due to solar wind [1.2]

The auroras are powered by the 'solar wind'. This wind is always pushing on the Earth's magnetic field, changing its shape. The compressed field around the Earth is called the magnetosphere. The Earth's field is compressed on the day side, where the solar wind flows over it. It is also stretched into a long tail, which is called the magneto-tail, and points away from the Sun. Squeezing the Earth's magnetic field

takes energy. The whole process is still not fully understood, but energy from the solar wind is constantly building up in the magnetosphere, and this energy is what powers auroras.

The Earth's magnetosphere, the solar wind squeezing the magnetosphere and charged particles everywhere in the field are responsible for auroras. Solar particles are always entering the tail of the magnetosphere from the solar wind and moving toward the Sun. Now and then, when conditions are right, the build-up of pressure from the solar wind creates an electric voltage between the magneto-tail and the poles. It can reach about 10 kV. The voltage pushes electrons toward the magnetic poles, accelerating them to high speeds. They zoom along the field lines towards the ground to the North and South, until huge numbers of electrons are pushed down into the upper layer of the atmosphere, called the ionosphere.



Fig. 1.4: Typical diagram of Aurora. [1.2]

In the ionosphere, the speeding electrons collide violently with gas atoms. This gives the gas atoms energy, which causes them to release both light and more electrons. In this way, the gases of the ionosphere glow and conduct flowing electric currents into

and out of the polar region. The electrons flowing back don't have as much energy as the speedy incoming ones had -that energy went into creating the aurora.

Atmospheric Gravity Waves

The stratification of the atmosphere in the presence of the Earth's gravity causes a parcel of air that is displaced in height to be subjected to a restoring force, known as the buoyancy force. This restoring force causes oscillations in the atmosphere with a characteristic frequency (known as Brunt-Väisälä frequency) with a period of the order of a few minutes in the thermosphere. Waves with periods longer than the Brunt-Väisälä period are known as the internal atmospheric gravity waves and those with shorter periods as acoustic gravity waves.

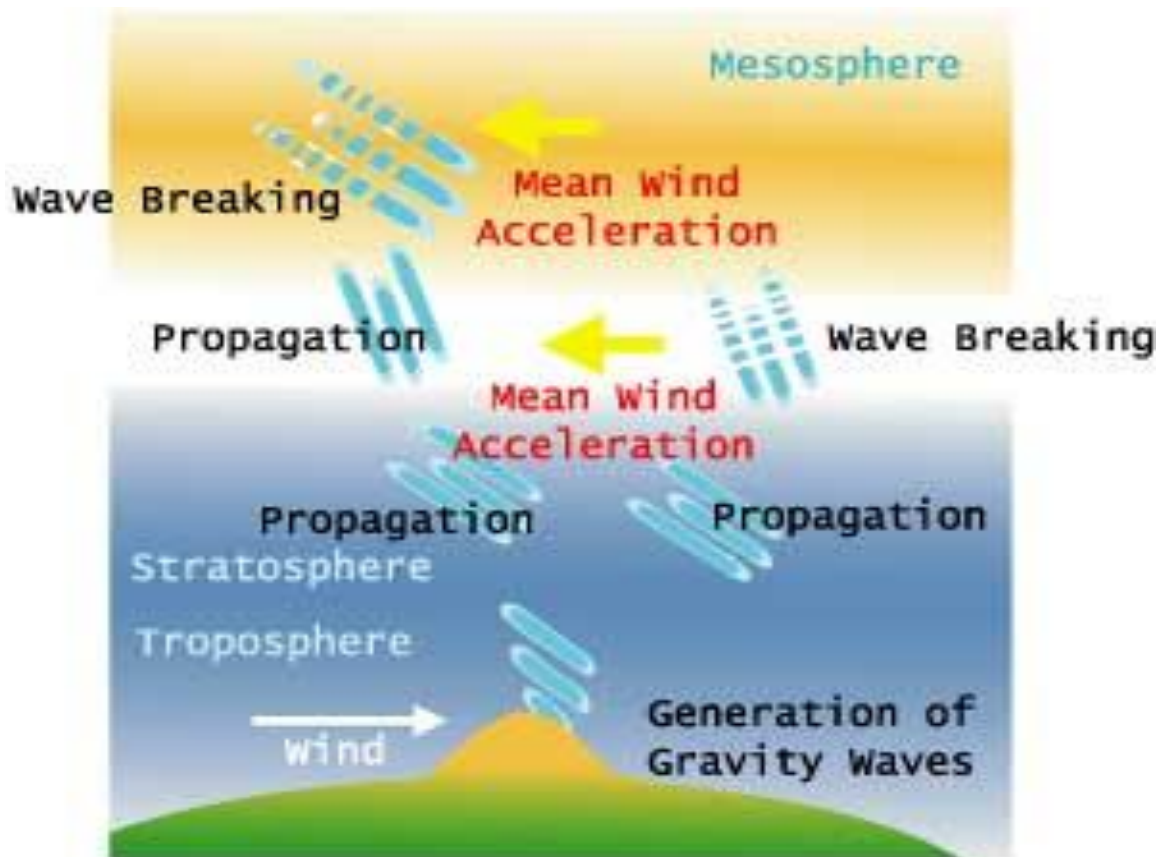


Fig. 1.5: Schematic formation of Atmospheric Gravity Waves and its propagation [1.2].

The AGWs propagate vertically as well as horizontally, and actively transport energy and momentum from the troposphere to the middle and upper atmospheres. These are caused by a variety of sources, e.g.,

- (i) including the passage of wind across terrestrial landforms
- (ii) interaction at the velocity shear of the polar jet stream and
- (iii) radiation incident from space.

AGWs can be seen in the higher atmosphere (100-200 km) by moving bands of atmospheric air glow. The air glow emits spectra from chemiluminescence of atmospheric molecules.

Traveling Ionospheric Disturbance (TID)

Traveling Ionospheric Disturbance is a class of phenomenon which manifests itself as periodic fluctuations in space or time or both in the atmospheric parameters (e.g., pressure, neutral density and neutral winds) and ionospheric parameters (e.g., electron densities and temperatures). Most of the observed characteristics of motions throughout the ionosphere could be satisfactorily explained on the basis of the internal AGWs. Thus, internal AGWs, generated in the lower atmosphere (stratosphere and mesosphere) as well as within the ionosphere, manifests themselves as TIDs.

LF, VLF, ELF

LF stands for low frequency (Range: 30 kHz – 300 kHz)

VLF stands for very low frequency (Range: 3 kHz – 30 kHz) and

ELF stands for extremely low frequency (Range: 3 Hz – 30 Hz)

Sferics: The waves in the range of 3-30 kHz, generated within the waveguide mainly due to lightning and thunderstorms are known as sferics. Sferics can propagate throughout the globe for a large distance by multiple reflections with less attenuation.

Waveguide: The ionosphere can be viewed as the positive plate of a spherical capacitor charged to a potential of about 260 kV and the earth surface as negative plate. The air medium in between the two plates behaves like the dielectric which is inhomogeneous and anisotropic in nature and sferics are trapped within spherical cavity called waveguide.

Schumann Resonance: Thunderstorm activity and lightning put the Earth-ionosphere waveguide into resonance producing characteristic spectra in ELF and VLF ranges. The discrete spectra of frequencies 8, 14, 20.... Hz are generated by the electromagnetic emissions from the lightning strokes are known as Schumann resonances (SR).

Columnar resistance: The total electrical resistance for a unit area of the atmospheric column from the surface upto the lower ionosphere is called the columnar resistance.

The propagation of electromagnetic waves through the Earth's ionosphere waveguide and their subsequent propagation have been of continuing interest since the beginning of the last century. Various investigations have contributed a lot to the understanding of the propagation of electromagnetic waves through different regions of the ionosphere. Ionospheric plasma is studied from theoretical as well as from experimental point of view which has contributed a lot to the understanding of the physical state and properties of such a magneto plasma. A Magneto plasma is one in which the ambient magnetic field is strong enough to significantly alter particle

trajectories and its various perturbations can be calculated through different mathematical formulations.

The electromagnetic waves are formed as a result of vibration of the electrons in the medium, in short, due to the elementary Hertzian oscillators. The directions of vibrations of electrons are solely determined by the directions of the forces experienced by them. Within the ionospheric plasma, in presence of collisions and geomagnetic field, the direction of the force which are really the direction of the displacement vectors are, however, not identical with the direction of the electric vector. So the polarization angle will depend on the orientation of the displacement vector instead of electric vector, for which the form of the electric permittivity will be tensorial in nature thereby developing plasma anisotropy. In the presence of geomagnetic field and irregularities, there are various types of interactions within the ionosphere. The plasma within the ionosphere interacts with the radio wave propagation through its index of refraction and collisional damping. If an intense wave, modulated in amplitude be incident within the ionospheric plasma, the perturbations which are caused in the plasma are also modulated and thus so for waves which pass through the perturbed region. Propagation of intense unperturbed waves perturb the plasma medium and introduce certain changes in the electron temperature, electron number density, and therefore, also in the conductivity and permittivity of the medium. Within the stated situation, the knowledge of the field solution of Maxwell's equations is of considerable importance for many applications [1.4–1.13].

Many articles are published for the experimental studies of the irregular ionospheric structure as well as for the generation of mechanism of ionospheric nonlinearities. The results of those investigations are given in different literatures [1.14,1.15 and references therein]. The generation mechanisms of the ionospheric

plasma density irregularities are considered through different types of plasma instability. In the presence of irregularities, the fluctuations of the physical quantities within the ionosphere may be expressed by the method of stretching. Thus,

$$\begin{aligned}
 (\mathcal{E}) &= \sum_{s=0}^{\infty} (\mathcal{E}_s) \\
 (n) &= \sum_{s=0}^{\infty} (n_s) \\
 (\vec{v}) &= \sum_{s=1}^{\infty} (\vec{v}_s) \\
 (\vec{H}) &= \sum_{s=0}^{\infty} (\vec{H}_s) \\
 (\vec{E}) &= \sum_{s=1}^{\infty} (\vec{E}_s)
 \end{aligned}$$

where the symbols have their usual meanings.

Introducing the propagation vector

$$(\vec{P} = \sigma \vec{E} = Ne\vec{r})$$

and using the relation of displacement vector,

$$\vec{D} = \vec{E} + 4\pi\vec{P}$$

the expression for the dielectric tensor may be evaluated.

The Earth is constantly immersed in the solar wind which may be considered as a rarefied flow of hot plasma, gas of free electrons and positive ions emitted by the Sun in all directions. The solar wind usually reaches the Earth with a velocity around 400 km s⁻¹, density around 5 ions cm⁻³ and magnetic field intensity around 2–5 nT. The Interplanetary Magnetic Field (IMF) may also be much stronger. The IMF originates on the Sun, related to the field of sunspots, and its field lines are dragged out by the solar wind. Earth's magnetosphere is formed by the impact of the solar wind on the Earth's magnetic field. The width of the magnetosphere abreast of Earth, is typically 190,000

km, and on the night-side a long magneto tail of stretched field lines extends to great distances ($> 200 R_e$), R_e is the radius of the Earth. Some magnetospheric plasma travel down along the Earth's magnetic field lines and lose energy to the atmosphere in the auroral zones. Magnetospheric electrons which are accelerated downward by field-aligned electric fields are responsible for the bright auroral features. The unaccelerated electrons and ions are responsible for the dim glow of the diffuse aurora.

The ionosphere consists of a region with rapid increase in density of free electrons, beginning at ~ 70 km, reaching a peak at ~ 400 km, and then falling off again as the atmosphere almost disappears entirely by $\sim 1,000$ km. The profile of the ionosphere is highly variable, changing constantly on timescales of minutes, hours, days, seasons, and years. This profile becomes even more complex near Earth's magnetic poles, where the nearly vertical alignment and intensity of Earth's magnetic field can cause physical effects like aurora. Using magneto hydrodynamic formalism, a model calculation could be performed through which the magnitude and the form of the anticipated atmospheric wave-train may be obtained.

The ionospheric medium is assumed to be a low density, electrically neutral cold plasma which is traversed by the geomagnetic field and irregularities. These charged particles within the plasma medium interact amongst themselves and also interact with electric and magnetic fields present in the medium, leading to the control of space plasma environments by an electrodynamic process. There are various types of interactions within the ionosphere and nonlinear self-interactions of radio waves. The self-interaction leads to a change in the depth of modulation and to the appearance of harmonics of frequency. If an intense wave is modulated in amplitude, the perturbations which it causes in the plasma are also modulated, and therefore, so for waves which pass through the perturbed region. Propagation of intense unmodulated waves perturbs

the plasma medium introducing certain changes in the electron temperature, electron number density and therefore, also in the conductivity and permittivity of the medium. Thus the conditions of wave propagation in the perturbed region are modified. Within the stated situation, the knowledge of the field solutions of Maxwell's equations is of considerable importance for many applications.

Since the first experimental radio wave sounding of the upper atmosphere, a substantial amount of information regarding the physical processes of the upper atmosphere has been explored. Different experimental techniques, e.g., vertical and oblique sounding techniques, absorption measurements etc. gave various information about the upper atmosphere under different circumstances at different heights. In the late 1950's and early 1970's, High Power (HP) radio transmitters have been put to a different kind of use – that of artificial heating of the ionosphere and study of various plasma phenomena. Disturbances are caused by the HP transmitter and the effects are observed with various other diagnostic tools. HP radio waves in the ionosphere cause perturbations in temperature and density of local plasma [1.16–1.25].

In passing through the ionized medium, the waves induce wide-ranging non-linear effects modifying the characteristic properties of the medium, producing a variety of wave propagation phenomena and generating parametric instabilities [1.24,1.26–1.34]. The nonlinear phenomena induce, among other effects, cross-modulation, self-focusing, artificial spread-F and scattering from field aligned irregularities, anomalous absorption and air-glow. Parametric instabilities are produced through interactions of radio waves with natural plasma modes – generating ion-acoustic waves.

The dynamical response of various phenomena to transient heating has been studied by different researchers [1.35–1.38] from which perturbation of density,

composition and electron-ion temperature within the ionosphere during HP radio wave propagation are recognized. The dissipation of energy by hydro magnetic waves, ionospheric currents, aurorally produced gravity waves, expansions of auroral oval are considered to be the sources of different types of perturbations in the upper atmosphere.

Theoretical studies of D-region showed that when the ionosphere is irradiated by HP HF electromagnetic waves, a substantial increase in electron temperature could be realized. If an enhanced electron temperature is maintained by continuous wave heating, the ion composition of the D-region plasma may also be modified due to the electron temperature dependence of the processes, e.g., electron-ion recombination and electron attachment [1.39,1.40]. The thermodynamics of low-latitude ionosphere have been studied with coherent and incoherent scatter radars, ionosondes, magnetometers, and space-based techniques. These measurements defined the morphology of E- and F-region plasma and current systems, and their dependence on the atmospheric and higher latitude ionospheric constituents [1.41–1.44].

Thunderstorms and the lightning that they produce are inherently interesting phenomena that have intrigued scientists and mankind in general for many years. The study of thunderstorms has rapidly advanced during the past century and many efforts have been made towards understanding lightning, thunderstorms and their consequences. Recent observations of optical phenomena above an active lightning discharge along with the availability of modern technology both for data collection and data analysis have renewed interest in the field of thunderstorms and their consequences in the biosphere. The upward lightning discharge can cause sprites, elves, jets, etc. which together are called transient luminous events. The wide spectrum of electromagnetic waves generated during lightning discharges couple the lower atmosphere with the ionosphere/magnetosphere.

During lightning discharge, an impulse current from cloud to ground removes charges from charge centre previously screened by neutralizing space charge. Distributions of electric charges in the electrified clouds introduce important effects in the ionosphere and into the region between the ionosphere and the Earth. Electrical properties of the medium changes greatly between thundercloud altitudes and the magnetosphere. The various types of coupling occur in case of transverse propagation of electromagnetic waves. The expression of second order current and field during the interaction between ordinary and extra-ordinary modes of propagation can be derived. Different models for the electric fields in the lower atmosphere by thunder clouds with a suitable charge distribution profile are known. Responses of the atmosphere are studied through–

- (i) Maxwell's equations
- (ii) Time-varying source charge distribution
- (iii) Conductivity having exponential graded functions of altitude.

Several field and laboratory experiments have been conducted to determine the electrical nature of storms and possible electrification processes are being studied in the laboratory and also through theoretical modeling and computer simulations [1.45-1.47]. Various research programmes such as the Thunderstorm Research International Programme (TRIP), the Down Under Doppler and Electricity Experiment (DUNDEE) [1.48], the Severe Thunderstorm Electrification and Precipitation Study (STEPS) [1.49] have been launched involving both ground and airborne measurements to study the electrical properties of thunderstorms and related phenomena. In India, theoretical and experimental works are being conducted in many institutions and universities of which IIT, Delhi; PRL, Ahmadabad; Indian Institute of Tropical Meteorology, Pune; Indian Institute of Geomagnetism, Mumbai; Department of Physics, Banaras Hindu

University, Varanasi; Tripura University and Institute of Radio Physics and Electronics under Calcutta University, Kolkata demand special mention. A brief account of researches carried out in Kolkata will be included in this thesis where the author is one of the co-workers in the group.

Lightning is a transient, high-current electrical discharge that occurs in the Earth's atmosphere. It is generally associated with thunderclouds. During a thunderstorm, large voltages are developed between the charged thunderclouds and the ground or between different parts of the thundercloud. So large electric fields are generated within the thundercloud. This electric field is enhanced by the roughly spherical shape of the cloud droplets. During collisions, this field enhancement is increased because several charged particles can act as a single object with an elongated shape [1.50]. When the electric field exceeds the critical value necessary for breakdown, electrical discharges take place in the air, leading to a lightning flash. Air is a good insulator in general, but at this critical electric field which is 1.5×10^6 V/m at 5 km above sea level or 3.0×10^6 V/m at sea level [1.51], it is converted into a conductor by the cumulative action of avalanches, streamers and leaders, making it capable of conducting electrical currents [1.52]. This electrical discharge gives rise to streamer discharges, and when the electric field exceeds 250 kV/m over a region, these streamer discharges propagate and initiate a leader discharge. Once a leader is created, it starts to propagate when the background electric field is about 100 kV/m leading to either a cloud or a ground flash [1.52]. At any moment, there are about 100 discharges per second worldwide [1.53]. When the electric field exceeds the critical value the rapid heating of the air from 25,000 to 30,000 K during a lightning flash causes a rapid increase in the atmospheric pressure, leading to a rapid expansion of the air, creating a shock wave before it transforms into a sound wave known as thunder [1.54].

Lightning can be categorized into two groups – ground flashes and cloud flashes [1.55]. Ground flashes make contact with the ground while cloud flashes do not. Cloud flashes, on the other hand, occur within a thundercloud, between the thunderclouds and between a thundercloud and clear air.

Lightning discharges radiate intense electromagnetic pulses ~20 GW peak power for ~1ms to ~1s duration as measured by electric and magnetic sensors on the ground or in space [1.56]. The electromagnetic power heats the partly ionized layers of the upper atmosphere, the mesosphere and the D and E layers of the ionosphere. The quasi-static electric field of up to ~1 kV/m produced during a lightning discharge at mesospheric heights can accelerate electrons to relativistic energies; some of these might travel up into the magnetosphere. Whistler mode waves propagating along dipolar geomagnetic field lines interact with counter-streaming energetic electrons and scatter them from the Van Allen radiation belts into the atmosphere. These energetic electrons produce additional ionization in the D-region [1.57] and modify the electrical conductivity of the atmosphere [1.58]. Inan et. al., [1.59] presented evidence of disturbances of electrical conductivity of the night time mesosphere and the lower ionosphere in association with lightning which lasted only 1 – 2 seconds. The resulting change in conductivity may subsequently cause changes in the amplitude/phase of VLF signals passing through the region. The most common perturbation observed follows within a few ms of the causative lightning discharge and has short onset duration of less than ~50 ms; usually referred as early/fast [1.60]. Recent observations show that early VLF amplitude perturbations for 90% cases were associated with +CG discharges which triggered sprites [1.61]. On the other hand numerous +GG and –CG discharges which did not trigger sprite were seldom associated with amplitude perturbations. Thus

sprites are nearly always accompanied by ‘early’ VLF perturbations while in a few cases ‘early’ VLF perturbations were found to be associated with elves also [1.56].

The electromagnetic signals generated during lightning discharges carry information about the source region and the ambient medium through which they propagate. They can be used to estimate the ionization density in the magnetosphere, and the existence and location of plasma pause [1.62,1.63]. The electromagnetic energy radiated from sprite-associated lightning in the ELF range can be used as a diagnostic of sprites because optical methods become ineffective during daytime. The global nature of the SR phenomena provides special incentive to examine very distant events, at ~20 Mm distance [1.64].

Thunderstorms generate and separate electrical charges, whereas lightning neutralizes electrical charges. Charging of thunderclouds may be initiated by inductive or non-inductive processes. An inductive process needs pre-existing electric field to induce charges on a particle so that when it rebounds from another charge, the field gets enhanced. Within the atmosphere, the fair weather electric field resulting from positive charges in the atmosphere and negative charges on the ground could be considered as the pre-existing field [1.65,1.66]. Non-inductive processes are based on collisions between graupel particles and cloud-ice particles and on the selectivity to transfer charge of a certain polarity to other particles. Here, charge transfer occurs when ice crystals collide with simulated graupel particles within a cloud of super cooled water droplets. In a thundercloud, the smaller ice-crystals are charged positively and move upward and the larger graupel particles are charged negatively which descend relative to the smaller particles.

This physical situation depends on the prevailing conditions of temperature, liquid water content and their mixing within the thunderstorm. The negatively charged

graupel particles become larger in size by accumulating the water droplets and fall down under the action of gravity with huge negative charges. Some of these negative charges are released as negative space charge in the lower zone of thundercloud that forms some stratification of charge centers. Due to convection, negative and positive charge centers mix up randomly and produce discharge phenomenon in the form of lightning. Due to the updraft, the upper part of the thundercloud with positively charged regions goes upward up to the lower ionospheric height and joins the global electric circuit, thereby, introducing itself as the generator.

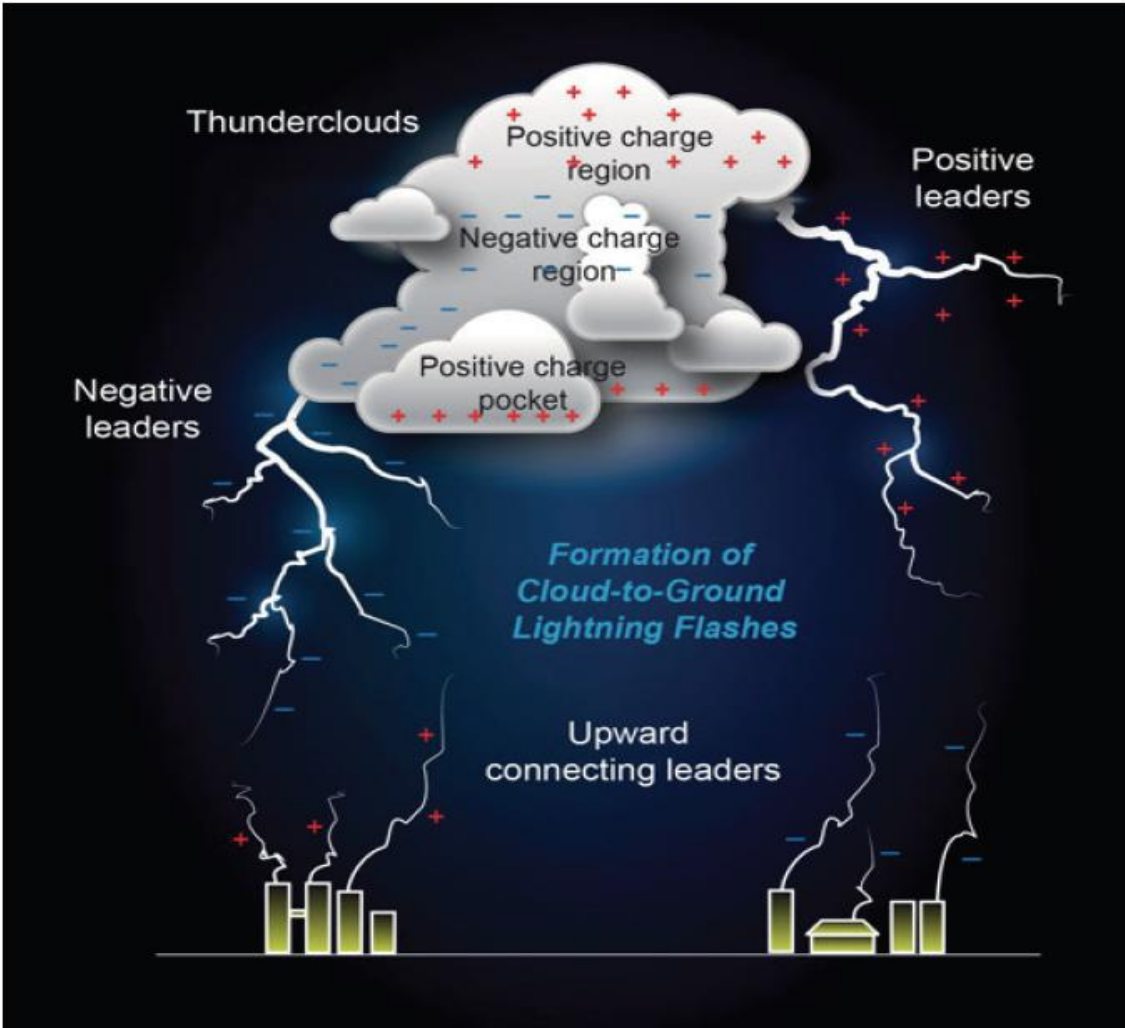


Fig.1.6: Typical tripolar model of thundercloud showing the formation of CG lightning [2].

In a tripolar model a typical thundercloud consists of three charged regions [1.67]. The main positive charge centre is located at the top while the main negative charge centre is located in the middle in a region of -15 to -10 °C isotherm. A smaller positive charge pocket is located below the main negative charge centre. This tripolar structure usually supports the occurrence of lightning.

Thunderstorms exhibit cloud (including intra-cloud, cloud-to-cloud, and cloud-to-air), cloud-to-ground and cloud-to-ionosphere lightning discharges. Cloud-to-ground (CG) discharges are the most studied as a good part of them is observed from the Earth's surface. The discharges occur mostly between the main negative or positive charge center and the ground. Each flash consists of several strokes, with each stroke consisting of a leader and a return stroke; thus, negative or positive charges are brought to the ground. On the other hand, most of the intra-cloud (IC) discharges occur between the positive and negative charge centers of the main dipole. The upward discharges from cloud to the ionosphere may occur as a result of electrical breakdown between the upper storm charge and the screening charge attracted at the cloud top. They could also occur due to electrical breakdown between the main mid-level charge and a screening depleted upper level charge that continues to propagate out of the top of the storm [1.68].

Lightning and atmospheric electricity have been studied for many years, but the existence of an electrical atmosphere on Earth was around even before life evolved on Earth about three billion years ago. It has even been suggested by some [1.69] that lightning played a role in producing the organic molecules necessary for the formation of every life form. Fossil evidence is also available of lightning strikes from 250 million years ago, called fulgurite (fossilized lightning). The first encounter of human

life and lightning may have been both frightening and fascinating and these civilizations incorporated lightning and thunder with religious beliefs. Serious studies of lightning and the electrical atmosphere were conducted by Benjamin Franklin, Thomas Francois D Alibard and John Canton more than 200 years ago [1.70].

It was Lord Kelvin who later introduced the concept of potential after he had recognized the electrical state of the atmosphere as a vertical electric field [1.71]. In the latest studies regarding the electrical nature of the atmosphere, climate change has been recognized as possible feature, as influenced by its importance in atmospheric science. More specifically, investigations have led scientists to correlate changes in atmospheric electricity with temperature changes across the globe. It has been in the forefront of these investigations with suggestions that as tropical near surface air temperatures increase by 1°C, lightning frequency will increase by 10% [1.72,1.73]. Variations of this hypothesis have resulted in similar conclusions using data limited to geographical areas. There are a number of studies which have looked at the change in the global distribution of lightning, the changes in tropospheric chemistry and the role of aerosols in the atmosphere the aspects which all linked to changes in the electrical circuit and a changing climate.

Global Electric Circuit (GEC) is a current system circuit where the current flows upward through the troposphere into the ionosphere and magnetosphere along the magnetic field lines to the opposite hemisphere. In course of time, it returns to the Earth's surface as the fair-weather air-earth current, thus closing the circuit. GEC links the electric field and current flowing in the lower atmosphere, ionosphere and magnetosphere forming a giant spherical condenser [1.74–1.78].

The GEC consists of the ionosphere, Earth surface, fair-weather current and thunderstorm current. The ionosphere is approximately 80 km in the upper atmosphere and is considered as a conductive plate that is positively charged with a potential (the Ionospheric potential, V_I) of about 250-300 kV [1.79,1.80]. The Earth surface is negatively charged and is part of the inner shell that can be compared loosely with a spherical capacitor, with the ionosphere making up the outer equipotential shell.

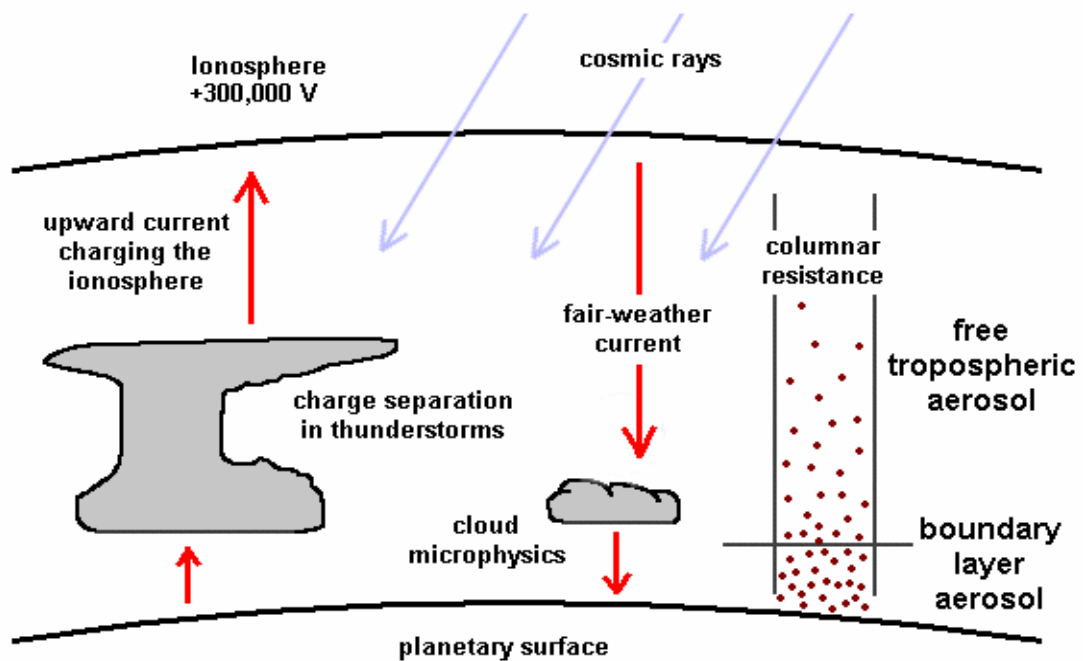


Fig. 1.7: Basic elements of Global Electric Circuit (schematic).

Within the global circuit, there is also an alternating current (AC) circuit which causes the neutral atmosphere to behave like a resonant cavity waveguide when excited by ultra-low frequency electromagnetic radiation, causing resonances at a range of frequencies at 7.8–45 Hz. A fair-weather condition is one where no local processes of charge separation that contributes any additional electric field (i.e., regions where no thunderstorm activity takes place) and where the electric field is steady, modulated only by the global circuit [1.81]. A voltage gradient can be measured that is caused by a large potential difference between the lowest layer of the ionosphere and surface. This

is a positive current (downward current) that has been estimated between 100–150 V/m [1.82,1.83]. Ionisation from cosmic rays and terrestrial sources produce cluster ions (small ions) which make the atmosphere weakly electrically conductive. These ions flow vertically because of the vertical potential difference, causing the air-Earth conduction current density, J_C , of order 10^{-12} Am^{-2} .

Both AC and DC circuits have been used to deduce the global electrical circuit and the range of time scale variations from diurnal to annual that correlate with lightning counts, global surface temperature and pollution occurrences. There is possibility that monitoring both the SR and the ionospheric potential can be used to infer a measure of global temperature and global rainfall rates suggests that if 60% of the average ionospheric potential arises from electrified rain cloud currents it can possibly be used as a proxy for global rainfall rates [1.80].

Sources of electromotive force driving the global circuit are: (i) thunderstorms, (ii) dynamo-interaction between the solar wind and the magnetosphere, (iii) dynamo effect of atmospheric tides in the thermosphere. Thunderstorms are the main sources of electric fields and currents in the GEC developing a vertical potential difference of several hundred kilovolts (kV) in atmospheric layers near the surface of the earth [1.84] and drives vertical current through the atmospheric columnar resistance (R_c) of about 10^3 A . The magnetospheric dynamo is driven by the interaction of solar wind with the Earth's geomagnetic field and generates a horizontal dawn-to-dusk potential drop of ~40–100 kV across the magnetic conjugate polar cap. On the other hand, the dynamo in the ionosphere is produced by tides which generate horizontal potential differences of 5–15 kV with the current flow of $\sim 10^5 \text{ A}$ within the ionosphere.

The upward current flow from thunderstorm to the ionosphere in an active thunderstorm is known as Wilson current. This current spreads around the globe

through the ionosphere/magnetosphere along the geomagnetic field lines to the opposite hemisphere [1.84]. The current returns to the surface of the earth as the fair-weather air-earth current. The ionosphere and magnetosphere are treated as the passive elements of the circuit. Horizontal current flows freely along the highly conducting earth surface and in the ionosphere, which is closed by the current flowing from the ground into the thunderstorm and from the top of the thunderstorm to the ionosphere and back from the ionosphere to the ground through the global fair-weather air-earth current having low load resistance ($\sim 100 \Omega$). The upward current from the Earth's surface to the bottom of the thundercloud consists of field dependent current, convection current, lightning current, precipitation current and displacement current [1.85]. Any perturbation in the interplanetary or atmospheric environment causes a variation in electrical conductivity and hence variation in current/electric field system of the atmosphere. The variations on solar surface causes variations in the solar wind parameters, which can be coupled with the stratosphere and troposphere leading to modulation of current density in the global atmospheric electric circuit from the ionosphere to the earth. Variation in solar wind inputs leads to very small changes (1– 3%) in the cosmic ray flux in the equatorial regions. These changes may affect the thunderstorm charging current and ionospheric potential.

The factors that affect the components of GEC include solar wind, solar flares, galactic cosmic rays, ionospheric-magnetospheric dynamo, thunder cloud, geomagnetic disturbances, solar magnetic sector boundary crossings, solar cycle variations, auroral activity etc. [1.74,1.86,1.87].

Solar wind and geomagnetic storm affect fair-weather current via aerosol distributions / cloud microphysics [1.86,1.88–1.91] by changing the pressure / temperature distribution of the troposphere or by changing its dynamics.

Lightning activity is mainly concentrated in three distinct zones - East Asia, Central Africa and America. Lightning is more prevalent in the northern hemisphere than in the southern hemisphere and mostly occurs over the land surface. The variation of lightning activity with latitude as observed from space shows that two of every three lightning flashes occur in tropical region [1.72]. Like the tropical lightning, extra-tropical lightning activity plays a major role in the summer season in the northern hemisphere, resulting in the global lightning activity having a maximum from June to August.

The earth's climate and climatic changes have direct connection with lightning activity [1.92], which has direct linkage with GEC. Thus, GEC may constitute a variable physical mechanism linking space weather and the Earth's weather and climate [1.77,1.93]. Present status of GEC is the possible linkage with other phenomena relating it to weather and climate. The major sources of GEC are thunderstorms, optical emissions, Schumann resonances, ionospheric dynamo and magnetospheric dynamo. Mathematical modeling of GEC should include the intense current between the top of the thunderstorm and the ionosphere during optical emissions. The electrical conductivity and columnar resistance component of GEC controls the magnitude of electric potential and current. The variation of global temperature (climate change) is related with global atmospheric electric circuit such a way that even 1% increase in global surface temperature could result into a 20% increase in ionospheric potential [1.94]. Aerosols act as a mediator of cloud microphysics, precipitation, cloud electrification and lightning.

The waves in the range of 3-30 kHz, called Very Low Frequency (VLF) generated over the globe mainly due to lightning and thunderstorms are known as sferics. Sferics are trapped between ground and lower boundary of the ionosphere and

propagate over long distances through the Earth-ionosphere waveguide by multiple reflections with very less attenuation. The source-detector distance, transmission conditions in the atmosphere, nature of dielectric properties in the medium and type of discharge can primarily affect the amplitude and waveforms of the sferics signals. Propagation of long range radio waves below 60 kHz is the Earth-ionosphere waveguide problem. The effects of geophysical events in the records of sferics or transmitted sub-ionospheric signals could be observed and analyzed. The atmospherics are significant with regard to electrical phenomena in different types of cloud during meteorologically active periods. Integrated Field Intensity of Sferics (IFIS) measurements are expected to provide different features for the study of ionospheric propagation. Lightning activity may be taken as an agent for global temperature change.

Lightning signals are spread out along the Earth-ionosphere waveguide. The world data about lightning are used for the study of weather prediction, storms, cyclones, tsunami and other irregular as well as complicated weather phenomena [1.95–1.100]. During severe thunderstorms, contribution to the radiation field from VLF band is greatly remarkable. The results of numerous investigations appeared during the past several decades suggesting solar-terrestrial relationship in atmospheric electricity. The sferics are very much significant in regard to electrical phenomena in different types of clouds during meteorologically active periods. Kolkata has its own privilege to study Atmospheric Radio Noise Field Strength (ARNFS) from the local cloud discharge as well as from the distant sources from Australia, Japan and Africa. Any change in source function will result in the variation of the received Integrated Field Intensity of the Atmospherics (IFIA). In the Department of Radio Physics and

Electronics, University of Calcutta, a permanent set up is developed for monitoring ELF-VLF sferics where author is a co-worker since 2006.

Thus, due to the occurrences of thunderstorm and lightning, the ionosphere can be viewed as the positive plate of a spherical capacitor charged to a potential of about 260 kV and the earth surface as negative plate. The air medium in between the two plates behaves like the dielectric which is inhomogeneous and anisotropic in nature. The space filled with gaseous medium in between the earth surface and lower boundary of the ionosphere is called the earth-ionosphere waveguide. Lightning discharges in thunderclouds radiate powerful radio noise bursts over a wide frequency range from a few Hz to several MHz. In the ELF/VLF frequency range waves can propagate over long distances in the Earth-ionosphere waveguide. Waves with frequencies less than 50 Hz can propagate globally with extremely low attenuation rates, allowing these radio waves to propagate a few times around the globe before dissipating. Interference between these waves results in the Earth-ionosphere cavity resonances known as Schumann resonances (SR) [1.101-1.102]. The waves generated by lightning discharges, suffer multiple reflection within the Earth-ionosphere waveguide to form standing electromagnetic waves. The spherical cavity between the Earth's surface and lower ionosphere acts as a resonator. When the wavelength of these standing waves is of the order of the dimension of the resonator, then the SR occurs. The resonant frequencies of SR modes are around 8 Hz, 14 Hz, 20 Hz, 26 Hz,.. etc. The parameters of SR are generally detected by ball antenna for vertical component of electric field and two induction coil-type antennas (magnetometers) for two horizontal magnetic field components and a square-loop antenna is used to measure the SR frequencies. These are set at remote locations far from artificial electrical interactions and any other types of noises.

The historical development of SR is an interesting story [1.103]. While Schumann [1.104] gets most of the credit for the first prediction of the existence of the SR, George F. Fitzgerald in 1893 and Nikola Tesla in 1905 [1.105] presented the formula about the idea of natural global electromagnetic resonances. However, Schumann together with Köning, who attempted to measure the resonant frequencies for the first time, but was not successful [1.104,1.106–1.108]. It was not until measurements made by Balser and Wagner [1.109-1.113] that adequate analytical techniques were available to extract the resonance information from the background noise. In recent time we require data for few minutes to detect the SR in the spectrum clearly.

Following Schuman's landmark article in 1952, there was an increasing interest in SR in a wide variety of fields. Due to the low attenuation of ELF waves in the SR band (~ 0.5 dB/Mm) it was discovered that not only lightning can produce SR, but any large explosion in the atmosphere will also induce SR transients [1.113–1.114]. Hence, until the ban of atmospheric nuclear explosions in the 1960s, there was great interest in using the SR to monitor the enemy's nuclear explosions in remote parts of the globe. Another application of ELF waves related to the SR, due to the low attenuations of the ELF waves, was the man-made transmission of these waves for long range communications with submarines [1.115–1.116]. However, due to the extremely long wavelengths at ELF, such transmitters need to be huge (>200 km length), with huge power outputs due to very low efficiencies of these transmitters. Nevertheless, since the signals propagate globally, the superpowers were still using these ELF transmitters until recently. The United States transmitter broadcasts at 76 Hz [1.117], while the Russian transmitter broadcasts at 82 Hz [1.118].

From the very beginning of SR studies besides the military uses of ELF resonances and propagation theory, there was an interest to track global lightning activity [1.111,1.119–1.123] and detection of extraterrestrial lightning may be studied using SR [1.124-1.126]. However, the recent focus on SR research since the 1990s was a result of the connection between lightning activity and the Earth's climate. It was first suggested in 1990 that global warming may result in significant increases in lightning activity [1.127]. Since the SR is one way to monitor global lightning activity, it was suggested that the SR may be used to monitor global temperature variations, acting as a global thermometer [1.128]. This started a new interest in SR research as related to global climate change that continues today.

With the discovery of transient luminous events (TLEs) such as sprites, elves, jets, etc., it was shown that SR transient pulses are closely linked to the occurrence of transient luminous events—sprites and elves [1.129-1.133]. Hence, SR research is now also a major part of this new field of research related to upper atmospheric discharges. Presently SR is being used to monitor global lightning activity [1.134,1.135], global variability of lightning activity [1.136,1.137] and sprite activity [1.135,1.138,1.139]. The relations between lightning and ELF noise levels on the global basis have been used to study the space-time dynamics of world-wide lightning activity showed that solar proton events cause increases in the frequency, Q-factor and amplitude of the SR modes [1.140,1.141].

Thundercloud electric fields may cause modifications of the atmosphere [1.142–1.146]. Modeling of the lightning discharges is a subject of high attention. The physics of vertical lightning discharges, predominantly, return strokes, are well-explored. An analysis may be performed on the heating of electrons in the lower ionosphere due to electromagnetic radiation from vertical and horizontal lightning discharges. Temporal

variations of the heating with the stroke model of Jones in 1970 may be shown graphically at a series of points distributed along the horizontal distance from the discharge [1.147]. The resonant modes due to constructive interference within the Earth-ionosphere waveguide with their peak frequencies close to 8, 14, 20,.. Hz. according to the theoretical prediction of Schumann, but due to their global nature, the SR represents a proxy for global lightning activity [1.148,1.149], and can also be reliably monitored from a single location on the Earth's surface [1.150,1.151]. In addition, changes in the diurnal SR frequency range are related to the areal variations of thunderstorm regions around the globe [1.152,1.153]. There have been a number of studies investigating the daily and seasonal variability of the SR parameters [1.154–1.156].

SR observations are being conducted time to time at Garhwal Himalayan region to study frequency variation from the spectral analysis of magneto telluric data recorded from eight different closely spaced stations (Lat. 30.45° to 31.02° N, Long. 78.26° to 78.51° E). (N-S) and (E-W) time-varying electric and magnetic field component data are recorded during 2006 [1.157]. FFT algorithm has been used to obtain a frequency spectrum with a resolution of 0.03 Hz. The observed frequency variation is found to be related to severity of thunderstorm and associated ionospheric conductivity. The frequency variations are found to be 1.9 to 4.2 %, 1.5 to 3.1% and 1.8 to 3.4% in the first, second and third SR modes.

SR frequency variations are also investigated at Allahabad (Lat. 22° N, Long. 81.51° E) with three search coils during 2005 [1.158]. Analyses of the recorded data reveal that there is dominance of power in the N-S component of SR, which is explained in terms of thunderstorm activities, which dominate more in the South-East

Asia than in Africa and American sectors. The seasonal dependence of SR amplitude and frequency was also obtained.

From the records of SR data over Kolkata, some analyses regarding amplitude and frequency fluctuations may be carried out. The analyses may be confined for a fixed period. The variation of global thunderstorm activity as inferred from monthly intensity fluctuations of global SR signals over Kolkata and Modra (Lat. 48.61° N, Long. 17.31° E) may be presented and the observed difference could be interpreted.

The diurnal and seasonal variations of SR have been reported in a number of experiments. A three-dimensional Finite Difference Time Domain (FDTD) model of the Earth-ionosphere cavity with a day-night asymmetric conductivity profile is employed to study the diurnal and seasonal variability of the power and frequency of the first SR mode. Comparison of the FDTD results and recent experimental measurements shows a clear modulation in the SR power related to the local ionospheric height and global lightning activity. It is found that SR frequencies are not only a function of the local time but also are controlled by the global lightning activity changing with universal time [1.159]. Also, a three-dimensional FDTD model of the Earth-ionosphere cavity with a realistic conductivity profile may be employed to study the global lightning activity using the observed intensity variations of SR [1.160]. Comparison of the results derived from the FDTD model and the previous studies by other authors on related subjects shows that SR is a good probe to indicate the seasonal variations of lightning activity in three main thunderstorm regions (Africa, South-east Asia, and South America).

Being a global phenomenon, Schumann resonances have numerous applications in lightning research. Background SR records can serve as a convenient and a low-cost tool for global lightning activity monitoring. The SR can provide a

global geo-electric index for monitoring climate changes. It provides one of the few tools that, through variations in global lightning activity, can provide continuous and long-term monitoring of such important global climate change parameters such as tropical land surface temperature, and tropical upper tropospheric water vapor (UTWV).

The three centers of global lightning activity are at Africa, Central and South America, and South Eastern Asia. Lightning occurs mainly in summer in the northern hemisphere. During the annual cycle it moves from one hemisphere to the other. SR field intensity variations are related to global thunderstorm activity. Due to this, the SR signal study became a very convenient tool for studying global lightning activity [1.161-1.163]. From the distribution of global lightning, the parameters of the SR modes, eg., amplitude, frequency and Q-factor are determined [1.164–1.167]. Long term recordings of SR enable to understand diurnal changes, seasonal and inter-annual tendencies of global lightning activity [1.168–1.170]. There is good connectivity between atmospheric temperature variation, the variation of SR signals during lightning flash rate and global climate change. Water vapour and lightning activity are closely linked through thunderstorms [1.171,1.172]. Thus it has been suggested to monitor global upper tropospheric water vapour changes by SR measurements. Hence the monitoring of global upper tropospheric water vapour changes by SR method would be used as a tool for global climate change observations [1.173,1.174].

SR transients (Q-bursts) can be used to geo-locate intense lightning strikes anywhere on the planet. These large-amplitude pulses are apparently related to the occurrence of sprites and elves above thunderstorms, and therefore TLEs can be studied using SR observations. SR may be used to detect and, if necessary, monitor lightning activity on the planets and moon satellites of the solar system.

The SR is also linked to the natural climate oscillation El Niño/ENSO that changes the Earth's climate in three to seven years. Variation in SR parameters is best utilized in monitoring the natural ENSO phenomena by the measurement of surface temperature and upper tropospheric water vapour [1.175]. The SR frequency mode intensity variation with Southward shift in global position of lightning activity during El Niño and Northward shift during La Niña in longitudinal range reported from the study of frequency and intensity variation of SR modes [1.176–1.177].

The SR record at Tahiti may be assigned to the release of latent heat in tropospheric convective in the equatorial region where in addition to the well-known three Chimneys the smaller 4th Chimney would be identified in the Pacific Ocean [1.178]. The maxima of SR records in the magnetic field component along north south direction (H_{NS}) show some Lightning activity. WN-4 (4th lightning centre/4th Chimney) structure and global lightning showed some electrical properties. Further information about the 4th Chimney is yet to be explored.

There are still many open questions in SR research: importance of the day–night variation in the ionosphere conductivity profile [1.179–1.181]; influence of the latitudinal changes in the Earth magnetic field; polar cap absorption; accuracy of source geolocation; the determination of the spatial lightning distribution from the background records; anomalous SR signals related to earthquakes [1.182,1.183]; and impacts of extra-terrestrial disturbances on the Earth-ionosphere cavity. The last topic has received considerable interest over the past few years. Effects primarily on SR frequencies have been detected during cosmic gamma-ray bursts [1.184,1.185], solar flares and solar proton events [1.185–1.187], as well as over the 11-year solar cycle [1.188-1.190]. Despite these remaining open problems, SR are one of the most promising tools in a variety of fields related to lightning electromagnetics.

Vast electric field can be generated from solar X-ray flares, solar proton events (SPE), meteor showers, seismo-associated electromagnetic waves and global thunderstorms and lightning. Electromagnetic radiations in the ULF to LF range are produced due to their interaction with the medium. Any of these sources introduce anomalous and significant perturbations in the amplitude of VLF/LF spheric signals as well as sub-ionospheric transmitted signals during their propagation through such disturbed regions. From the data, the seismo-ionospheric perturbations are investigated through the statistical studies on the correlation between ionospheric perturbations and seismic activity. Both precursory and post-seismic variations in ELF-VLF amplitudes and in ionospheric parameters are known from satellite-based as well as from ground-based observations surrounding the earthquake zones [1.191–1.194].

Seismo-electromagnetic emissions are different from lightning induced emissions and technogenic emissions. On the event of strong earthquakes, the near ground of the atmospheric layer becomes ionized and generates strong electric field that introduces particle acceleration, exciting local plasma instabilities. Ion cluster mass and plasma concentration during the process of lithosphere-ionosphere coupling vary with the vastness of the earthquake. As a result, the seismo-electromagnetic emissions would be expected to cover almost the whole of ULF-ELF-VLF band. In the process, there will be increase of thermal plasma noise along with other types of emissions, eg, Cerenkov and Bremsstrahlung.

Quite a good number of articles have been published on ionospheric perturbations associated with earthquakes through the use of sub-ionospheric VLF/LF propagation [1.195–1.197] which can influence the VLF propagation characteristics. From the VLF/LF data, the seismo-ionospheric perturbations are investigated through

the statistical studies on the correlation between ionospheric perturbations and seismic activity [1.198,1.199]. The emission and propagation of electromagnetic waves from large earthquakes in the ULF-ELF-VLF bands have been reported [1.198,1.200]. Both precursory and post-seismic variations in ELF-VLF amplitudes and in ionospheric parameters are well-known from satellite-based observations surrounding the earthquake zones [1.196, 1.201,1.202].

Electromagnetic anomalies before the destructive earthquake in Greece covering wide range of frequencies have been analyzed by Eftaxias et al. [1.203]. They detected spiky nature of electromagnetic signals at 3 kHz which is similar to the VLF pre-seismic signals of Kozani Grevena earthquake. In the observations of the 1995 Hyogo-Ken Nanbu Earthquake, similar records at VLF frequencies are reported [1.204,1.205]. Spiky signatures are also reported in the publications of other investigators [1.206,1.207].

There are different models on seismic waves and also on the generation of electric field within the atmosphere due to seismo-ionospheric coupling during the occurrence of strong earthquakes [1.208,1.209]. Emission and propagation of electromagnetic waves in the ULF-ELF-VLF bands from large earthquakes are reported earlier [1.196, 1.200–1.202]. During the occurrence of any strong earthquake, electric field is generated within the upper atmosphere due to seismo-ionospheric coupling phenomenon [1.210–1.212]. In the earthquake preparation zones, underground gas discharges carry sub-micron aerosols with them which enhance the intensity of electric field close to the Earth's surface in the earthquake preparation zone due to the drop in air conductivity created by aerosols [1.213,1.214]. Seismo-electromagnetic emissions have been observed in the ULF-ELF-VLF bands in the seismically active zones prior to

the incidence of any large earthquake [1.205,1.215]. The propagation of electromagnetic waves in these frequency bands is reported [1.198]. It is inferred that the ionospheric perturbations as detected by VLF-LF propagation may be a significant tool for short-term earthquake prediction [1.216]. Several days before the occurrence of any earthquake, electron density of the plasma in the upper ionosphere over the epicenters increases abnormally [1.217].

Moreover, an inter-relation between the tectonic activity and the anomalous change of the orographic, geochemical and geohydrological parameters characterizing the Earth's lithosphere have been noticed. Electromagnetic Anomalies (EA) preceding the destructive earthquakes in Greece, covering a wide range of frequencies, have been studied [1.203]. They are correlated with the fault model characteristics of the associated earthquake and on the degree of geotectonic heterogeneities in the focal zone. The time evolution sequences in EA revealed striking similarities to the acoustic and electromagnetic emissions observed in the laboratory. Some significant effects are obtained in the data of VLF sferics and VLF sub-ionospheric transmitted signals at various frequencies, recorded from and near Kolkata (Lat: 22.56° N, Long: 88.5° E) as well as at Agartala (Tripura University site; Lat.23° N and Long. 91.4° E) during the occurrences of different earthquakes for the past several years.

Surrounding the earthquake zones, both precursory and post-seismic variations in the amplitudes of the transmitted VLF-LF sub-ionospheric signals and in the sub-ionospheric parameters are well-known from ground-based as well as satellite-based observations [1.218–1.220]. Electric field is generated during the occurrence of any strong earthquake within the upper atmosphere due to seismo-ionospheric coupling phenomena. The intensity of electric field increases when underground gas discharges

carry submicron aerosols at the near ground in the earthquake preparation zone due to the drop in air conductivity created by aerosols [1.221,1.222]. In the seismically active zones, siesmo-EM emissions have been observed in the ULF-ELF-VLF-LF bands prior to the incidence of any large earthquake [1.223].

Amplitude and phase of VLF sub-ionospheric and sferic signals are being monitored continuously from Kolkata. These are directly influenced by global thunderstorm activity, solar X-radiation and ionization of ionospheric constituents at the D-region of the atmosphere along with the conductivity of the medium [1.224,1.225]. The ionization in the lower ionospheric regions modifies the Earth-ionosphere waveguide parameters. As a result, the VLF signals, when recorded after their journey through a long distance, exhibit anomalous variations both in their amplitude and phase. For these reasons, it may be used as a tool to study the ionospheric perturbations and their association with the naturally occurring events.

Global temperature changes have been suggested as a source of variability in the global atmospheric electrical circuit. Changes in the global atmospheric electric circuit are important with regard to modern climate change issues as a possible increase in lightning frequency can indirectly regulate tropospheric ozone and CO₂. These greenhouse gases are important constituents of the enhanced greenhouse effect and lead to increases in global temperature.

In the fair-weather part of the circuit, small ions dominate the charge transport since they have a large electrical mobility. Therefore an increase in small ion concentration will increase the air conductivity by providing more charge carriers. Aerosol in the atmosphere removes small ions by attachment. An increase in aerosol number concentration therefore reduces the ion number concentration and decreases the

air conductivity. A change in aerosol number concentration subsequently modifies the total columnar resistance (R_C) between the ionosphere and the surface, and therefore J_C directly and consequently has an indirect effect on PG.

During fair-weather days there is an electrical current that travels vertically downwards from the upper atmosphere towards the Earth surface. The electric field measured at the Earth's surface is approximately 100-300 volts per meter (V/m) but this is not apparent in everyday life, as virtually everything around us is a good conductor compared to air. The ionospheric potential and the Earth-air current form part of the Direct Current (DC) circuit.

The Carnegie research showed a strong diurnal, seasonal and annual variation in the fair-weather electric field. This original data is now seen as an important discovery in the variation of the global electrical circuit and many other studies have resulted from this. Figure 1.8 shows the diurnal variation of the PG as measured during the Carnegie research. The diurnal variation in the global electric field shows a maximum at ~18:30 UT (Universal Time) and a minimum at ~02:30 UT.

Aerosol in the atmosphere is very important and is sourced from both natural and anthropogenic processes. The biggest natural primary contributor to natural aerosols is sea-salt and charged windblown dust production. Anthropogenic aerosols are formed from a range of emitted pollutants and it is the finer of these aerosol particles that have a significant effect on the electrical conductivity of air. Smoke, for instance is composed of many particles that are less than 0.1 μm in diameter and falls into a category referred to as Aitken condensation nuclei [1.226].

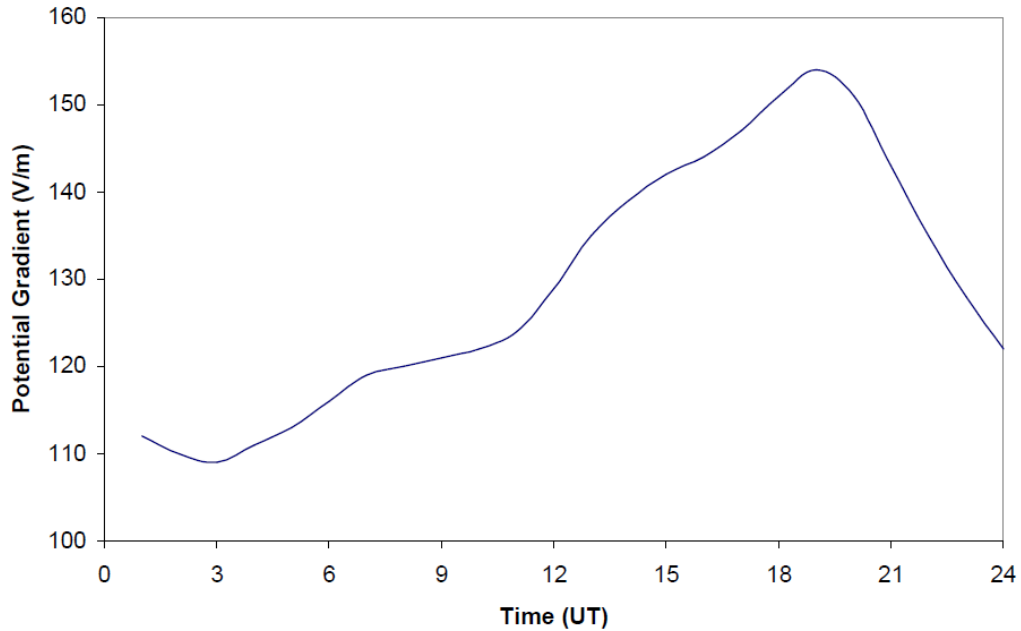


Fig: 1.8: The average diurnal variation of PG as measured by the Carnegie research vessel during 1915-1919. [1.94]

If the concentration of Aitken nuclei is large, the concentration of small ions in the air is reduced because the small ions are often captured by the aerosol particles. This leads to a reduction in the conductivity of the air and therefore an increase in the local PG (figure 1.9). There have been some studies to establish the magnitude of the change in PG but it is firstly important to investigate the natural background conductivity. Aitken nuclei have a natural seasonal variation which has studied in detail by measuring the concentration at five remote sites in the southern hemisphere [1.227]. All of the five sites showed a seasonal variation with a minimum ranging from 0-400 /cm³ in the austral winter (southern hemisphere winter). Similar studies in the northern hemisphere showed similar concentrations (300-600 /cm³) [1.228]. For comparison, concentrations of Aitken nuclei were measured at land stations that ranged from 10 000 /cm³ in coastal areas to nearly 150 000 /cm³ in the centre of a large city [1.226].

The seasonal variation of Aitken nuclei in populated areas of the world follow a trend that is opposite to that of the natural variations. There is a maximum in the local winter and a minimum in the local summer [1.227]. This is most likely due to the increased production of fossil fuels in the winter time when temperatures are low and even atmospheric dispersion characteristics favour suppression of pollutants. If there is any pollution at a site where atmospheric electricity is being monitored then it is highly likely that the low conductivity of the local atmosphere will increase the PG, reducing the likelihood of a global signal.

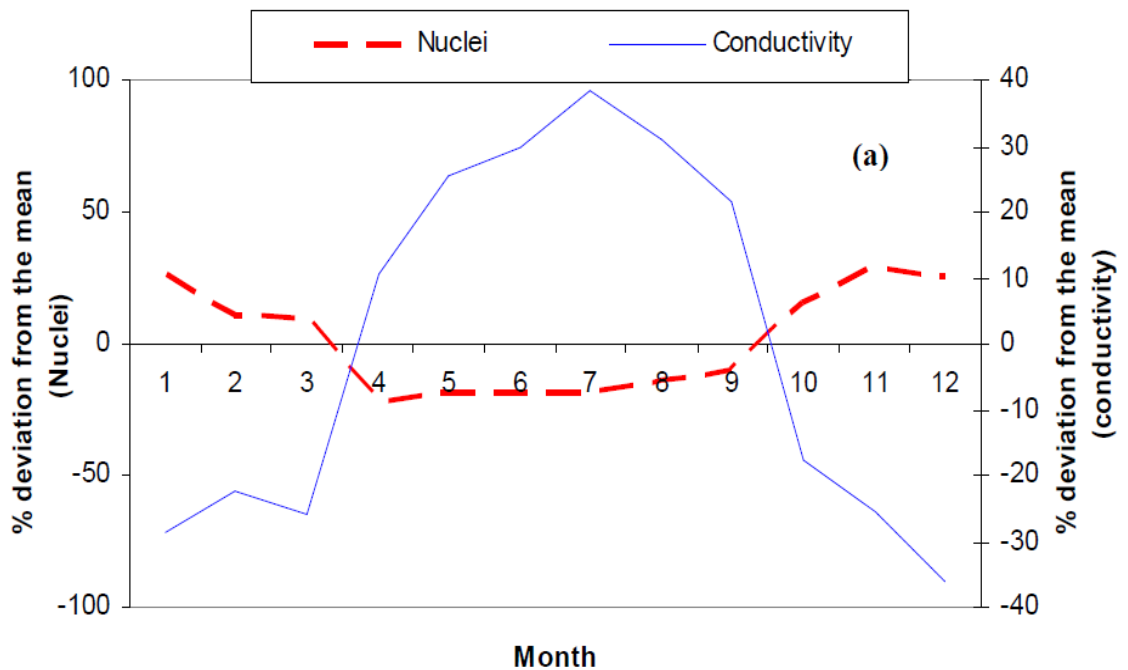


Fig. 1.9: Seasonal variation of concentration of Aitken nuclei and electrical conductivity in Poona, India [1.79].

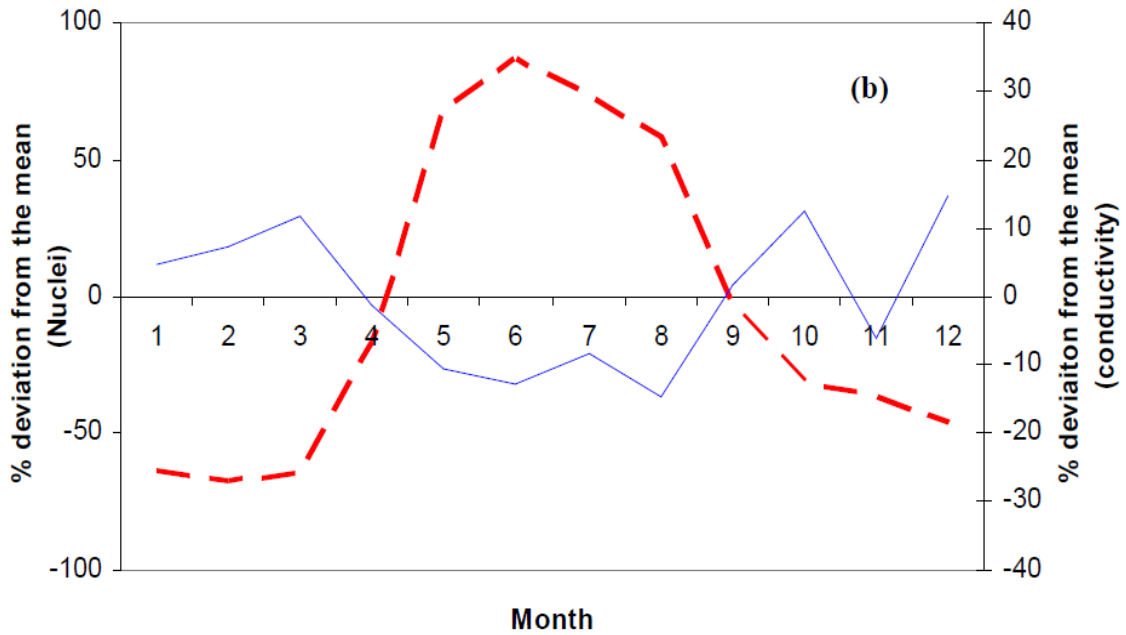


Fig. 1.10: Seasonal variation of concentration of Aitken nuclei and electrical conductivity in Huancayo, Peru [1.79].

Measurements of atmospheric electricity have been used to provide details of pollution occurrences during the nineteenth century in Paris. Because of the effect of aerosol on the PG Harrison and Aplin used the measurements on the Eiffel Tower (285 m) from 1889 to determine the air pollution levels in the late nineteenth century [1.229,1.230]. Measurements were also made at the surface at the Bureau Central Meteorologique in order to make comparison between a polluted boundary layer and clean air measurements (surface and on top of the Eiffel Tower respectively). Harrison and Aplin [1.229] results show the clean air PG followed the diurnal Carnegie curve. This indicates that measurements made at this level above the polluted Parisian boundary layer can be used to measure the global electrical circuit. The diurnal variation of the PG at the surface was found to have a double maximum in summer and autumn, with a minimum in the middle of the day. The authors of this study suggested the maximum PG at the beginning and end of the day are comparable to the smoke concentration measurements made simultaneously with the PG [1.231].

During the past several years, some works have been carried out under the joint collaboration between the Institute of Radio Physics and Electronics, University of Calcutta and Tripura University the study of Atmospheric Electricity Parameters, Schumann resonances, middle & lower atmospheric dynamics and Precursors of Earthquakes from experimental as well as theoretical point of views.

Time to time observations of SR spectra from Kolkata (Lat. 22.56° N, Long. 88.5° E) had been taken since 1999 using two square-loop antennas connected in series. Some frequency changes were observed in different modes which have been interpreted in terms of uncertainties arising from spatial distribution of lightning sources exciting the SR modes [1.232]. The Kolkata group recorded the shift in the frequency of the first SR mode during the solar proton event (SPE) on July 14, 2000 [1.233]. The recorded data shows increase of frequency during X-ray bursts and decrease during the period of occurrence of SPE. Some attempts are made to explain the observed variation during solar proton event in terms of perturbations within the Earth-ionosphere waveguide on the basis of two-layer-model.

Some studies of SR data over Kolkata recorded during Jan.-Dec. 2000 are made about the amplitude and frequency fluctuations along with other aspects of SR during the period [1.234]. The variation of the global thunderstorm activity as inferred from monthly intensity fluctuation of global SR signals over Kolkata and Modra (Lat. 48.61° N, Long. 17.27° E) has been shown and the observed difference has been interpreted.

The changes in the fourth Schumann resonance mode amplitude and peak frequency due to two earthquakes on August 2009 are recorded from Kolkata from the propagation paths of VLF subionospheric transmitted signals at 40 kHz from Fukushima, Japan and 19.8 kHz from North West Cape, Australia [1.235]. The epicenters of two earthquakes were at Andaman Island, India and at South coast of

Honsu, Japan. About 1.25 Hz shift in peak frequency is obtained. Around the time of main shocks of both the earthquakes, amplitude sustains higher values about 2.4 in arbitrary unit, which is nearly 17 % increase from the pre- and post-seismic values.

In order to make a systematic study regarding the upper tropospheric water vapour variability and other meteorological parameters affecting the global climatic change via Schumann resonance, the experiments records of SR signals through the ball antenna and induction coil antenna are necessary.

1.2 Scope of Investigation

During the last several decades, various investigations on thunderstorm and lightning, SR variation and its various modern aspects, PG and its variation, precursor of earthquake and other problems related to lower ionosphere are resulted in opening up a new dimension towards the study of various physical processes and different parameters of Atmospheric Electricity within the middle and lower ionosphere. However, different areas are also indicated where further studies are necessary to gather more information and to reconcile, where possible, with experimental results and also for predicting new features. Thus, with a view to fill up some gaps that remained in the investigation to be reported in the different aspects of Schumann resonance and Atmospheric Electricity, the author carried out researches on some of stated topic at the Department of Physics, Jadavpur University and Department of Radio Physics and Electronics, University of Calcutta, during the period from 2006 to till to date. The present thesis embodies the results of some investigations in the areas indicated.

In chapter 1, a general background about the contents of the thesis is narrated along with the outline of the chapters following.

An overview of the rudimentary concepts, measurement setup and techniques used in the study regarding the description antenna systems, buffer electronic circuits

and system calibration are described in chapter 2.

In chapter 3, the diurnal and seasonal variations of atmospheric potential gradient are analysed. The results of measurement of the atmospheric vertical potential gradient (PG) in Kolkata (Lat: 22.56° N) on the ground surface for 90 fair weather days during 2006–2009. The results are compared with those reported by others at various stations. The observed records of PG, PDC and conductivity during the stated period are analysed. Also, the correlations studies are carried out among PG and PDC and interpreted.

The characteristic of Schumann Resonance (SR) spectra from Kolkata are investigated from the recorded data. Various aspects of SR phenomena are presented in the thesis. Variation in SR parameters is best utilized in monitoring the natural ENSO phenomena by the measurement of surface temperature and upper tropospheric water vapour. The details of all are presented in chapter 4.

In chapter 5, some typical variations of maximum temperature, relative humidity, air pressure, wind speed and rainfall during a large earthquake are presented by graphical analysis. The outcomes are considered as the precursor of earthquake.

A model calculation is set up to estimate the changes in the electron concentration and the electron temperature in the ionospheric regions through energy balance equation, continuity equation and ionization balance equation. Also, statistical analyses are pictured on the three sub-ionospheric VLF transmitted signals from the recorded data at Kolkata investigated during the occurrence of several earthquakes having $M \geq 5.0$. These all are considered as the precursor of earthquake included in chapter 6.

In chapter 7, the works presented in different Chapters of this thesis are summarized. Problems for extensional work on different topics at various chapters of this thesis have been contemplated.

1.3 Main Objectives:

The electromagnetic fields generated by the lightning flashes are of importance in lightning studies. Features of the electromagnetic fields (e.g., the temporal and spatial variations) can be used to understand the physical mechanism behind the lightning processes. The electromagnetic fields can be used to estimate the voltages and currents induced in structures due to lightning strikes.

The investigations presented in this thesis, concern mainly on the studies of responses of atmospheric electricity during geophysical and extra-terrestrial events. Both experimental and theoretical investigations are initiated that led to solution of different problems closely related to the stated fields. Results of statistical analyses have also been presented in the concerned areas of researches. In some of the stated areas, further explorations would be necessary to explain aspects of the physical processes involved other than what have been considered.

There are ample scopes to extend the analysis of the various problems presented in different chapters in this thesis. Thus, in the thesis, different problems are studied in the areas of nonlinear phenomena of Earth's atmospheric electricity parameters during geophysical and extra-terrestrial events. Further works are suggested which are expected to cover in future research works.

Spectral characteristics of VLF atmospherics are recorded from Calcutta that showed some connectivity between atmospheric and ionospheric parameters. The outcome of the analysis of problems at different area has been published in research journals of national and international repute.

The thesis is based on the electric fields generated by the lightning flashes. In the proposed thesis, attempts will be made to explore problems related to different aspects of various Global Electricity Parameters based on theoretical interpretations, experimental observations and graphical analyses. Measured PG value will be critically analyzed and compared with the standard Carnegie result and deviation is explained including local factors. Different aspects of SR and Correlation between the occurrence of lightning and other geophysical activity such as earthquake with the variation of the electricity parameters like air-earth current, potential gradient, air temperature, current density, conductivity of air, UTWV, El-Niño etc.

Analysing the variation of these parameters, we can predict the occurrence and intensity of different geophysical events so that we can save the society from the devastation of this kind of natural calamities.

1.4 References

- [1.1] www.windows2universe.org
- [1.2] www.exploratorium.edu/learning_studio/auroras/happen.html
- [1.3] www.climate.nasa.gov
- [1.4] Sen, H. K. & Wyller, A. A., *J. Geophys. Res.*, **65**, (1960), 3931.
- [1.5] Chen, H. H. C. & Cheng, D. K., *J. Appl. Phys.*, **36**, (1965) 3320.
- [1.6] Motz, H., *Radio Sci.*, **69D**, (1965) 671.
- [1.7] Burman, R. & Gould, R. N., *Radio Sci.*, **69D**, (1965) 693.
- [1.8] Tai, C. T., *Radio Sci.*, **69D**, (1965) 401.
- [1.9] Chen, H. H. C. & Cheng, D. K., *IEEE Trans. Antennas Propagate.*, **14**, (1966) 497.
- [1.10] Liu, C. H., *J. Mathematical Phys.*, **8**, (1967) 2236.
- [1.11] De, S. S., *Proc. Inst. Elect. Electronics Engrs.*, **38**, (1969) 765.
- [1.12] De, S. S., *Pure and Appl. Geophys.*, **83**, (1970) 38.
- [1.13] Dyson, P. L. & Newbery, S. M., *J. Atmos. Terr. Phys.*, **44**, (1982) 363.
- [1.14] Fejer, B. J., Kelley, M. C., *Review of Geophys.*, **18**, (1980) 401.
- [1.15] Kelley, M. C., *Academic Press, San Diego, CA*, (1989).
- [1.16] Carlson, H. C., Gordon, W. E. and Snowden, R. L., *J. Geophys. Res.*, **77**, (1972) 1242.
- [1.17] Utlaut, W. F. and Violette, E. J., *Radio Sci.*, **9**, (1974) 895.
- [1.18] Bowhill, S. A., *Radio Sci.*, **9**, (1974) 975.
- [1.19] Fialer, P. A., *Radio Sci.*, **9**, (1974) 923.
- [1.20] Fejer, J. A., *Phil. Trans. Roy. Soc. London, A. Ser.* **280**, (1975) 151.
- [1.21] Utlaut, W. F., *Proc. IEEE* **63**, (1975) 1022.

- [1.22] Gurevich, A. V., Milikh, G. M. and Shlyuger, I. S., *JETP Lett.* **23**, (1976), 356.
- [1.23] Gurevich, A. V., *Excitation of ionosphere instabilities*, Springer, New York (1978).
- [1.24] Walker, J. C., *Rev. Geophys. Space Phys.* **17**, (1979), 534.
- [1.25] Mantas, G. P., Carlson, H. C. and LaHoz, C. A., *J. Geophys. Res.*, **86**, (1981), 561
- [1.26] DuBois, D. F. and Goldman, M. V., *Rev. Lett.*, **164**, (1967), 207.
- [1.27] Perkins, F. W. and Flick, J., *Phys. Fluids.*, **14**, (1971), 2012.
- [1.28] Fejer, J. A. and Leer, E., *Radio Sci.*, **7**, (1972), 481.
- [1.29] Cohen, B. I., Kaufman, A. N. and Watson, K. M., *Phys. Rev. Lett.*, **29** (1972), 581.
- [1.30] Chen, H. H. C. and Fejer, J. A., *Radio Sci.*, **10** (1975), 167.
- [1.31] Dystne, K. B., Leer, E., Trulsen, J. and Stenflo, L., *J. Geophys. Res.*, **82** (1977), 717.
- [1.32] Fejer, J. A., *Geophys. Res. Lett.*, **4**, (1977), 289.
- [1.33] Cragin, B. L., Fejer, J. A. and Leer, E., *Radio Sci.*, **12**, (1977), 273.
- [1.34] Fejer, J. A., *Rev. Geophys. Space Phys.*, **17**, (1979), 135.
- [1.35] Lin, S. C., *Phys. Fluids*, **4**, (1961), 1277.
- [1.36] Papa, R. J., *Can. J. Phys.*, **43**, (1965), 38.
- [1.37] Chakrabarti, A. K. and De, S. S., *Indian J. Radio Space Phys.* **11**, (1982), 236.
- [1.38] Sulzer, M. P., Mathews, J. D. and Tomko, A. A., *Radio Sci.* **17**, (1982), 435.
- [1.39] Tomko, A. A., Ferraro, A. J., Lee, H. S., Mitra, A. P., *J. Atmos. Terr. Phys.* **42**, (1980), 273.
- [1.40] Mitra, A. P., *Proc. Ind. Nat. Sci. Acad.*, **41**, (1975), 537.

- [1.41] Fejer, B. G., *J. Atmos. Sol.- Terr. Phys.* **59** (1997), 1465.
- [1.42] Fejer, B. G, *J. Atmos. Terr. Phys.*, **53** (1991), 677.
- [1.43] Richmond, A. D., *Handbook of Atmospheric Electrodynamics, CRC Press, Boca Ratan*, 249-290, (1995).
- [1.44] Stenning, R. J., *J. Atmos. Terr. Phys.*, **57** (1995) 1117.
- [1.45] Balakrishnan, N. and Dalgarno, A., *J. Geophys. Res.*, **108**, (A2), (2003).
- [1.46] Barr, R., Llanwyn Jones, D. and Rodger, C., *J., Atmos. Terr. Phys.*, **62**, (2000) 1689.
- [1.47] Barrington, R. E., Belrose, J. S., Nelms, G. N., *J. Geophys.Res.*, **70**, (1966) 1647.
- [1.48] Rutledge, S.A., Williams, E.R., Keenan, T.D., *American Meteorological Society*, **73**, (1992), 3.
- [1.49] Lang, et al., *Bull. Amer. Met. Soc.*, **85**, (2004) 1107.
- [1.50] Cooray V., *Lightning and Human: The Early Days, in: An Introd. To Light., 1st ed., Springer Netherlands*, 1 (2015), 1–5.
- [1.51] M.A. Uman, *Lightning, Dover, Dover Publications, Inc. New York*, 1984.
- [1.52] Cooray V., *Mechanism of Lightning Flashes, in: An Introd. to Light., Springer Netherlands*, **7**, (2015), 1–386.
- [1.53] Cooray V., *Basic Physics of Electrical Discharges, in: An Introd. to Light., 1st ed., Springer Netherlands*, **02** (2015), 7–27.
- [1.54] Cooray V., *Direct and Indirect Effects of Lightning Flashes, in: An Introd. to Light., 1st ed., Springer Netherlands*, **15** (2015), 247–280.
- [1.55] J.R. Dwyer, M.A. Uman, *The physics of lightning, Phys. Rep.* **534** (2014) 147.
- [1.56] Neubert, T., Rycroft, M., et. al., ‘*Recent results from studies of electric discharges in the mesosphere*’, *Surv. Geophys.*, **29**, (2008), 71.

- [1.57] Inan, U.S., Piddyachiy, D., Peter, W.B., Sauvaud, J.A. and Parrot, M., *Geophys. Res. Lett.*, **34**, (2007), L 07103.
- [1.58] Hu, H., Li, Q. and Holzworth, R.H., *J. Geophys. Res.*, **94**, (1989), 16429.
- [1.59] Inan, U.S., Sampson, W.A. and Taranenko, Y.N., *Geophys. Res. Lett.*, **23**, (1996), 133.
- [1.60] Inan, U.S., Bell, T.F., Pasko, V.P., Sentman, D.D., Wescott, E.M. and Lyons, W.A., *Geophys. Res. Lett.*, **22**, (1995), 3461-3464.
- [1.61] Mika, A., Haldoupis, C., Marshall, R.A., Neubert, T. and Inan, U.S., *J. Atmos. Sol.-Terr. Phys.*, **67**, (2005), 1580-1597.
- [1.62] Storey, L.R.O.: 1953, 'An investigation of whistling atmospheric', *Philosophical Transactions of the Royal Society (London) A* (**246**), (1953), 113-141.
- [1.63] Singh, R.P., Singh, A.K. and Singh, D. K., *J. Atmos. Solar-Terr. Phys.*, **60**, (1998a), 495.
- [1.64] Williams, E.R., Downes, E., Boldi, R., Lyons, W.A. and Heckman, S., *Radio Sci.*, **42**, (2007a) RS2S17.
- [1.65] Yair, Y., *Space Sci. Rev.*, **137**, (2008) 119.
- [1.66] Saunders, C., *Space Sci. Rev.*, **137**, (2008) 335.
- [1.67] Cooray V., *Charge Generation in Thunderclouds and Different Forms of Lightning Flashes, in: An Introd. to Light.*, Springer Netherlands, **06**, 2015.
- [1.68] Krehbiel, P.L., Rioussset, J.A., Pasko, V.P., Thomas, R. J., Rison, W., Stanley, M.A. and Edens, H.E., *Naturegeoscience*, **1**, (2008) 233.
- [1.69] Miller, S.L., *Science*, **117**, (1953), 528.
- [1.70] Chalmers, J.A., (1967). *Atmospheric Electricity, 2nd Edition*. Pergamon Press.

- [1.71] Israel, H., *Atmospheric Electricity, Israel Program for Scientific Translations. Jerusalem, Israel.*, **1**, (1970)
- [1.72] Williams, E.R., *Science*, **256**, (1992) 1184.
- [1.73] Williams, E.R., *Mon Weath Rev*, **122**, (1994) 1917.
- [1.74] Lakhina, G.S., *Current Science* **64**, (1993) 660.
- [1.75] Bering III, E.A., *Rev. Geophys.* (supplement copy Part II) (1995) 845-862.
- [1.76] Bering III, E.A., Few, A. A., Benbrook, J.R., *Phys. Today* (Oct. issue), (1998) 24-30.
- [1.77] Rycroft, M.J., Israelsson, S., Price, C., *J. Atmos. Solar Terrs. Phys.*, **62**, (2000) 1563.
- [1.78] Siingh, Devendraa, Singh, R.P., Kamra, A.K., Gupta, P.N., Singh, R., Gopalakrishnan, V., Singh, A.K., *J. Atmos. SolarTerr. Phys.*, **67**, (2005) 637.
- [1.79] Alderman, E.J., Willaims, E.R., *J. Geophys Res.*, **101**, (1996) D23, 29679.
- [1.80] Bering E.A., Few, A.A., Benbrook, J.R., *Physics today*, **51**(10), (1999), 24.
- [1.81] Harrison, R.G., *Atmospheric Research*, **70**, (2003) 1.
- [1.82] Rakov, V.A. Uman, M.A., *Lightning: Physics and Effects. Cambridge University Press.*, (2003).
- [1.83] Harrison, R.G., *Geophys. Res. Lett.*, **29**, (2002), 14.
- [1.84] Roble, R.G., Tzur, I., *National Academy Press, Washington, D. C.*, (1986), 206-231.
- [1.85] Roble, R.G., *J. Atmos. Solar-Terr. Phys.*, **53**, (1991), 831.
- [1.86] Tinsley, B.A., *Space Sci. Rev.*, **94**, (2000), 231.
- [1.87] Singh, D.K., Singh, R.P., Kamra, A.K.. *Space Sci. Rev.*, **113**, (2004), 375.
- [1.88] Pudovkin, M.I., Babushkina, S.V., *J. Atmos. Terr. Phys.*, **54**, (1992), 1135.
- [1.89] Carslaw, K.S., Harrison, R.G., Kirkby, J., *Science.*, **298**, (2002), 1732.

- [1.90] Harrison, R.G., Carslaw, K.S., *Rev. Geophys.*, **41**, (2003), 10.
- [1.91] Tinsley, B.A., Yu, F., *American Geophysical Union Press, Washington, D.C.* (2003), 19.
- [1.92] Williams, E.R., Mushtak, V.C., Rosenfeld, D., Goodman, S.J., Boccippio, D.J., *Atmos. Res.* **76**, (2005), 288.
- [1.93] Rycroft, M.J., Fullekrug, M., *J. Atmos. Solar –Terr. Phys.*, **66**, (2004), 1103.
- [1.94] Price, C., *Geophys. Res. Lett.*, **20**, (1993) 1363.
- [1.95] Molinari, J., Moore, P. K., Idone, V. P., Henderson, R. W., Saljoughy, A. B., *J. Geophys. Res.*, **99**, (1994), 16665.
- [1.96] Molinari, J., Moore, P. K. and Idone, V. P., *Mon. Weather Rev.*, **127**, (1999), 520.
- [1.97] Alexander, G. D., Weinman, J. A., Karyampudi, V. M., Olson, W. S., Lee, A. C., *Mon. Weather Rev.*, **127** (1999), 1433.
- [1.98] Lay, E. H., Holzworth, R. H., Rodger, C. J., Thomas, J. N., Pinto Jr., O. and Dowden, R. L., *Geophys. Res. Lett.*, **31**, (2004), L03102.
- [1.99] Rodger, C. J., Werner, S., Brundell, J. B., Lay, E. H., Thomson, N. R., Holzworth, R. H. and Dowden, R. L., *Ann. Geophys.*, **24** (2006), 3197.
- [1.100] www.imd.gov.in/section/nhac/dynamic/aila.pdf.
- [1.101] Polk, C., ‘Schumann resonance’, *In CRC Handbook of Atmospheric*, **1**, (1982), 11.
- [1.102] Siingh, Devendraa, Gopalakrishnan, V., Singh, R.P., Kamra, A.K., Singh, Shubha, Pant, V., Singh, R and Singh, A.K., *Atmos. Res.*, **84**, (2007) 91.
- [1.103] Besser, B.P. *Radio Sci.*, **42**, (2007) 2.
- [1.104] Schumann, W.O., *Z. und Naturf.*, **7**, (1952), 149.
- [1.105] Tesla, N. *Electr. World Eng.*, **7**, (1905), 21.

- [1.106] Schumann, W.O. *Z. und Naturf.*, **7**, (1952), 250.
- [1.107] Schumann, W.O. *Nuovo Cimento.*, **9**, (1952), 1116.
- [1.108] Schumann, W.O., König, H. *Naturwiss.*, **41**, (1954), 183.
- [1.109] Balsler, M., Wagner, C, J. *Res. NBS*, **64**, (1960), 415.
- [1.110] Balsler, M., Wagner, C. *Nature*, **188**, (1960), 638.
- [1.111] Balsler, M., Wagner, C. *J. Geophys. Res.*, **67**, (1962), 619.
- [1.112] Balsler, M., Wagner, C, *J. Geophys. Res.* **67**, (1962), 4081.
- [1.113] Balsler, M., Wagner, C, *J. Geophys. Res.*, **68**, (1963), 4115.
- [1.114] Gendrin, R., Stefant, R, *C.R., Acad. Sci. Paris*, **255**, (1962), 2273.
- [1.115] Wait, J.R., *IEEE Trans. Commun.*, **22**, (1974), 353.
- [1.116] Wait, J.R., *IEEE J. Oceanic Eng.*, **2**, (1977), 161.
- [1.117] Fraser-Smith, A.C. Bannister, P.R., *Radio Sci.*, **33**, (1998), 83.
- [1.118] Yano, M., Ida, Y., Hobara, Y., Hayakawa, M., Nickolaenko, A.P., *Radio Sci.*, (2010), 45.
- [1.119] Holzer, R.E., *In Recent Advances in Atmospheric Electricity*; Smith, L.G., Ed.; Pergamon Press: Oxford, UK, (1958), 599.
- [1.120] Nickolaenko, A.P., Rabinowicz, L.M., *J. Atmos. Terr. Phys.*, **57**, (1995), 1345.
- [1.121] Nickolaenko, A.P., Rabinowicz, L.M., Hayakawa, M., *J. Atmos. Electr.*, **18**, (1998), 1.
- [1.122] Heckman, S.J., Williams, E., Boldi, B., *J. Geophys. Res.*, **103** (1998), 31775.
- [1.123] Yang, H., Pasko, V.P., Satori, G., *J. Geophys. Res.*, (2009), 114.
- [1.124] Nickolaenko, A.P.; Rabinowicz, L.M., *Space Res.*, **20**, (1982) 82.
- [1.125] Nickolaenko, A.P.; Rabinowicz, L.M., *Space Res.*, **25**, (1987), 25301.

- [1.126] Pechony, O., Price, C., *Radio Sci.*, (2004) 39.
- [1.127] Price, C., Rind, D., *AMS 16th Conference on Severe Storms; American Meteorological Society: Alberta, AB, Canada*, (1990).
- [1.128] Williams, E.R., *Science*, **256**, (1992) 1184.
- [1.129] Boccippio, D.J., Williams, E.R.; Heckman, S.J.; Lyons, W.A.; Baker, I.T.; Boldi, R., *Science*, **269**, (1995), 1088.
- [1.130] Haug, H.G., Williams, E., Boldi, R., Heckman, S., Lyons, W., Taylor, M., Nelson, T., Wong, C., *J. Geophys. Res.*, **104**, (1999), 16943.
- [1.131] Price, C., Asfur, M.; Lyons, W., Nelson, T., *Geophys. Res. Lett.*, (2002), 29.
- [1.132] Sato, M.; Fukunishi, H.; Kikuchi, M.; Yamagishi, H.; Lyons, W.A., *J. Atmos. Terr. Phys.*, **65**, (2003), 607.
- [1.133] Sato, M.; Fukunishi, H. *Geophys. Res. Lett.*, 2003, 30.
- [1.134] Heckman, S.J., Williams, E.R. and Boldi, R., *J. Geophys. Res.*, **103**, (1998) 31775.
- [1.135] Rycroft, M.J., Israelsson, S., Price, C., *J. Atmos. Solar-Terr. Phys.*, **62**, (2000) 1563.
- [1.136] Satori, G., *J. Atmos. Terr. Phys.*, **58**, (1996) 1483.
- [1.137] Nickolaenko, A.P., Satori, G., Zieger, B., Rabinowicz, L.M., Kuduntseva, I.G., *J. Atmos. Solar-Terr. Phys.*, **60**, (1998) 387.
- [1.138] Boccippio, D.J., William, E.R., Heckman, S.J., Lyons, W.A., Baker, I.T. and Boldi, R., *Science*, **269**, (1995) 1088.
- [1.139] Cummer, S.A., Inan, U.S, Bell, T.F., Barrington-Leigh, C.P., *Geophys. Res. Lett.*, **25**, (1998a) 1281.
- [1.140] Magunia, A., *J. Atmos. Solar-Terr. Phys.*, **56**, (1996) 1683.
- [1.141] Schlegel, K. and Fullekrug, M., *J. Geophys. Res.*, **104**, (1999) 10111.

- [1.142] Boccippio, D. J., Williams, E. R., Lyons, W. A., Baker, I., Boldi, R., *Science*, **269**, (1995), 1088.
- [1.143] Dowden, R., Brundell, J., Rodger, C., Molchanov, O., Lyons, W. and Nelson, T., *Antennas and Propag. Mag.*, **38**, (1996), 7.
- [1.144] Glukhov, V. S., Inan, U. S., *Geophys. Res. Lett.*, **23**, (1996), 2193.
- [1.145] Pasko, V. P., Inan, U. S., Taranenko, Y. N. and Bell, T. F., *Geophys. Res. Lett.*, **22**, (1995), 365.
- [1.146] Rycroft, M. J., *J. Atmos. Terr. Phys.*, **56**, (1994), 343.
- [1.147] Sentman, D. D., Westcott, E. M., Osborne, D. L., Hamptue, D. L. and Heavner, M., *J. Geophys. Res. Lett.*, **22**, (1995), 1205.
- [1.148] Jones, D. L., *J. Atmos. Terr. Phys.*, **32**, (1970), 1077.
- [1.149] Heckman, S. J., Williams, E., Boldi, B., *J. Geophys. Res.*, **103**, (1998), 31775.
- [1.150] Mushtak, V. C. and Williams, E. R., *J. Atmos. Sol.- Terr. Phys.*, **64**, (2002), 1989.
- [1.151] Füllekrug, M. and Fraser-Smith, A. C., *Geophys. Res. Lett.*, **23**, (1996), 2773.
- [1.152] Price, C., *Nature*, **406**, (2000), 290.
- [1.153] Nickolaenko, A. P., Rabinowicz, L. M., *J. Atmos. Sol.- Terr. Phys.*, **57**, (1995), 1345.
- [1.154] Nickolaenko, A. P., Satori, G., Zieger, B., Rabinowicz, L. M., Kudintseva, I. G., *J. Atmos. Sol.- Terr. Phys.*, **60**, (1998), 387.
- [1.155] Ogawa, T., Tanaka, Y., Yasuhara, M., *J. Geophys. Res.*, **21**, (1969), 447.
- [1.156] Satori, G., Zieger, B., *J. Geophys. Res.*, **101**, (1996), 29663.
- [1.157] Chand R., Israil M., Rai J., *Annn. Geophys.*, **27**, (2009) 3497.
- [1.158] Hazra S., Sinha A. K., Pathan B. M., *Indian Journal of Radio and Space Physics*, **39**, (2010), 308.

- [1.159] Yang, H., V. P. Pasko, *Radio Sci.*, **41**, (2006) RS2S14, Printed 42(2), 2007
- [1.160] Yang, H., V. P. Pasko, and G. Satori, *J. Geophys. Res.*, **114**, (2009) D 01103.
- [1.161] Sentmann, D. D., Fraser B. J., *J. Geophys. Res.*, **96**, (1991) 15973.
- [1.162] Nickolaenko A. P., Rabinwicz L. M., *J. Atmos.Terr. Phys.*, **57**, (1995), 1345.
- [1.163] Satori G., Szendroi J., Vero J., *J. Atmos. Terr. Phys.*, **58**, (1996) 1475.
- [1.164] Nickolaenko A. P., Satori G., Zieger B., Rabinowicz L. M., Kudintseva L. G.,
J. Atmos.Terr. Phys., **60**, (1998) 387.
- [1.165] Heckman, S.J., Williams, E.R. and Boldi, R., *J. Geophys. Res.*, **103**, (1998)
31775.
- [1.166] Belyaev et al., (1999).
- [1.167] Ogawa and Komatsu, (2009).
- [1.168] Fullekrug M., Fraser-Smith A.C., *Geophys. Res. Let.*, **23**, (1996) 2773.
- [1.169] Satori G., Zieger B., *Geophys. Res. Let.*, **26**, (1999) 1365;
- [1.170] Price C., Melnikov M., *J. Atmos.Terr. Phys.*, **66**, (2004), 1179.
- [1.171] Price C., *Nature*, **406**, (2000), 290.
- [1.172] Rycroft, M. J., Price, C., *J. Atmos. Sol.-Terr. Phys.*, **62**, (2000) 1563.
- [1.173] Price, C., Rind, D., *Geophys. Res.*, **97**, (1992) 9919.
- [1.174] Price C., Asfur M., *Bull. Amer. Met. Soc.*, **34** (2006).
- [1.175] Price et al., **24** (2016) 123.
- [1.176] Wan, W., Liu, L., Pi, X., et al., Wavenumber 4 patterns of the total electron
content over the low latitude ionosphere, *Geophys. Res. Lett.*, **35**, (2008), 12.
- [1.177] Pedatella N. M., *J. Geophys. Res.*, **114**, (2009), A12316.
- [1.178] Satori, G., Ortega, P., Guha, A. and Williams, E., *2nd TEA-IS Summer
School*, June 23rd–June 27th, 2014, Collioure, France.
- [1.179] Pechony, O., Price, C., *Radio Sci.*, **41**, (2006).

- [1.180] Pechony, O., Price, C., Nickolaenko, A.P., *Radio Sci.*, **42** (2007).
- [1.181] Satori, G., Mushtak, V., Williams, E. *In Lightning: Principles, Instruments and Applications; Springer: Berlin, Germany*, (2009), 347–386.
- [1.182] Nickolaenko, A., Hayakawa, M., *Geomat. Nat. Haz. Risk.*, (2014).
- [1.183] Zhou, H., Zhou, Z.; Qiao, X., Yu, H., *J. Geophys. Res. Atmos.*, **118**, (2013) 13338.
- [1.184] Price, C., Mushtak, V., *J. Atmos. Terr. Phys.* , **63**, (2001) 1043.
- [1.185] Nickolaenko, A.P., Kudintseva, I.G., Pechony, O., Hayakawa, M., Hobara, Y., Tan, Y.T., *Ann. Geophys.*, **30**, (2012) 1321.
- [1.186] Singh, B., Tyagi, R., Hobara, Y., Hayakawa, M., *J. Atmos. Sol-Terr. Phys.*, **113**, (2014) 1.
- [1.187] Dyrda, M., Kulak, A., Mlynarczyk, A., Ostrowski, M., *J. Geophys. Res. Space Phys.*, **120**, (2015) 2255.
- [1.188] Satori, G., Williams, E., Price, C., Boldi, R., Koloskov, A., Yampolski, Y., Guha, A., Barta, V., *Effects of energetic solar emissions on the Earth-ionosphere cavity of Schuman Resonances. Surv. Geophys.*, (2016).
- [1.189] Nickolaenko, A.P., Koloskov, A.V., Hayakawa, M., Yampolski, Y.M., Budanov, O.V., Korepanov, V.E., *Sun Geophys.*, **10**, (2015) 39.
- [1.190] Ondraskova, A., Sevicik, S., Kostecky, P., *J. Atmos. Sol-Terr. Phys.*, **73**, (2011) 534.
- [1.191] Liu, J. Y., Chuo, Y. J., Shan, S. J., Tsai, Y. B., Pulinets, S. A., Yu, S. B., *Ann. Geophys.*, **22**, (2004) 1585.
- [1.192] Molchanov, O. A., Hayakawa, M., *J. Geophys. Res.*, **103**, (1998) 17489.
- [1.193] Parrot, M., *J. Geophys. Res.*, **99**, (1994) 23339.
- [1.194] Izutsu, J., *Terr. Atmos. Ocean. Sci.*, **18**, (2007) 923.

- [1.195] Hayakawa, M., Molchanov, O. A., Ondoh, T. & Kawai, E., *J Communication Res. Laboratory*, **43**, (1996) 169.
- [1.196] Molchanov, O. A., Hayakawa, M., *J. Geophys. Res.*, **103**, (1998) 17489.
- [1.197] Biagi, P. F., Piccolo, R., Castellana, L., Ermini, A., Martellucci, S., Bellecci, C., Capozzi, V., Perna, G., Molchanov, O. & Hayakawa, M., *Phys. Chem. Earth*, **29**, (2004) 551.
- [1.198] Fujinawa, Y. & Takahashi, K., *Physics of the Earth and Planetary Interiors*, **105**, (1998), 249.
- [1.199] Maekawa, S., Horie, T., Yamauchi, T., Sawaya, T., Ishikawa, M., Hayakawa, M., Sasaki, H., *Ann. Geophys.*, **24**, (2006) 2219.
- [1.200] Gokhberg, M. B., Morgounov, V. A., Yoshino, T., Tomizawa, I., *J. Geophys. Res.*, **87(B9)**, (1982) 7824.
- [1.201] Pulinets, S. A., *Adv. Space Res.*, **22**, (1998b) 903.
- [1.202] Liu, J. Y., Chuo, Y. J., Shan, S. J., Tsai, Y. B., Chen, Y. I., Pulinets, S. A., Yu, S. B., *Ann. Geophys.*, **22**, (2004) 1585.
- [1.203] Eftaxias, K., Kapiris, P., Polygiannakis, J., Peratzakis, A., Kopanas, J., Antonopoulos, G., Rigas, D., *Nat. Hazards Earth Syst. Sci.*, **3**, (2003) 217.
- [1.204] Yamada, T., Oike, K., *J. Phys. Earth*, **44**, (1996) 405.
- [1.205] Nagao, T., Enomoto, Y., Fujinawa, Y., Hata, M., Hayakawa, M., Huang, Q., Izutsu, I., Kushida, Y., Maeda, K., Oike, K., Uyeda, S. & Yoshino, T., *J. Geodynamics*, **33**, (2002) 401.
- [1.206] Ohta, K., Umeda, K., Watanabe, N. & Hayakawa, M., *Nat. Hazards Earth Syst. Sci.*, **1**, (2001) 37.
- [1.207] Izutsu, J., *Terr. Atmos. Ocean. Sci.*, **18**, (2007) 923.
- [1.208] Hayakawa, M. & Fuzinawa, Y., *Terra Scientific, Tokyo*, (1994), 247.

- [1.209] Mareev, E. A., Iudin, D. I. & Molchanov, O. A., *Mosaic source of internal gravity waves associated with seismic activity, Seismo Electromagnetics: Lithosphere-Atmosphere-Ionosphere Coupling, (Editors) M. Hayakawa, & O. A. Molchanov, TERRAPUB, Tokyo, (2002), 335–342.*
- [1.210] Pulinets, S. A., Legen'ka, A. D., Gaivoronskaya, T. V. & Depuev, V. K., *J. Atmos. Sol.-Terr. Phys.*, **65**, (2003) 1337.
- [1.211] Hayakawa, M., (Ed.), *Atmospheric and Ionospheric Electromagnetic Phenomena Associated with Earthquakes (Tokyo: TERRAPUB) (1999).*
- [1.212] Hayakawa, M., Molchanov, O. A., NASDA/UEC Team, *Terr. Atmos. Oceanic Sci.*, **15**, (2004), 311.
- [1.213] Chemyrev, V. M., Isaev, N. V., Serebryakova, O. N., Sorokin, V. M. & Sobolev, Y. P., *J. Atmos. Sol.-Terr. Phys.*, **59**, (1997), 967.
- [1.214] Krider, E. P. & Roble, R. W. (Eds.), *The Earth's Electrical Environment*, National Academy Press, Washington D.C., (1986).
- [1.215] Fuzinawa, Y. & Takahasi, K., Paper presented at IUGG Meeting Boulder, Colorado, 2-4 July, 1995, (1995).
- [1.216] Yamauchi, T., Maekawa, S., Horie, T., Hayakawa, M. & Soloviev, O., *J. Atmos. Sol.-Terr. Phys.*, **69**, (2007) 793.
- [1.217] Utsunomiya, T., *IEICE Trans.*, **E83-B**, (2002) 838.
- [1.218] Pulinets, S. A., *Adv. Space Res.* **22** (1998), 903.
- [1.219] Molchanov, O. A., Hayakawa, M., *J. Geophys. Res.* **103** (1998), 17489.
- [1.220] Liu, J. Y., Chuo, Y. J., Shan, S. J., Tsai, Y. B., Chen, Y. I., Pulinets, S. A., Yu, S. B., *Ann. Geophys.* **22** (2004), 1585.
- [1.221] Chmyrev, V. M., Isaev, N. V., Serebryakova, O. N., Sorokin, V. M. and Sobolev, Y. P., *J. Atmos. Sol.- Terr. Phys.* **59** (1997), 967

- [1.222] Krider, E. P., Roble, R. W., (Eds.): The Earth's Electrical Environment, *National Academy Press, Washington D.C.* (1986).
- [1.223] Nagao, T., Enomoto, Y., Fujinawa, Y., Hata, M., Hayakawa, M., Huang, Q., Izutsu, I., Kushida, Y., Maeda, K., Oike, K., Uyeda, S. and Yoshino, T., *J. Geodynamics* **33** (2002), 401.
- [1.224] De. S. S., De, B. K., Bandyopadhyay, B., Paul, Suman, Haldar, D. K. & Barui, S., *J.Atmos. Sol.- Terr. Phys.*, **72**, (2010) 829.
- [1.225] Nickolaenko, A. P., *J. Atmos. Terr. Phys.* **59**, (1997), 806.
- [1.226] Israel, H., (1970). Atmospheric Electricity, Vol I. *Israel Program for Scientific Translations*. Jerusalem, Israel.
- [1.227] Bigg, E.K., Gras, J.L., Evans, C., *J. Atmos. Chem.*, **1**, (1984) 203.
- [1.228] Flyger, H.K., Hansen, K., Megaw, W.J., Cox, L.C., *J. Appl. Meteorol.*, **12**, (1973) 161.
- [1.229] Aplin, K. L., Harrison, R. G., *Proc. R. Soc. Lond.*, **459**, (2003) 353.
- [1.230] Chauveau, B., (1925). Electricite Atmospherique, Vol. 3, *Librairie Octave Doin*, Paris, France.
- [1.231] Harrison, R.G., Aplin, K.L., *Atmospheric Environment*, **37**, (2003) 5319.
- [1.232] De, S.S., De, B.K., Guha, A., Mondal, P.K., *Indian J. Radio Space Phys.*, **35**, (2006) 396,
- [1.233] De S. S., De B. K., Bandyopadhyay B., Paul S., Haldar D.K., Barui S., *J. Atmos. Sol-Terr. Phys.*, **72** (2010) 829.
- [1.234] De, S. S., De, B. K., Sarkar, B. K., Bandyopadhyay, B., Haldar, D. K., Paul, S. and Barui S., *Indian J. Radio Space Phys.* **38** (2009), 208.
- [1.235] De S. S., Bandyopadhyay B., Das T. K., Paul S., Haldar D. K., Barui S., Snfui M., Pal P., Chattopadhyay G., *Indian Journal of Physics*, **85**, (2011), 447.

CHAPTER 2

Rudimentary concepts, Experimental setup & measuring techniques

This chapter provides an overview of the rudimentary concepts, measurement setup and techniques used in this work. The brief descriptions of antenna systems, buffer electronic circuits and system calibration are also presented.

2.1 Rudimentary concepts

Electric field E and electric potential ϕ are related by the formula

$$E = -\frac{\partial\phi}{\partial r} \quad \text{wheresymbols have their usual meaning.}$$

Thunderstorms and shower clouds cause separation of electric charges between the ground and ionosphere, an electrically conductive layer about 60 km above the surface. Here, the term electrically conductive layer refers to a layer with sufficiently high conductivity compared to the lower (tropospheric) atmosphere to be considered a perfect conductor. This charge separation causes the ionosphere to have a potential (V_I) of approximately +300kV with respect to the surface. Ionisation from cosmic rays and terrestrial sources produce cluster ions (small ions) which make the atmosphere weakly electrically conductive. These ions flow vertically because of the vertical potential difference, causing the air-Earth conduction current density, J_C , of order 10^{-12} Am^{-2} . The total electrical resistance for a unit area of the atmospheric column from the surface to the ionosphere is called the columnar resistance, R_C .

The ionosphere-earth potential difference (V_I), columnar resistance and conduction current are related by Ohm's law,

$$V_I = J_C \times R_C$$

The physical unit of R_C is $\Omega.m^2$ (or more commonly $P\Omega.m^2$) due to the inherently large values. This is because R_C is the integral of resistivity (units $\Omega.m$) with height, V_I represents the electric potential of a layer at a height above the surface (the zero potential reference) so the unit is in volts (or in kV).

The negative of potential gradient (PG) is equal with the electric field intensity (E). So

$$PG = - E$$

At the surface, the PG arises because of J_C flowing through the electrically conductive air. It is, therefore, J_C that permits the effect of the global circuit to be measured at the surface, either directly through measurement of J_C itself, or by PG. However, PG is also a function of the local air conductivity. Away from sources of charge separation, the air conductivity (σ_T), potential gradient (PG) and conduction current density are related by Ohm's Law

$$PG = J_C / \sigma_T$$

Among the quantities which can be measured at the surface, the air-Earth conduction current density (J_C) presents one of the most fundamental parameters of the global circuit [2.1]. It is, therefore, of great importance in this study, with its continuous measurement being one of the aims of this work. A positive current density occurs when positive charge is moved downward. The conduction current density is one of several components contributing to the total current density, J_S , received by a horizontal conducting electrode at the earth's surface, electrically isolated from the ground. J_S comprises of contributions from turbulence J_T , conduction J_C , displacement J_D and precipitation J_P ,

$$J_S = J_C + J_D + J_T + J_P$$

where, J_C is the component flowing as a result of the global electric circuit [2.2]. The displacement current density (J_D) is induced by changes in the PG. The turbulent current density (J_T) arises due to the transport of space charge by air turbulence. Charged precipitation falling on the electrode will also transfer a precipitation charge J_P .

Ion-aerosol theory explained here has been summarised from work carried out by Harrison and Aplin [2.3]. In air of varying conductivity, the PG and air-earth current (J) can be explained by Ohm's law

$$PG = \frac{J}{\sigma}$$

when negative and positive ion concentrations are considered equal.

Now $\sigma = 2n\mu e$

where; n is the ion number concentration,

μ is the mean ion mobility,

and e is the electronic charge.

The production and removal of ions in the atmosphere is assumed balanced and the time variation in the ion number concentration can be represented as [2.4]

$$\frac{dn}{dt} = q - \alpha n^2 - \beta nZ$$

Where; q is the volumetric ion formation rate,

n is the ion number concentration,

α is the ion recombination coefficient,

β is the ion-aerosol attachment coefficient, and

Z is the monodisperse (all aerosols have same radius) aerosol number concentration.

In a steady state situation with a clean air atmosphere, the removal of ions via aerosol interaction is negligible and nZ becomes zero. Therefore, [2.3]

$$n = \sqrt{\frac{q}{\alpha}}$$

So we can write,

$$PG = \frac{\sqrt{\alpha}}{2\mu e} \frac{J}{\sqrt{q}}$$

In a polluted atmosphere ion-aerosol attachment dominates over ion recombination, i.e., $nZ \gg n^2$ as the mechanism of ion removal and the steady state ion concentration becomes [2.3]

$$n = \frac{q}{\beta Z}$$

Use of ion-aerosol theory can explain how a polluted site such as Kew Observatory, country UK may show higher PG values than at clean air sites. The PG measured on the Carnegie research vessel show lower values that are typical of an aerosol-free atmosphere. Research at Eskdalemuir, Scotland shows PG values that are typical of both a clean air site and polluted site. Harrison in 2004 [2.5] reports that PG data at Eskdalemuir shows the Carnegie global circuit diurnal variation in the winter months, but PG values are greater than would be expected from ion-aerosol theory.

Electrified clouds and lightning play important role in the global electric circuit. The electromagnetic responses of the atmosphere are presented through Maxwell's equations together with a time-varying source charge distribution. The conductivities are taken to be exponentially graded function of altitude. Mathematically, the expression of electric potential has been deduced from which the expressions of electric field components have been derived. The vertical component of the electric field would

relate the global electric circuit while the radial component would show the electrical coupling between the lower atmosphere and the ionized Earth's environment.

If $z = 0$, represents the surface level;

Z is the axis of symmetry of the charge density distribution;

z_E is the height between 100 Km to 120 Km;

z_L = the lower boundaries of the electrified cloud;

z_U = the upper boundaries of the electrified cloud;

Φ = the electric potential of the electric field of the electrified cloud;

\hat{e}_0 = the unit vector in the direction of the external magnetic field;

\vec{j}_s = source current density to generate a charge center at the height z_C , in the cloud;

$\sigma_0, \sigma_1, \sigma_2$ are the longitudinal, Pedersen and Hall conductivities respectively;

ζ and δ are the unit Heaviside and Dirac function; [2.6]

$Q(t)$ = the source function which gives the total current injected at time t ;

\hat{e}_s = the vertical unit vector;

Let us assume that, the electric conductivity is isotropic in the atmospheric region $(0, z_L)$. where $z_L = 70$ Km and anisotropic above $z = z_L$, the conductivity is anisotropic so tensorial in nature [2.7]. Now, the field equations can be written as,

$$\nabla^2 \Phi = \frac{-\rho_T}{\epsilon_0}(r, z) \quad \text{at } 0 \leq z \leq z_E \quad (1)$$

$$\nabla \cdot \vec{j} = 0 \quad \text{at } 0 \leq z \leq z_L \quad (2)$$

$$\vec{j} = (\sigma_0 - \sigma_1)(\vec{E} \cdot \hat{e}_0)\hat{e}_0 + \sigma_1 \vec{E} - \sigma_2 \vec{E} \times \hat{e}_0 + \vec{j}_s \quad \text{at } z_L \leq z \leq z_E \quad (3)$$

$$\vec{j}_s = \frac{Q(t)}{2\pi r} \delta(r) \zeta(z - z_e) \hat{e}_s \quad (4)$$

For $110 < z_E < 125$ Km, the longitudinal conductivity σ_0 becomes very large compared to transverse conductivities. The charge is assumed to have an ellipsoidal Gaussian distribution given by eq. (4).

The radial and the vertical component of electric field are given by,

$$E = -\frac{\partial\phi}{\partial r} \quad \text{and}$$

$$E_z = -\frac{\partial\phi}{\partial z}$$

For isotropic region ($0 \leq z \leq z_L$ and $z_U \leq z \leq z_I$) solution for electric potential is,

$$\Phi(r, z) = \int_0^{\infty} J_0(rk) [a_i(k) \exp(c_1 z) + b_i(k) \exp(c_2 z)] dk$$

For anisotropic region, $z_I \leq z \leq z_E$ the solution becomes,

$$\Phi(r, z) = [f(z)]^n \int_0^{\infty} \left[J_0(rk) \{A(k)I_n[kf(z)] + B(k)K_m[kf(z)]\} + \left[(r^2 + \frac{k^2}{r_k^2}) J_0\{kf(z)\} - k^2 \right] \right] dk$$

For the thundercloud region, $z_L \leq z \leq z_U$

$$\Phi_n(r, z) = \int_0^{\infty} J_0(kr) [C(k) \exp(-kz) + D(k) \exp(+kz) + \nu(z, k)] dk$$

Hence electric field around the electrified cloud, $z_L \leq z \leq z_U$

$$E_r = -\frac{\partial\Phi}{\partial r} = \int_0^{\infty} kJ_1(rk) [C(k) \exp(-kz) + D(k) \exp(+kz) + \nu(z, k)] dk$$

$$E_z = -\frac{\partial\Phi}{\partial z} = \int_0^{\infty} J_0(rk) [kC(k) \exp(-kz) + kD(k) \exp(+kz) - \nu'(z, k)] dk$$

The variation of the values of field components for different heights can be evaluated with these expressions.

The upward Maxwell current can be determined by using the transient electric field solution as

$$I_{\text{Max}}(\text{upward}) = \int \int_{-\infty-\infty}^{+\infty+\infty} \left(\sigma E_z + \varepsilon \frac{\partial E_z}{\partial t} \right) dx dy.$$

During sudden removal of thundercloud charge at low latitude by lightning discharges, the quasi-electromagnetic fields are supposed to heat up the mesospheric electrons producing ionization and light (red sprites type of discharges). Strong lightning discharges associated with sprites excite ULF transients and Schumann resonance bursts which are impulsive events [2.8-2.11].

Now, Maxwell equations for the ionized medium can be written as

$$\left. \begin{aligned} \nabla \times \vec{H} &= \frac{1}{c} \frac{\partial \vec{D}}{\partial t} \\ \nabla \times \vec{E} &= -\frac{1}{c} \frac{\partial \vec{H}}{\partial t} \\ \nabla \cdot \vec{D} &= 4\pi e(n - n') \\ \nabla \cdot \vec{H} &= 0 \end{aligned} \right\} \quad (5)$$

Based on the highly ionised plasma columns above sprite associated lightning discharges in the upper mesosphere and lower ionosphere, a model is formed by which the ULF transients in the magnetic field are explained in terms of magnetic signatures caused by induced current flowing in the short-lived, highly ionised plasma columns. Generation of ULF field by local variation of the ionospheric conductivity in the presence of an ambient electric field is known [2.12].

Here, the upper mesospheric height range with enhanced ionization has been considered to be subjected to a time-varying current in presence of anisotropic conductivity of the medium.

Solving Maxwell's equations with appropriate boundary conditions, the expression of current has been evaluated as

$$J = \frac{\omega^2}{c^2} E_0 e^{-(k_1'' + k_2'')y} [\xi_1 \{ (\zeta_1 k_2'' + \zeta_2 k_2') \cos(ky - \omega t) + (\zeta_1 k_2' - \zeta_2 k_2'') \sin(ky - \omega t) \} \hat{x} \pm \xi_2 \{ (\zeta_3 k_2'' + \zeta_4 k_2') \cos(ky - \omega t) + [\zeta_3 k_2' - \zeta_4 k_2''] \sin(ky - \omega t) \} \hat{y}]$$

Where,

$$\xi_1 = \frac{e \Omega_z \omega_p^2 E_r}{mc \omega (\eta^2 + 4\omega^2) \{ (\Omega_z + \eta^2 - 4\omega^2)^2 + 16\eta \omega^2 \}}$$

$$\xi_2 = \frac{e \omega_p^2 E_r}{mc \omega \{ (\Omega_z + \eta^2 - 4\omega^2)^2 + 16\eta^2 \omega^2 \}}$$

$$\zeta_1 = \eta (\Omega_z^2 + \eta^2 - 4\omega^2 - 8\eta \omega^2)$$

$$\zeta_2 = \{ 2\omega (\Omega_z^2 + \eta^2 - 4\omega^2) + 4\eta^2 \omega \}$$

$$\zeta_3 = (\Omega_z^2 + \eta^2 - 4\omega^2)$$

$$\zeta_4 = 4\eta \omega$$

$$k_{y_1} = k_1' + ik_1''$$

$$k_{y_2} = k_2' + ik_2''$$

$$k = k_1' + k_2'$$

$$\omega = \omega_1 \pm \omega_2$$

$$\Phi_n(r, z) = \int_0^\infty J_0(rk) [C(k) \exp(-kz) + D(k) \exp(+kz) + v(z, k)] dk$$

These waves may develop ultra-slow tails of sprite-associated lightning discharges at the upper mesospheric height range [2.13].

Again, to explain the EM radiation associated with earthquakes and volcanic activities, one has to calculate the attenuation of ELF/VLF waves in dry crust and wet soil.

Now, the electric field of EM waves may be expressed as

$$\vec{E} = \vec{E}_0 \exp\{j(\omega t + \vec{k} \cdot \vec{r})\} \quad (6)$$

Where \vec{k} is the wave vector given by, $k^2 = \epsilon\mu\omega^2 - j\sigma\mu\omega$.

ω is the angular wave frequency;

\vec{r} , the radial vector from the radiation source;

μ , the permeability;

ϵ , the dielectric constant and

σ is the electrical conductivity.

The complex wave number is given by $k = \alpha + j\beta$, ($\alpha > 0, \beta \geq 0$), α represents the propagation constant and β is the attenuation constant. The attenuation constant is derived as

$$\beta = \omega \left\{ \frac{\epsilon\mu}{2} \left[\sqrt{1 + \left(\frac{\sigma}{\epsilon\omega} \right)^2} - 1 \right] \right\}^{1/2} \quad (7)$$

$$= (\sigma\mu\omega / 2)^{1/2} = 1/\delta \text{ for } \sigma / \epsilon\omega \gg 1, \text{ where } \delta \text{ is the skin depth.}$$

The dielectric constant is expressed by $\epsilon = \epsilon_o \epsilon_r$. $\epsilon_o = 1/(36\pi \times 10^9) F/m$ is the dielectric constant or permittivity of free space and ϵ_r is the relative dielectric constant. The magnetic permeability μ is usually approximated by the permeability of vacuum $\mu_o = 4\pi \times 10^{-7} H/m$, if the material concerned is not ferromagnetic. Relative dielectric constants ϵ_r of the material concerned are as follows: 1 for gas, 80 for water at 20° C. For water $\epsilon_r = 55$ at 100° C. The electric conductivities σ of the material concerned are as follows: 10^{-2} mho/m for wet soil and 10^{-5} mho/m for dry crust.

The expression of $\beta = 1/\delta$ can be properly used for EM wave attenuation below 100 kHz in wet soil and below 10 kHz in dry crust. For frequencies from 100 Hz

to 10 kHz, the attenuation of EM waves in dry crust is less than 4 dB/km, while it is from 17.3 dB/km at 100 Hz and above 100 dB/km at 1 kHz in wet soil. Therefore, if EM radiation is generated in dry crust by rock fractures over a vast region before and after the main shock of a shallow earthquake, anomalous EM waves will be observed even in the VLF band.

2.2 Experimental Set-up and measuring techniques

2.2.1 Experimental Arrangement for measuring Potential Gradient (PG)

In our work continuous measurement of atmospheric vertical Potential Gradient (PG) is done by the apparatus named Field-mill, placed at a height 26 m above the ground. Its aluminium rotor plate is 11.4 cm in diameter while the stator has the same dimension. The alternating signal from the field-mill is being amplified by using a signal processor having one-second time constant. IC LF356N has been used at the input stage of the amplifier because of its high input resistance ($\sim 10^{12} \Omega$) and good signal to noise ratio (SNR). The r.m.s. value of the amplified signal is used to find the required electric field from the calibration chart. It has been calibrated in a vertical field set-up between two large aluminium cover plates, electrically isolated at a given potential, through a fixed distance between them. The outer shield of the Field mill is grounded properly to ensure protection from any field distortion. The sensitivity of the Field-mill is measured to be $(0.33 \pm 0.03) \text{ Vm}^{-1}$.

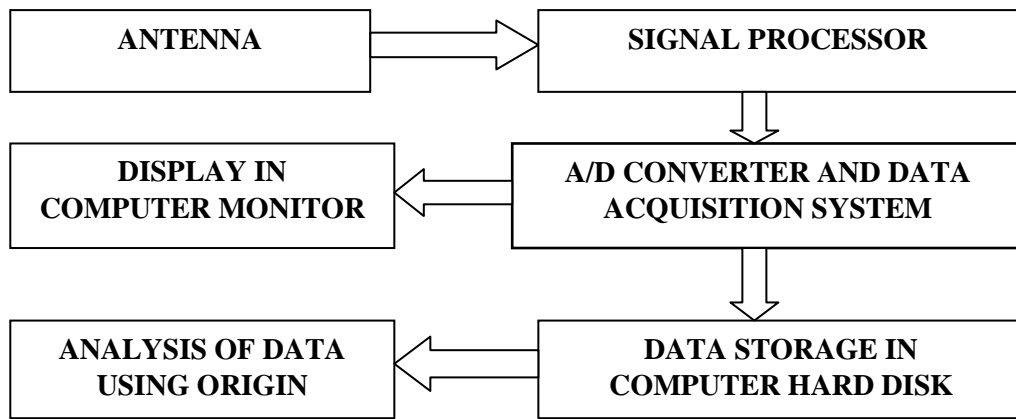


Fig. 2.1: Block diagram of the receiver system.

Regular records of sferics (<30 kHz) at frequencies 1,3,5,7,9,12 kHz are taken. The output of the amplifier is recorded at a sample rate of 1 data per sec, through a data acquisition system that uses a PCI 1050, 16 channels 12 bit DAS Card (Dynamlog), having 12 bit A/D converter, 16 digital inputs and outputs. One of the input–output channels is used for PG measurement and another is for PDC signal measurement. The recorded data are analyzed through graphing software (Origin). A set of 15 data have been averaged and then plotted. A block diagram is shown in Fig. 2.1.



Fig. 2.2: A standard Field mill apparatus that shows the modulator, pressure cover, and electric connector.

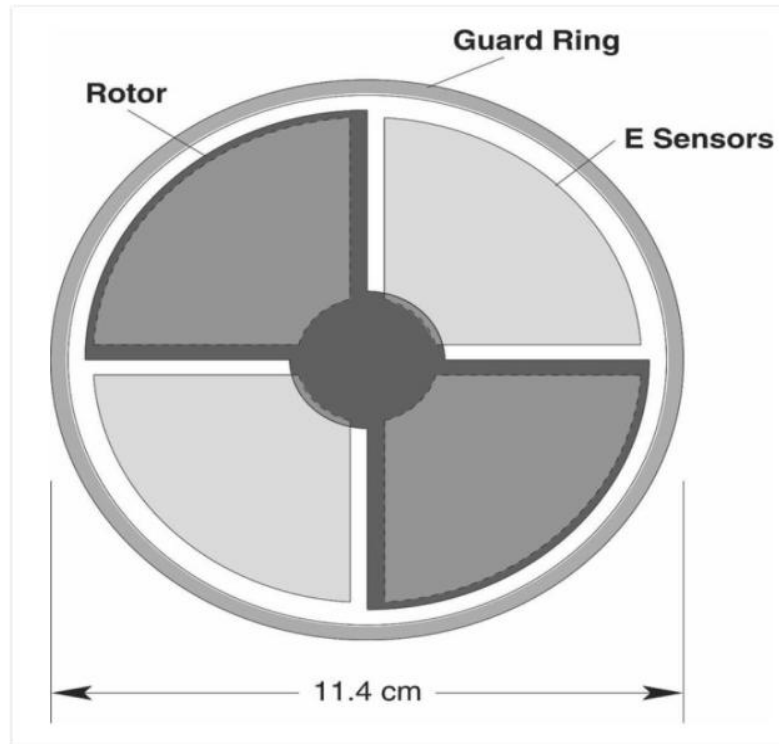


Fig. 2.3: Top view of the E-field sensor. The grounded rotor is 'bow tie' shaped, so that it covers one pair of sensors.

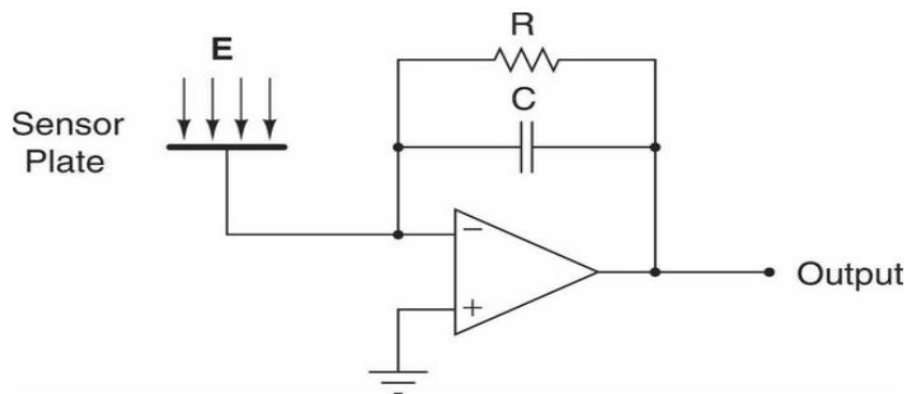


Fig. 2.4: The circuit diagram of a charge amplifier.

The ambient electric field, E , induces charge (Q) on the sensor plate, which is measured by the charge amplifier. The output voltage is given by $V = Q/C$. The feedback resistor (R) slowly bleeds off charge from the capacitor, keeping the output from saturating. This also sets the high-pass cutoff frequency of the circuit at $1/RC$.

2.2.2 Measurement of Point Discharge Current (PDC)

The continuous measurement of PDC has been made by using a steel wire having diameter 3 mm and length 8 cm, one end of which is tapered to a sharp edge. The tip of the sharp edge is about 0.02 mm. The other end is soldered to a co-axial cable which is made perfectly insulated by Teflon coating. The entire junction is tightly covered by a Teflon insulated wire. The cable is surrounded by thermoplastic polystyrene which is coated by a very thin honeycomb winding copper wire. The external surface is kept within the cylindrical plastic cover. This process ensures efficient heat insulation also. The other end of the cable is connected to the receiving system. The pointer is erected on a wooden support which is at a height of 8 m from the ground. Proper precautions are taken to avoid any other object with sharp edges at the site. The transient responses from the tip are amplified. The overall gain of the amplifier is around 40 dB. IC LF356N used here ensures good signal to noise ratio.

The output of the amplifier is recorded at a sample rate of 1 data per sec, through a data acquisition system that uses a PCI 1050, 16 channels 12 bit DAS Card (Dynamlog), having 12 bit A/D converter, 16 digital inputs and outputs. One of the input–output channels is for PDC signal measurement. The recorded data are analyzed through graphing software (Origin). A set of 15 data have been averaged and then plotted. A block diagram is shown in Fig. 2.1.

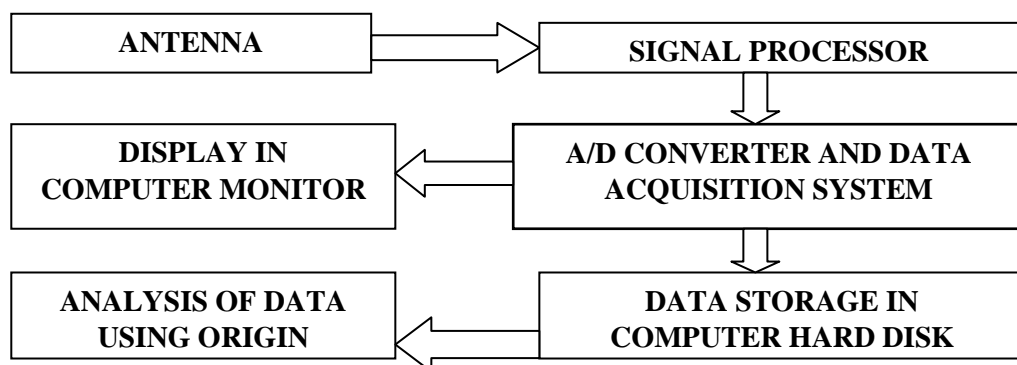


Fig. 2.5: Block diagram of the receiver system.

2.2.3 Measurement of Conductivity

The conductivity is measured near ground through a Gerdien condenser, where air between the electrodes (two co-axial cylinders) is supplied by a fan. Air-ions with desired polarity and mobility are forced by electric field to supply their charge to the collecting electrode which gives the generating current $I=neQ$. Here, Q is the amount of air flow through the electrode (~ 0.0022 to 0.0026) $\text{m}^3 \text{s}^{-1}$ and e is 1.609×10^{-19} C. Current is measured by an electrometer [2.14]. It is represented as the concentration of air-ions cm^{-3} . Polarizing voltage (U) and air flow determine the critical mobility μ_c of the measured ions given by the following expression:

$$\mu_c = \frac{V_s(R_{12} - R_{22}) \ln\left(\frac{R_2}{R_1}\right)}{2LU}$$

where, R_1 , R_2 are the radii of the polarizing and collecting electrodes; L is the electrode length and V_s is the speed of air-flow. The instrument is used for air conductivity measurements under varying concentrations and scanning of air-ions through mobility. Alternating ion polarities would require alternative supply of applied polarizing voltage that produces capacitive current spikes [2.14, 2.15]

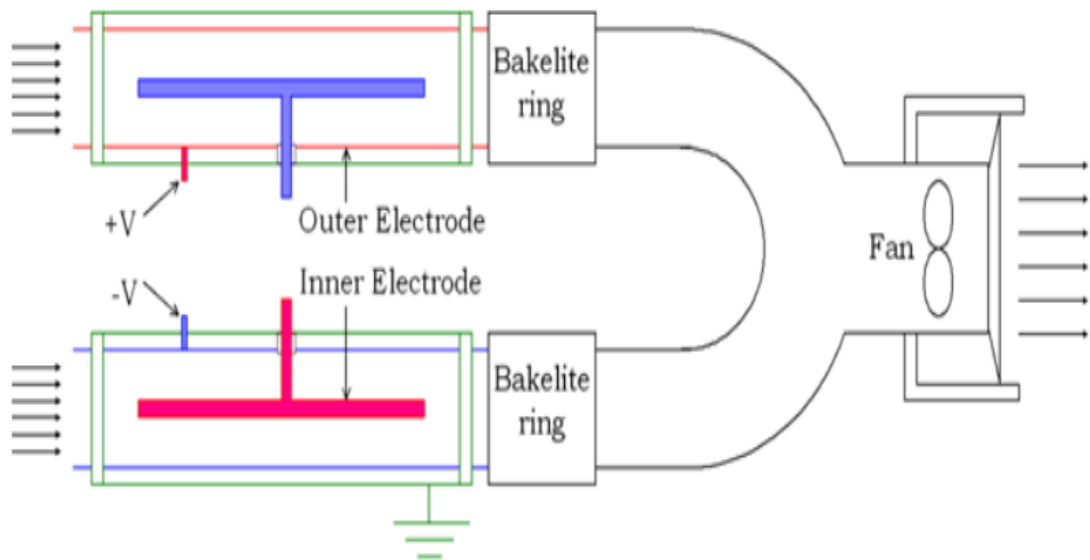


Fig 2.6: Schematic representation of Gerdien condenser.

2.2.4 Experimental arrangement for recording of VLF transmitted signals

The VLF transmitted signal at frequencies 16.4 kHz, 19.8 kHz and 25 kHz have regularly been recorded over the last several years from Kolkata (lat: 22.56⁰N, long: 88.5⁰E). For the reception of these signals, a straight horizontal copper wire of 8 SWG having 120 m length has been used in the form of an inverted L type antenna. The antenna, installed 30 m above the ground, is capable of receiving vertically polarized transmitted signals in the ELF–VLF bands. The VLF transmitted signals are recorded by computerized data acquisition system through a PCI 1050, 16 channel 12 bit DAS card. These are then processed and stored in a computer. The r.m.s. value of the filtered data are analyzed regularly using graphing software (Origin). The receiver system is presented by the block diagram in Fig. 2.7.

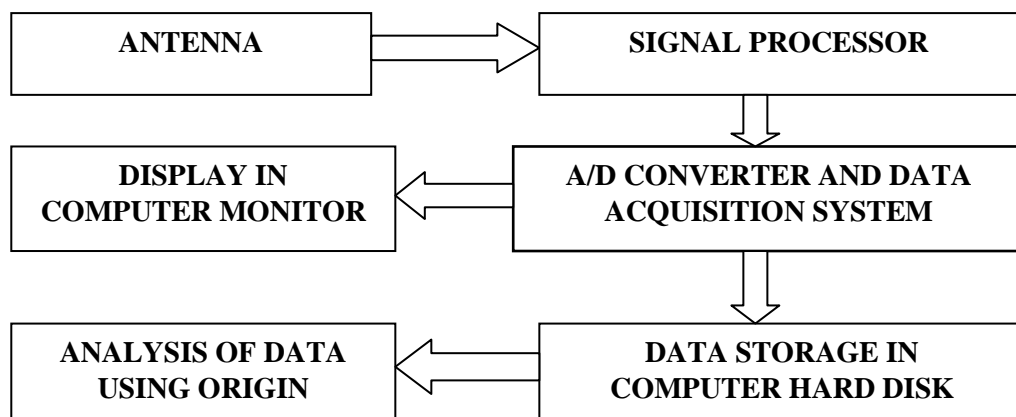


Fig. 2.7: Block diagram of the ELF / VLF receiver.

2.2.5 Measurement of Schumann Resonance (SR) parameters

We developed a calibrated wide-band ELF measurement technique at the Institute of Radio Physics and Electronics, University of Calcutta, India. Observations of signals on SR spectra have been made during the period 1997 to 2003 regularly and after 2004 as and when required. The records were taken from different noise free regions as far as

practicable. Parameters of SR which are of significance are: (i) SR frequency. (ii) amplitude of electric field component. (iii) amplitude of magnetic field components.

A square-loop antenna is used to measure the SR frequency. The vertical electric field is determined by using a ball antenna. The magnetic field components are recorded in by induction coil magnetometer.

2.2.5.1 Square-loop Antennas

In a Square-loop antenna there are two square loops. one square loop has 1 m side with a total of 75 turns and the other square loop with 90 turns has 1.3 m side. The antenna system for the experiment has been erected on the ground at a vast bare land of Salt Lake area, Kolkata. Square-loop antennas are made for the detection of ELF signals. Two such loops have been mounted on wooden structures connected in series and their effective gain is increased beyond 5 dB with this arrangement.

A co-axial cable of length 50 m is used to transfer the signal from the antenna to the input of the receiver where it is pre-amplified. A stereo-preamplifier-integrated circuit with LA3161 chip is chosen whose low frequency response starts below 5 Hz and extends to a few kHz. It is superior to others to handle the input voltage in the range of few microvolts to millivolts. The frequency selective stages are designed with active circuit elements. A wide-band amplifier whose output is taken through an active low-pass filter having cut-off frequency nearly 35 Hz further amplifies it. This signal information is now stored in a computer by the data acquisition process in which a 40 Hz generator is used to convert the analog signal into digital signal. A wide-band, very low input voltage-sensitive and low frequency sensitive receiver, has been designed which can detect input signal from 100 μ V to 500 μ V.

2.2.5.2 Ball Antenna

The vertical electric field of SR has been regularly measured by using a ball-antenna at the field of observations. The ball-antenna made of stainless steel having 30 cm in diameter is set-up at a height of 7 m above the ground. The block diagram of the receiver is shown in Fig. 2.8. The southern side of this centre is the sandy land rising out of the bed of the river above the water level. The East- West and Northern regions are spread out mostly with paddy-fields, wheat and vegetable fields. The ELF to VLF electric fields are measured regularly with this ball-antenna. The wide band wave-forms in general are largely free from the influence of non-essential sferics. The ball-antenna has the frequency response from 1 Hz to 12.5 kHz. Signals received by the antennas are introduced directly to a computer through an AD converter (44 kHz). A co-axial cable of length 70 m is used to transfer the signal from the antenna to the input of the receiver where it is pre-amplified. The r.m.s. values of the filtered data are analyzed regularly using graphing software (Origin).

The East-West and Northern regions are spread out mostly with rice, wheat and vegetable fields. The ELF to VLF electric fields are measured regularly for about three hours within 04:00 – 09:00 hrs UT, during the tranquil period in the global lightning activity. During the time, the wide band wave-forms in general are largely free from the influence of non-essential sferics. The ball antenna has the frequency response from 1 Hz to 12.5 kHz. Quite a good number of Q-bursts have been obtained with transient pulse oscillations lasting more than 0.2 second are selected for analyses. Signals which are received by the antennas are introduced directly to a computer through an AD converter (44 kHz).



Fig. 2.8: Ball antenna

2.2.5.3 Induction Coil Magnetometer

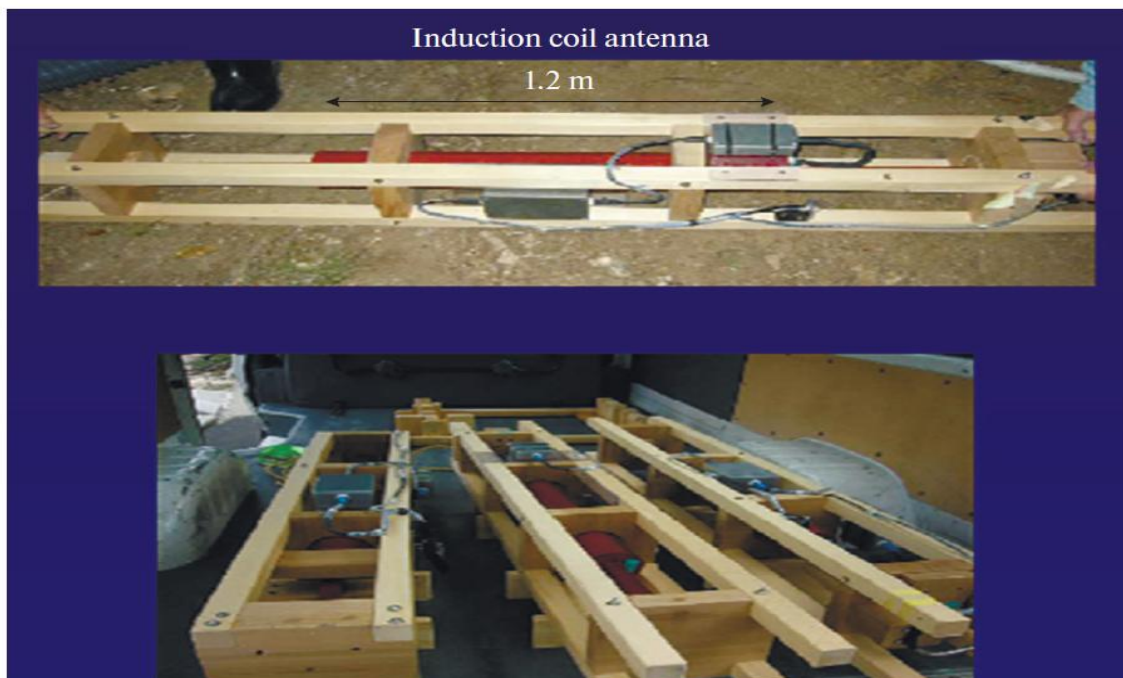


Fig. 2.9: A typical induction coil magnetometer.

2.3 References

- [2.1] Book Review: Research in Electric power - B. J. Chalmers 1967
- [2.2] Rycroft M. J., Israelsson S., Price C., *J Atmos Sol-Terr Phys.*, **62(17-18)**, (2000) 1563.
- [2.3] Harrison R.G., Aplin K.L., *Atmospheric Environment*, **36(25)**, (2002), 4037.
- [2.4] Harrison R.G., Carslaw K.S., *Review of Geophysics*, **41(3)**, 2003.
- [2.5] Harrison R.G., *Long-term measurement of the global atmospheric circuit at Eskdalemuir, Scotland, 1911-1981*, **70** (1), (2004), 1-19.
- [2.6] Tonev P. T., Velinov P. I. Y., *J Atmos Terr Phys.*, **58**, (1996), 1117.
- [2.7] Fullekrug M., & Sukhorukov A. I., *Geophys Res Lett.*, **26**, (1999), 1109.
- [2.8] Sorokin V. M., Yashchenko A. K., *Geomagnetism and Aeronomy*, **30**, (1990), 358.
- [2.9] Fullekrug M., Fraser-Smith A. C., Reising S. S., *Geophys Res Lett.*, **25** (1998) 3497.
- [2.10] Fukunishi H, Takahashi Y, Sato M, Shono A, Fujito M & Watanabe Y, *Geophys Res Lett.*, **24**, (1997), 2973.
- [2.11] Shalimov S. L., Bösinger T., *J Atmos Sol-Terr Phys.*, **68**, (2006), 814.
- [2.12] Sorokin, V. M., Yashchenko, A. K., *Geomagnetism and Aeronomy*, **30**, (1990), 358.
- [2.13] Shalimov, S. L., Bösinger, T., *J. Atmos. Sol.-Terr. Phys.*, **68**, (2006), 814,
- [2.14] Kolarz P., Milijkovic B., Curguz Z., Air-ion counter and mobility spectrometer, Nuclear Instruments and Methods in Physics Research Section B: Beam Interactions with Materials and Atmos., **279**, (2012), 219.
- [2.15] Vojtek T., Steinbauer M., Fiala P., Bartusek K., Gerdien condenser measuring and numerical modeling of air ion fields, *International Conference on Applied Electronics*, (2006), 225-228.

CHAPTER 3

A Study on the Seasonal Variation of Atmospheric Vertical Potential Gradient (PG) at a Tropical Station in Kolkata

3.1 Introduction

Among different sources of electromotive force driving the global electric circuit, thunderstorms are considered to be the most powerful ones. Dynamo-interaction between the solar wind and the magnetosphere, and the dynamo effects of atmospheric tides in the thermosphere are considered as sources not as powerful as the thunderstorm generated by the creation of electric field driving the global circuit at the lower atmosphere. Further, the Earth–ionosphere potential difference directs the air–earth current downward from the lower region of the ionosphere to the ground surface which varies in accordance with the ionospheric potential and columnar resistance.

Thunderclouds in the troposphere updraft the charges producing current into the ionosphere and magnetosphere that maintains an electric potential difference of nearly 250 kV between the Earth and the ionosphere which produces vertical electric potential gradient (PG) on the surface of the Earth. At the ground, this is maintained by the negative quasi-steady charge on the Earth and by the ‘electrode effect’. The ‘electrode effect’ is defined as the accumulation of an excess of ions of positive sign in the neighborhood of a negative electrode, and vice versa, when ions are continuously produced in the space above the electrode and move under the influence of the electrode’s field. Positive charge is buildup in the air near the surface of the Earth and this is because of the flow of positive charge from the ionosphere to negatively charged Earth [3.1]. Negative charges do not flow from the Earth because of the want of any mechanism except the process of radioactive phenomena that yield the emanation from

the Lithospheric origin. Vertical electric field of about $100\text{--}120\text{ Vm}^{-1}$ is found at the ground surface of the Earth.

Major thunderstorm activities of the globe and local environmental factors maintain electric PG at any point on the Earth's surface. Various models for thundercloud electric field have been presented to investigate their behaviour in the region between the surface of the Earth and the lowest layer of the ionosphere [3.2–3.6]. It is worth-mentioning that pollutant particles due to smoke from various combustion processes of domestic and industrial origin, reaction of natural and anthropogenic gaseous species, and windblown dust can reduce the conductivity giving higher value of PG [3.7–3.9]. Aerosol particles, which are smaller than $5\text{ }\mu\text{m}$ in diameter, tend to form stable suspension in air [3.10]. The nuclei present (pollutant particles: artificial or natural) combine with the ions and decrease the concentration or immobilize the small ions, thereby reducing the conductivity. The impact of fossil fuels (CO_2 emission) within the pollutants is also responsible for higher trend in the value of electric field than the fair-weather value. There are changes in ionization rate, recombination and attachment rate, and also different meteorological conditions, which affect the variation of electrical conductivity. As a result, atmospheric electric field and air–earth current are affected. The interdependence of these parameters is important. Meteor showers, solar flares, sudden meteorological disturbances like severe cyclonic storms can affect the parameters of global electric circuits through the variation in atmospheric conductivity [3.11].

The variations in the meteorological conditions can give rise to rapid changes in the value of PG during rain, showers, snow as well as fog. The changes in wind direction can also produce variations in PG [3.12]. Rain and rain-clouds are often highly charged. As a result, the value of PG may increase. The absolute value of PG

and its variation are largest during the thunderstorms. Moreover, surface PG should also depend on change of pressure, temperature and formation of dense fog which governs the conductivity of the medium. Thus, the meteorological effects play some role in the enhancement of PG [3.13–3.15]. Hence, seasonal variations are to be taken into consideration. In many observations, the diurnal variation of PG matches closely with the Carnegie curve, which is the generally accepted global unitary variation of PG on Earth with a maximum around 19:00 UT (Universal Time) and a minimum around 04:00 UT [3.16–3.18]. But, based on the observations of the atmospheric electric field in the Indian Ocean, Bay of Bengal and Arabian Sea, Kamra et al. [3.19] showed large changes in PG value, in which 40-day average field curve showed a maximum at 10:00 UT and a minimum at 00:00 UT with a small secondary peak at 19:00 UT. The observations at the Indian station Maitri at Antarctica (Lat: 70.75° S) are also in contrast to the unitary diurnal variation of Carnegie curve [3.20]. The diurnal and seasonal variations of ground surface electric field over Pune (Lat: 18.32°N) during fair-weather days of 1993 are measured and the influences of meteorological factors over the observed results have also been reported [3.21].

Some recent measurements of electric field for 69 fair weather days during local summer at the Indian station at Antarctica, Maitri, showed the maximum and minimum period of occurrence similar to the Carnegie curve although the field values are much higher than the Carnegie results [3.22]. Analysis of daily and seasonal variations at different locations on the globe is important as it will provide additional information for the study of the GEC.

This chapter deals with the results of measurement of the atmospheric vertical potential gradient (PG) in Kolkata (Lat: 22.56° N) on the ground surface for 90 fair weather days during 2006–2009. The variations of PG have been studied extensively to

investigate their values during monsoon (when the Sun is in Northern Solstice) and winter (when the Sun is in Southern Solstice) seasons. The results are compared with those reported by others at various stations. The observed records of point discharge current (PDC), conductivity and PG during the period from January 2006 to December, 2009 at Kolkata are analyzed. The measured values of PG at Kolkata are seemed to be higher and these values are compared with the results of Potsdam station (Lat: 52° N) and Johannesburg station (Lat: 26° S), with 9 years data and 2 years data respectively. The correlations studies are carried out among PG, PDC (Point Discharge Current) as well as negative and positive carrier conductivities. The corresponding correlation coefficients are obtained as 0.93, -0.842 and -0.844 .

3.2 Experimental arrangement

- (i) The vertical electric field has been measured on a continuous basis by using an ac field-mill.
- (ii) The continuous measurement of PDC has been made by using a steel wire having diameter 3 mm and length 8 cm, one end of which is tapered to a sharp edge. The tip of the sharp edge is about 0.02 mm. The other end is soldered to a co-axial cable.
- (iii) The conductivity is measured near ground through a Gerdien condenser.

The details about the apparatus are discussed in section 2.2.

3.3 Observations and Interpretations

The PG shows a diurnal variation with maxima and minima. Values are found to be higher than the usual trend of fair-weather results. Fig. 3.1 depicts diurnal variations averaged over 90 fair-weather days available during the period from January 2006 to February 2009. Standard deviations are shown by error bars. The measured diurnal

variation in PG was obtained by 15 min average. Maximum PG exhibits 193 Vm^{-1} that occurred at about 04:00 UT (09:30 Local time (LT), late morning period). It is followed by a secondary maximum between 08:00 and 08:30 UT. It then decreased showing a minimum at around 10:30–11:00 UT (16:00 LT) which is before the local afternoon period. Another secondary maximum occurred at about 16:00 UT. The potential level started to decrease gradually and exhibited lowest value at around 00:00 UT (05:30 LT), about half an hour before sunrise. It then rises to a maximum value with a repetition at around 04:00 UT following the new cycle. So the fair day features consist of one principal maximum and two secondary maxima.

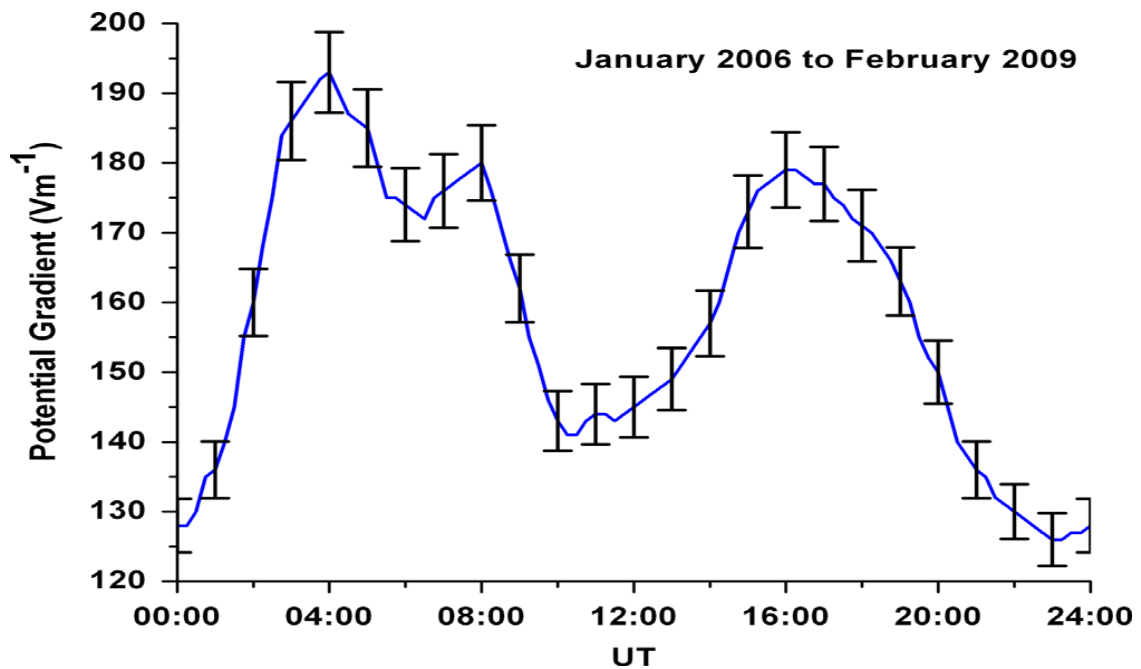


Fig. 3.1: Hourly average diurnal variation of Potential Gradient (PG) of 90 fair weather days at Kolkata during January 2006–February 2009. Error bars represent standard deviation.

Our observation shows a marked variation from Carnegie's oceanic field curve, which is the generally accepted global unitary variation of electric field on Earth. Maxima and minima in Carnegie curve differ from the present results of 90 days

average field curve. The overall average, irrespective of seasons, shows a primary maximum at about 04:00 UT (09:30 LT) and one secondary maximum at about 16:00 UT (21:30 LT) instead of a single maximum at 18:00–19:00 UT of Cranegie curve. Similar deviations have been reported by Kamra et al. [3.19] and Deshpande & Kamra [3.20]. Sunrise and its prolonged effects are responsible for the primary maximum at about 04:00 UT (09:30 LT). Sunrise effect is explained by a two layer electrode model [3.1,3.23]. By sunrise, the upliftment of dense electrode layer due to convective mixing above the sensing height of 2 m increases the value of PG [3.24]. Near Earth surface conductivity, seasonal variation of ionospheric potential and distance from active thunderstorm areas may also influence the vertical PG [3.25]. The commonly accepted thunderstorm occurrence frequency curve of Whipple and Scarce [3.26] with the maximum at around 19:00 UT and minimum around 04:00 UT is the average of three major continental thunderstorm activity centers viz., Asia–Australia, Africa–Europe and America [3.27]. Moreover, each continental average was taken over 81 years span.

Our results also indicate a tendency to manifest the thunderstorm activity over the Asia–Australia region which becomes maximum at 08:00 UT. It is worthwhile to mention that the measurements at the Asiatic tropical zones exhibit the resemblance of peak thunderstorm activity at 08:00 UT of Asia–Australia region. Thus, in a tropical region, continental thunderstorm activity plays an important role in modulating the global electric circuit. Observations of global lightning distribution during January 1998–February 2009 taken from LIS (Lightning Imaging Sensor), NASA, confirm that the thunderstorm activity in the Himalayan region is more prominent than in the Asia–Australia region [3.28].

The Asia–Australia has long been thought of as one of the largest thunderstorm producing regions, but recent records confirm that the thunderstorm from the Himalayan region is also strong enough to be one of the distinguished lightning centres all over the world. So the peak at 04:00 UT is higher than that at 08:00 UT. After morning period, solar heating near the surface of the Earth initiates convective instability which returns the PG value to its typical fair-weather value (minimum around 10:00–12:00 UT). But the secondary maxima around 16:00 UT (21:30 LT) is neither due to GEC nor sunrise effect. It may be due to regional thunderstorm activity mainly in the Himalayan region.

Fig. 3.2 shows the comparative study of vertical electric potential gradient of the atmosphere over Kolkata for the period June 2008 to January 2009 (blue coloured curve) along with the results of earlier data recorded at this centre for the same period of duration, June 2005 to January 2006 (black coloured curve). Standard deviations from the mean are represented by corresponding error bars. The two periods of study are separated by a gap of 3 years. The figure 3.2 depicts that the nature of diurnal variation remains almost the same for the two periods. But with the progress in time, the PG shows a tendency to decrease on an average. The decrease of both kinds of ions at the ground level is one of the significant reasons for the higher value of PG at Kolkata.

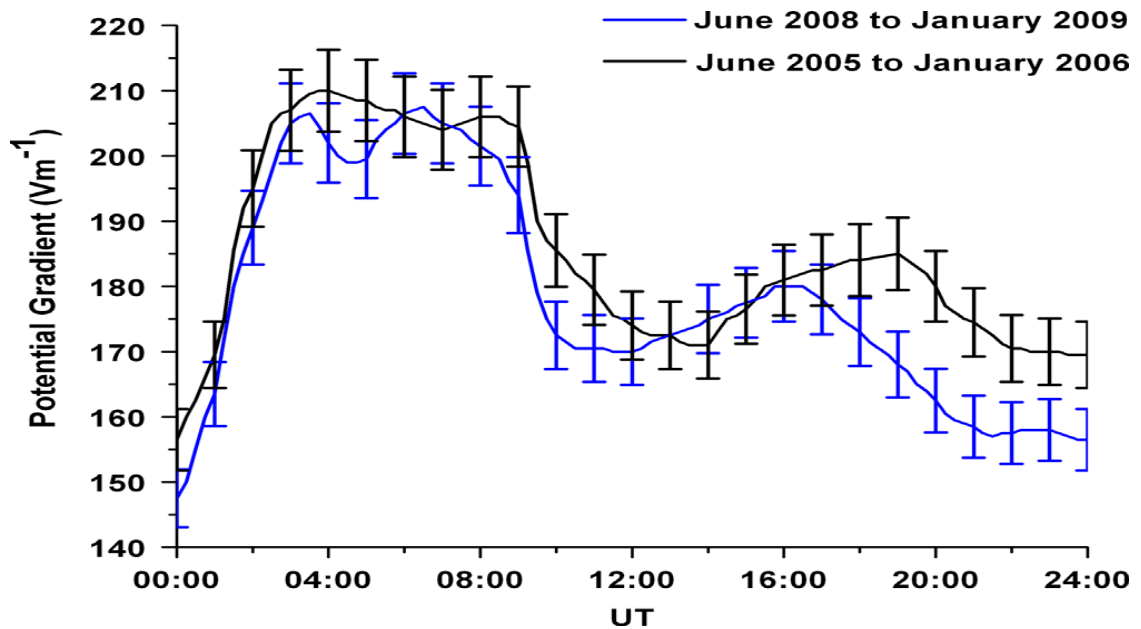


Fig. 3.2: Vertical electric Potential Gradient (PG) of the atmosphere at Kolkata for the period June 2008-January 2009 is shown by blue coloured curve, while the black coloured curve depicts the results for the period from June 2005-January 2006. Corresponding standard deviations are shown by error bars.

The atmospheric turbulence forces the positive space charges to higher altitudes against the forces of the existing electric field. It can be taken as the generator effect of the turbulence which influences the atmospheric electric field locally. The decrease of ions in the process of transportation lowers the conductivity. Kolkata is a densely populated city surrounded by small and large scale industries. Air is greatly invaded by pollutant particles emitted from various industries. Fine particles having a diameter less than $1 \mu\text{m}$ (Aitken nuclei) are distributed in air. They can capture both kinds of ions. Since ions are attached to pollutant particles of comparatively large mass, the mobility of the ions decreases [3.29,3.30]. So near the Earth surface, conductivity is low. The magnitude of relative abundance of different aerosol particles as well as the presence of Aitken nuclei distributed in air at this tropical station is lower than its value during the

period 5–6 years earlier [3.31]. The existence of their variation introduces a change in the value of vertical PG in the atmosphere. The variation of energy consumption of traffic in Kolkata would contribute to a high Aitken count resulting in changes in atmospheric dispersion that also reduce the conductivity of the medium.

During the period June 2008–January 2009 in comparison to the period of June 2005–January 2006 many industries surrounding Kolkata have been shifted to the suburban areas and some were abandoned. The reduction in the variation of energy consumption of traffic (oil and gasoline) and fossil fuels (CO₂ emission) during the later period of study increases the conductivity of the medium near the surface of the Earth. Hence the value of PG shows a tendency to decrease on an average.

In order to explore the seasonal effect of diurnal variations of PG, the whole year is divided into four seasons, viz., winter (December, January and February), pre-monsoon (March, April and May), monsoon (June, July and August) and post-monsoon (September, October and November). Fig. 3.3 shows the diurnal variations of PG at different seasons averaged over the period from January 2006 to February 2009 along with their standard deviations plotted as error bars. During all the seasons, the first maximum which is very much prominent occurred at around 03:30–04:00 UT (local late morning hour). During winter and pre-monsoon, the first secondary maximum obtained around 08:00–09:00 UT is comparable to the principal maximum. The second secondary maximum occurred at 13:30 UT, 19:00 UT, 14:30 UT and 16:00 UT respectively during winter, pre-monsoon, monsoon and post-monsoon seasons.

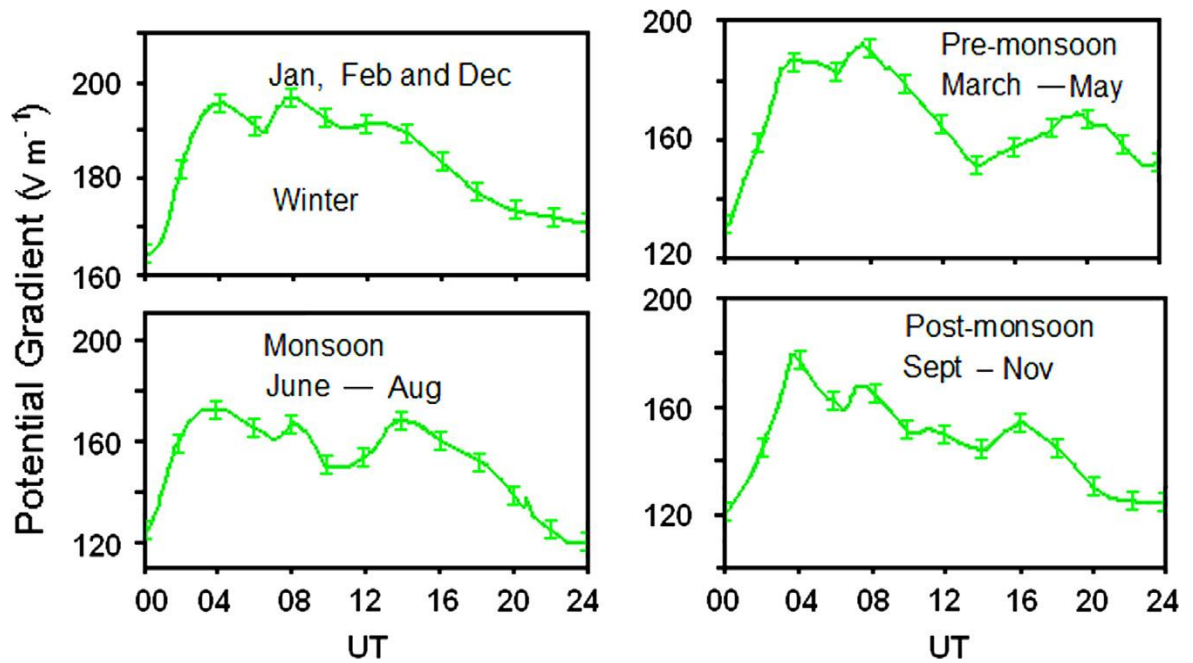


Fig. 3.3: Diurnal variations of Potential Gradient (PG) at different seasons during January 2006–February 2009.

The values at the principal peak of PG in winter, pre-monsoon, monsoon and post monsoon are 195, 190, 170 and 180 V m^{-1} , respectively. It is evident that the primary maximum PG value during monsoon is 170 V m^{-1} which is a comparatively low value during the year. It is due to the fact that during the monsoon season aerosol concentration in the near Earth surface is reduced. Also, the patterns in Fig. 3.3 indicate that the sunrise effect affects all the seasons almost similarly. Although, in Kolkata, which is a site of observation in the tropical region of Northern hemisphere, significant variations in local sunrise time occur during different seasons, no shift in principal maxima of PG value is found. One such shift in the morning peak about 45 min was reported from Suva, Fiji station in Southern hemisphere during Wet and Dry seasonal measurement [3.32].

The mean value of vertical electric potential gradient versus the number of fair-weather days observed during the period of study (2006–2009) is plotted in Fig.3.4. The potential gradient is high around 152 Vm^{-1} which is also the mean value at Kolkata.

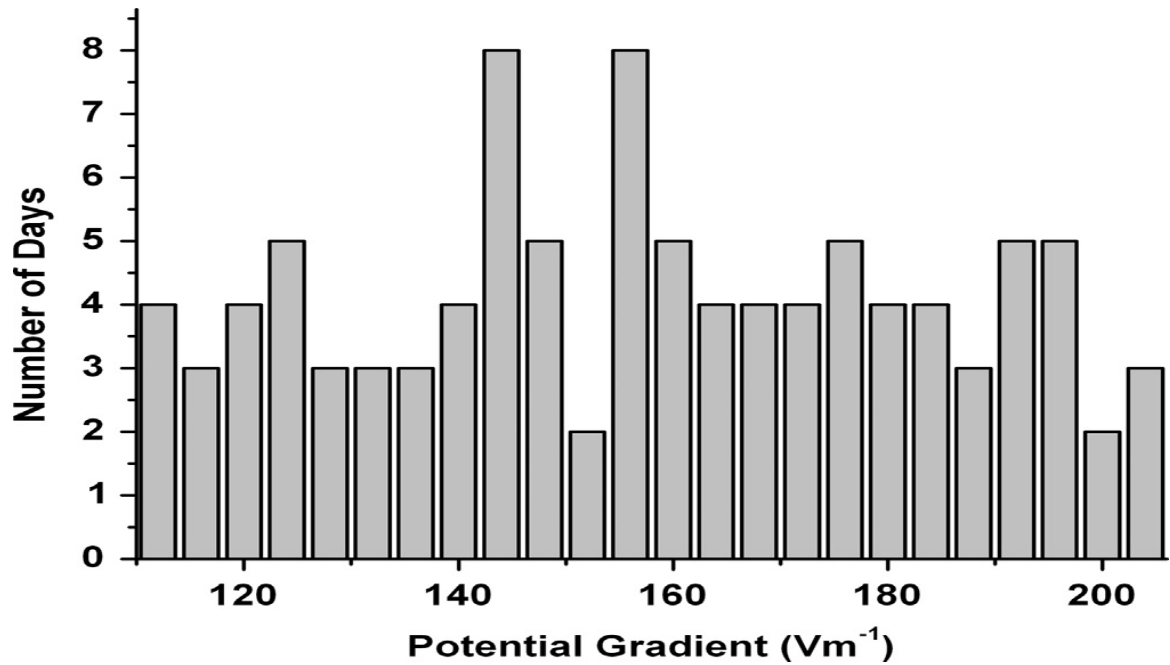


Fig. 3.4: Mean value of vertical electric Potential Gradient (PG) against the number of days observed during 2006–2009.

The hourly variations of PDC and PG at Kolkata averaged over monsoon season and winter are shown in Fig. 3.5 separately for the years 2006, 2007, 2008 and 2009.

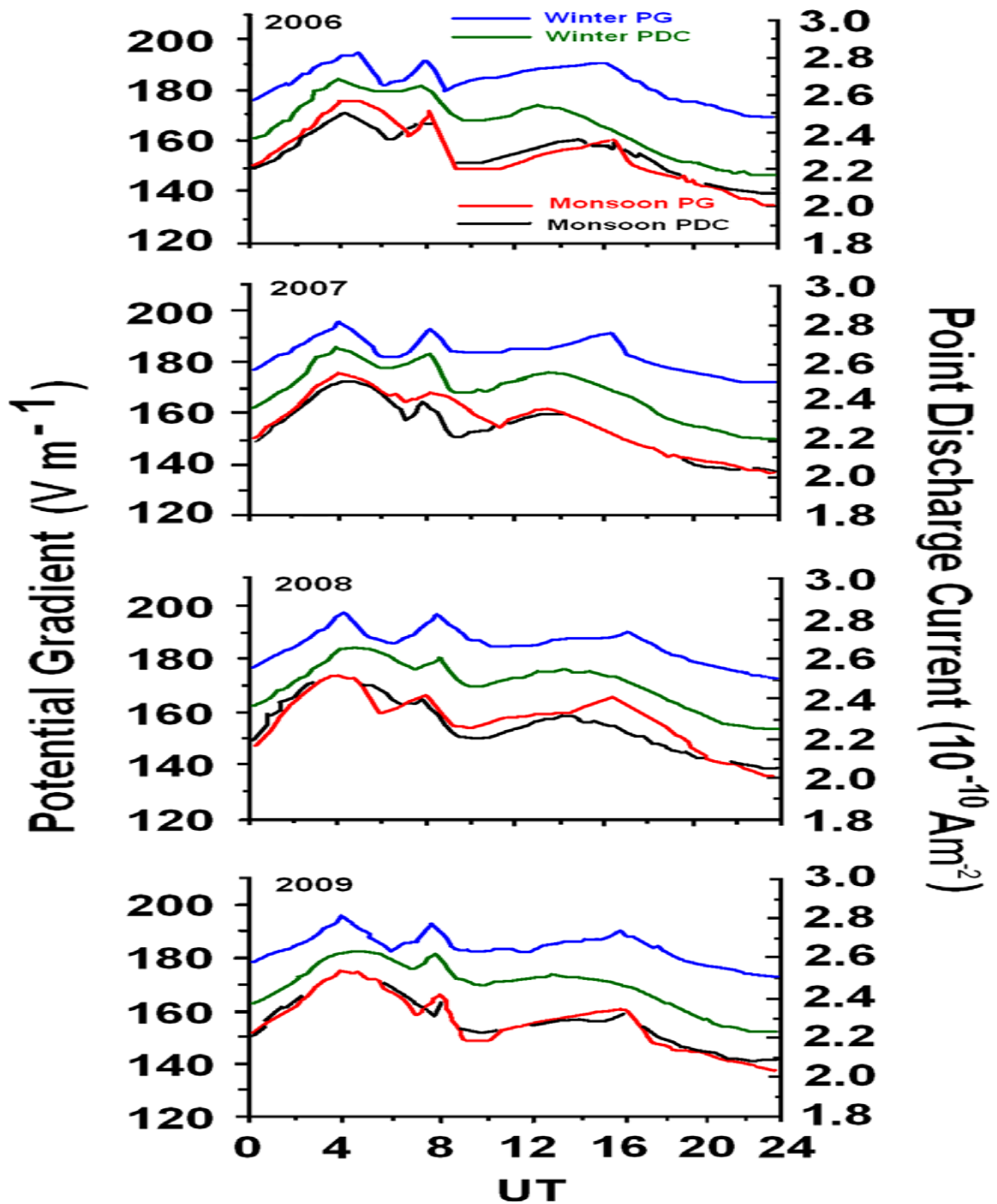


Fig. 3.5: Diurnal variation of Point Discharge Current (PDC) and Potential Gradient (PG) at Kolkata during monsoon and winter of 2006, 2007, 2008 and 2009.

The PG and PDC show the same trend in their diurnal variations. During monsoon, minimum and maximum values of PDC are $2.0 \times 10^{-10} \text{ Am}^{-2}$ and $2.55 \times 10^{-10} \text{ Am}^{-2}$ respectively. During winter, the PDC varies between a minimum value of

$2.2 \times 10^{-10} \text{ Am}^{-2}$ and a maximum value of $2.62 \times 10^{-10} \text{ Am}^{-2}$. The minimum value is obtained at 24:00 UT (half an hour before the sunrise) and maximum value is obtained around 04:00 UT (local late morning hour). The PG is observed to vary from 130 Vm^{-1} to 170 Vm^{-1} during monsoon and from 170 Vm^{-1} to 195 Vm^{-1} in winter.

The correlation coefficient between PDC and PG is remarkably high as shown in Table 3.1. The measurements of PG and PDC in this work are two different ways of measuring the same strong electric field. So, high correlation is expected and data presented in Table 3.1 also support the phenomenon. But, the influence of wind speed always prevails in the process which forces the space charges away from the point of discharge, thereby serving to unshield those that increase the coronal current. This effect of the additional parameter enhancing the coronal current if taken into account, the said correlation should not maintain one-to-one correspondence as stated by E. R. Williams [3.33].

Table 3.1: Observed correlation coefficient between PDC and PG in monsoon and winter during the period 2006 to 2009.

Year	Monsoon	Winter
2006	0.79	0.84
2007	0.89	0.91
2008	0.87	0.88
2009	0.85	0.87

Typical annual variations of PG are shown in the upper panel of Fig. 3.6 and the negative carrier conductivity (NCC), positive carrier conductivity (PCC) and PDC averaged over the period from 2006 to 2009 are shown in the lower panel of Fig. 3.6. The average range of variation of PG over four years is between 160 Vm^{-1} and

190 Vm^{-1} . This is associated with the variation of PDC between $2.2 \times 10^{-10} \text{Am}^{-2}$ and $2.6 \times 10^{-10} \text{Am}^{-2}$. The corresponding variations in NCC and PCC are between $2.2 \times 10^{-14} \text{S m}^{-2}$ and $2.5 \times 10^{-14} \text{S m}^{-2}$.

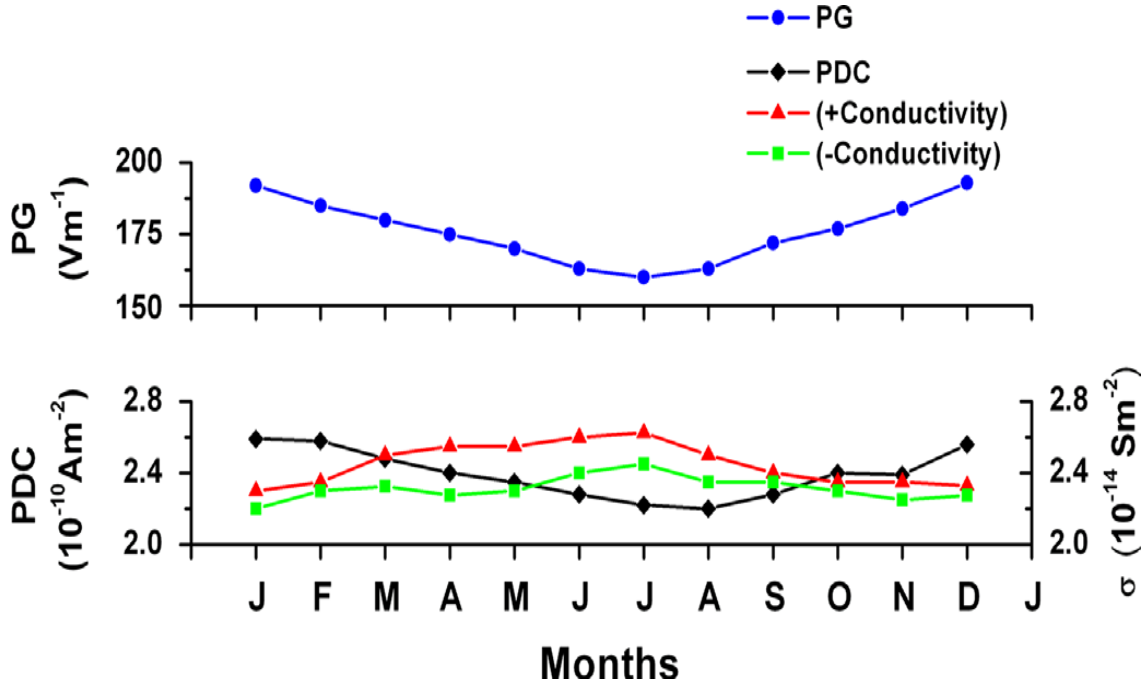


Fig. 3.6: Seasonal variations of Potential Gradient (upper panel) and negative, positive conductivities and Point Discharge Current (lower panel) at Kolkata during January 2006–December 2009.

The correlation coefficient of PG with PDC, NCC and PCC are respectively 0.93, -0.842 and -0.844 . These are obtained through the analysis presented in Fig. 3.7.

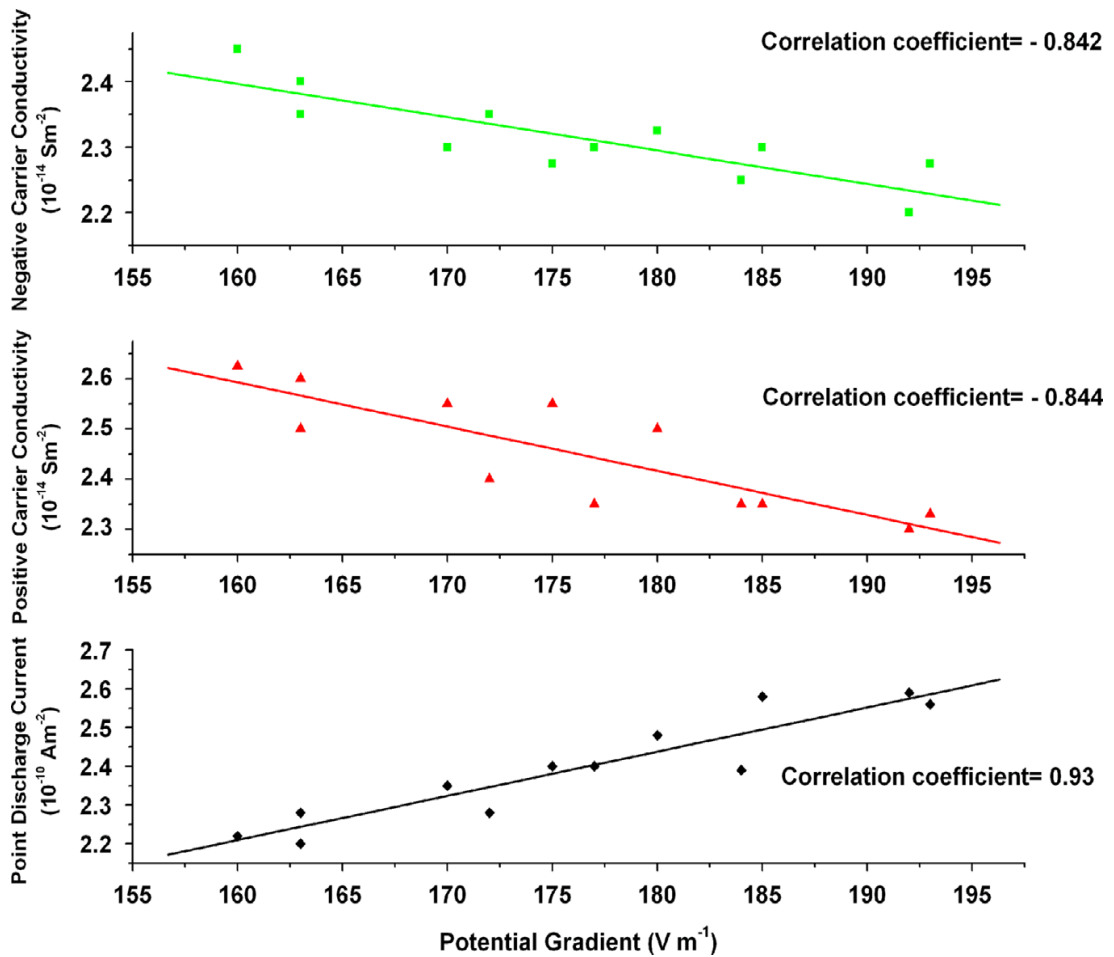


Fig. 3.7: Correlations of Negative Carrier Conductivity (NCC), Positive Carrier Conductivity (PCC) and Point Discharge Current (PDC) with Potential Gradient (PG) at Kolkata during January 2006–December 2009.

Fig. 3.8 shows the seasonal variation in PG at Kolkata, Potsdam (Northern hemisphere) and Johannesburg (Southern hemisphere) stations. The monthly variation of PG at Kolkata (Lat: 22.56° N) is almost the same as observed at Potsdam (Lat: 52° N). It reveals that the electric PGs at these two stations yield the maximum value during winter and minimum value during the monsoon months. But at the Johannesburg station (Lat: 26° S), the picture is just the reverse. It exhibits a maximum during monsoon while a minimum is found to occur during winter [3.34]. This is due to the effects of opposite seasonal changes in insolation and convection in the two hemispheres [3.35].

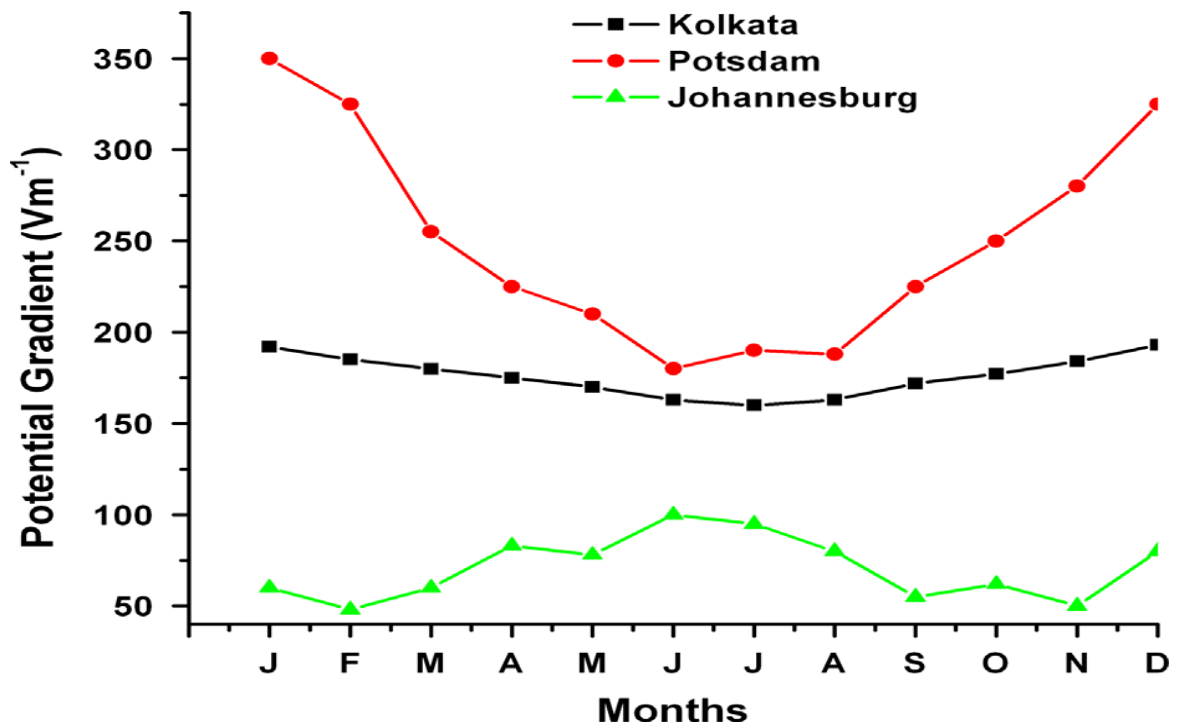


Fig. 3.8: The monthly variation of PG at Kolkata, Potsdam and Johannesburg.

3.4 Conclusions

From the analyses of the experimental data various conclusions can be drawn. The diurnal curve of PG shows a marked deviation from Carnegie curve. The PG measured at Kolkata is higher than the values observed over the ocean and it is due to the local meteorological parameters. With the progress in time, PG showed a tendency to decrease on an average. It may be due to reduction of pollution in Kolkata during the tenure of measurements. Seasonal variation shows that the monsoon level is lower than the winter level because of a lower amount of aerosol content in air. PG exhibits good correlations with PDC both in monsoon and winter. The monthly variations in PG observed in the stations of Northern hemisphere are identical, whereas, an opposite nature of variations is observed between the results of Northern and Southern hemispheres.

3.5 References

- [3.1] Marshall, T.C., Rust, W.D., Stalzenburg, M., Roeder, W.P., Krehbiel, P.R., *Journal of Geophysical Research*, **104**, (1999) 24455.
- [3.2] Wilson, C. T. R., *A* **221**, (1920) 73.
- [3.3] Park, C.G., Dejnakintra, M., *Journal of Geophysical Research* **78**, (1973) 6623.
- [3.4] Yeboah-Amankwah, D., *Journal of Atmospheric and Terrestrial Physics* **51**, (1989) 1035.
- [3.5] Kumar, R., Jagdish, R., Singh, V., *Journal of Atmospheric and Terrestrial Physics* **57**, (1995) 1247.
- [3.6] Tonev, P.T., Velinov, P.T.Y., *Journal of Atmospheric and Terrestrial Physics* **58**, (1996) 1117.
- [3.7] Prospero, J.M., Aerosol particles in Global Tropospheric Chemistry. *National Academy Press, Washington D C*, (1984).
- [3.8] Harrison, R.G., Aplin, K.L. *Atmospheric Environment* **36**, (2002) 4037.
- [3.9] Harrison, R.G., Aplin, K.L., *Atmospheric Environment*, **37**, (2003) 5319.
- [3.10] Malm, W.C., Sisler, J.F., Huffman, D., Eldred, R.A., Cahill, T.A., **99**, (1994) 1347.
- [3.11] Herman, J.R., Goldberg, R.A., *Journal of Atmospheric and Terrestrial Physics*, **40**, (1978) 121.
- [3.12] Bennett, A.J., Harrison, R.G., *Weather* **62**, (2007) 227.
- [3.13] Anbar, O.M.Y., 2006. Solar eclipse effects on the air layer near the surface over Makkah Region. Department of Meteorology, Environment and Arid Land Agriculture, King Abdulaziz University, Jeddah, Saudi Arabia.

- [3.14] Founda, D., Melas, D., Lykoudis, S., Lisaridis, I., Gerasopoulos, E., Kouvarakis, G., Petrakis, M., Zerefos, C., *Atmospheric Chemistry and Physics* **7**, (2007) 5543.
- [3.15] Kachakhidze, N., Kachakhidze, M., Kereselidze, Z., Ranishvili, G., *Natural Hazards and Earth System Sciences*, **9**, (2009) 1221.
- [3.16] Takagi, M., Kanada, M., *Pure and Applied Geophysics*, **100**, (1972) 44.
- [3.17] Kasemir, H.W., *Pure and Applied Geophysics*, **100**, (1972) 70.
- [3.18] Yeboah-Amankwah, D., *Journal of Atmospheric and Terrestrial Physics*, **51**, (1989) 1035.
- [3.19] Kamra, A.K., Deshpande, C.G., Gopalakrishnan, V., *Journal of Geophysical Research* **99**, (1994) 21043.
- [3.20] Deshpande, C.G., Kamra, A.K., *Journal of Geophysical Research* **106**, (2001) 14207.
- [3.21] Latha, R., *Earth, Planets and Space*, **55**, (2003) 677.
- [3.22] Panneerselvam, C., Selvaraj, C., Jeeva, K., Nair, K.U., Anilkumar, C.P., Gurubaran, S., *Journal of Earth System Sciences*, **116**, (2007) 179.
- [3.23] Hoppel, W.A., Anderson, R.V., Willett, J.C., *National Academic Press, Washington, D.C.* (1986) 149–165.
- [3.24] Kamra, A.K., *Journal of Geophysical Research*, **37**, (1982) 4257.
- [3.25] Takagi, M., On the regional effect of global electric field. In: Dolezalek, H., Rieter, R. (Eds.), *Electrical Processes in Atmosphere*, (1977) pp. 477.
- [3.26] Whipple, F.J.W., Scarce, F.J., 1936. *Geophys. Mem.* Vol. **68** (1986). Meteorological Office, Air Ministry, London, UK.
- [3.27] Orville, R.E., Henderson, R.W., 1986. *Monthly Weather Review* **114**, (1986) 2640.

- [3.28] <http://thunder.nsstc.nasa.gov>
- [3.29] Pawar, S.D., Kamra, A.K., *Atmospheric Research*, **54**, (2000) 105.
- [3.30] Tinsley, B.A., *Space Science Reviews* **09**, (2000) 1.
- [3.31] Raj, P.E., Devara, P.C.S., Maheshkumar, R.S., Pandithurai, G., Dani, K.K.,
Atmospheric Research **45**, (1997) 201.
- [3.32] Kumar, V.V., Ramachandran, V., Buadromo, V., Prakash, J., *Earth, Planets
and Space*, **61**, (2009) 747.
- [3.33] Williams, E.R., 2013. (personal communication).
- [3.34] Alderman, E.J., Williams, E.R., *Journal of Geophysical Research*, **101**, (1996)
29679.
- [3.35] Williams, E.R., *Atmospheric Research*, **91**, (2009) 140.

CHAPTER 4

Measurement of Schumann Resonance Spectra over Kolkata and Some Its Recent Observed Characteristics

4.1 Introduction

Discrete spectra of frequencies at 8, 14, 20, 26, ... Hz generated by electromagnetic emission from lightning sources can be regarded as excitation of AC global circuit. These electromagnetic emissions originating within the Earth-ionosphere waveguide occur in the ULF, ELF and VLF frequency ranges. These include Schuman Resonances (SR), ELF-VLF sferics, sprites etc. During 1990s and later, the scenario with these sub-ionospheric ELF SR waves changed and several new aspects emerged. The SR power varies with respect to the receiver position and the lightning centers, commonly referred as source-observer distance. Both electric and magnetic components of SR intensity vary with the spatial shifts of the thunderstorm regions under El-Niño and La-Niña conditions. The magnitude of the lightning in the lower atmospheric region varies with time of the day. The electromagnetic waves thus generated at SR frequencies resonate due to multiple reflections in the Earth-ionosphere cavity. The total signal may be dependent on the waves from the different lightning sources. In this context, different groups of researchers throughout the globe are investigating and published many interesting results. In this work, few results of different observatories are discussed. Also, an attempt was made to detect experimentally the discrete signals at Kolkata (Lat. 22.56° N, Long. 88.5° E) from the year 1999. Some frequency changes in the peak values are observed in the recorded data which may be attributed to

uncertainty arising from spatial distribution of lightning sources exciting the Schuman Resonance modes. Some of those results are presented in this chapter.

SR is global electromagnetic phenomenon occurring in the spherical waveguide between the Earth's surface and the lower boundary of the ionosphere. The Earth-ionosphere waveguide acts as a resonator. In the presence of fair-weather electric field between the ionosphere and the Earth's surface, electric discharges take place in the atmosphere, through (i) thunderstorms, (ii) dynamo interactions between solar wind and magnetosphere and (iii) dynamo effect of the tides in the thermosphere introducing electromotive force in the ionosphere. Thunderstorms are considered to be the most powerful of these sources. Resonance phenomena within the cavity are due to the interaction of direct and reflected (round the world) waves arriving at an observer.

The waves generated by lightning discharges, suffer multiple reflections within the waveguide to form standing electromagnetic waves. When the wavelength of these standing waves is of the order of the resonator, then the Schumann Resonance occurs. Radio waves of a few Hz frequencies travelling along the surface of the ground are able to circle the globe and return back by ionosphere to the starting point. The global resonance occurs when the phase delay due to propagation is proportional to 2π .

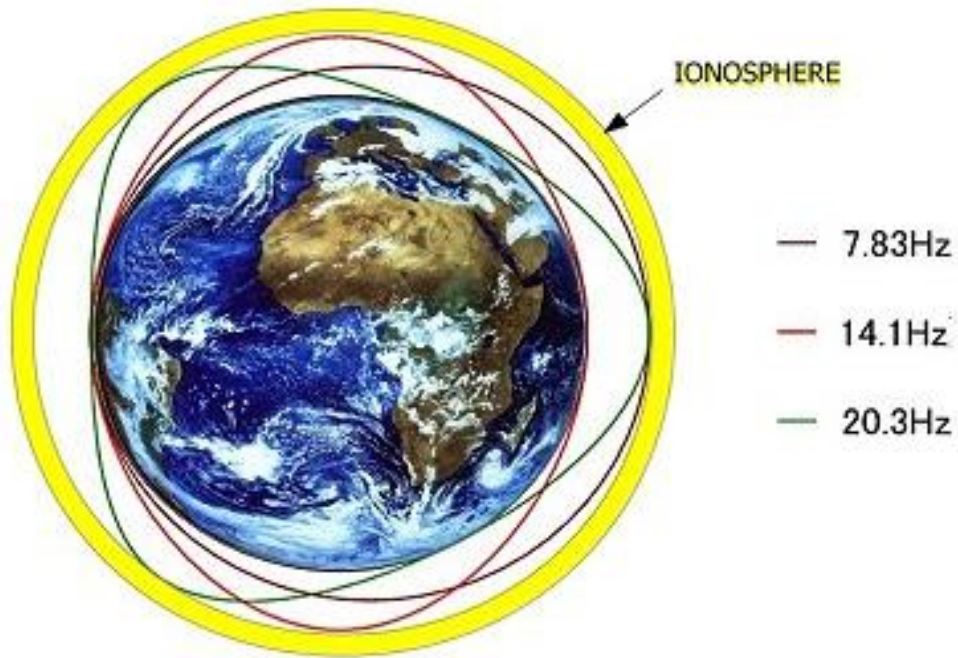


Fig. 4.1: Fundamental and higher order modes of Schumann Resonance.

Here, Fundamental mode or first order mode suffers one reflection, second order mode suffers two reflections and third order mode suffers three reflections from ionosphere.

Winfried Otto Schumann (1952) first predicted about the existence of such resonance and theoretically derived that the eigen frequency of the n-th SR mode ' f_n ' is determined by the formula:

$$f_n = \frac{c}{2\pi a} \sqrt{n(n+1)}$$

Where, a = radius of earth, c = velocity of light in free space.

He calculated the Eigen frequencies as 10.6, 18.4 ...Hz etc.

4.2 Measurement of SR parameters

Parameters of SR are: (i) SR frequency, (ii) Amplitude of vertical component of Electric field and (iii) Amplitudes of two horizontal components of Magnetic field.

The SR frequency is measured by a square-loop antenna. The vertical electric field is determined by using a ball antenna. Two horizontal magnetic field components were recorded in Kolkata by Induction coil magnetometer. The details are discussed in chapter 2 (section 2.2.5).

4.3 Experimental evidences of SR

Balser and Wagner in 1960 first observed experimentally and obtained the SR frequencies as 8, 14, 20, 26...Hz etc [4.1]. Gradually more realistic and analytical models were developed by many workers which confirmed independently the experimental value as Balser and Wagner [4.2-4.9]. In 2002, amplitude spectrum of SR with various peaks (modes) measured by Nickolaenko and Hayakawa [4.2] are shown in Fig. 4.2.

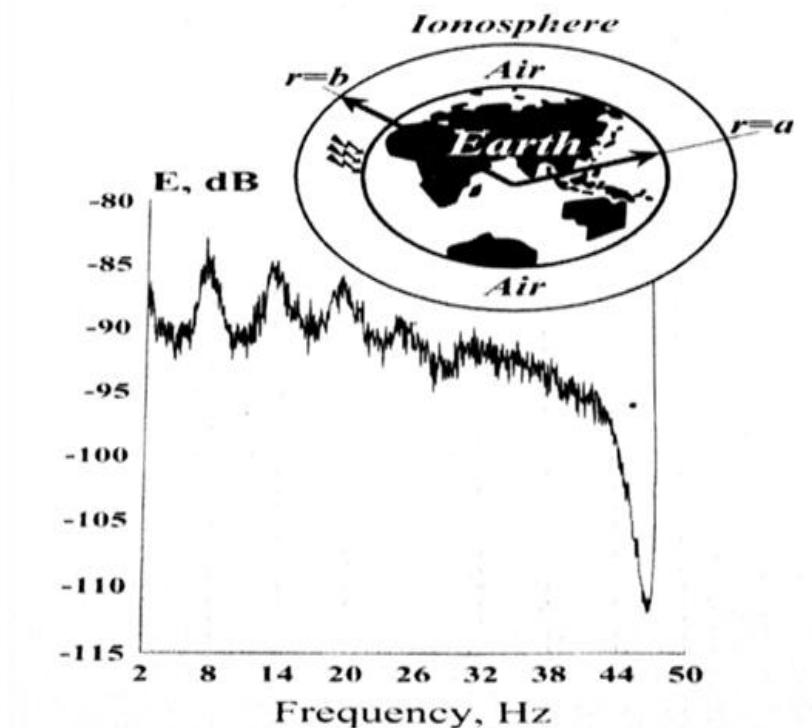


Fig. 4.2: Schumann resonance spectra 8, 14, 20, 26, ... Hz etc. along with Earth-ionosphere cavity is displayed here. This is formed by the dielectric layer of air bounded by spherical conducting surfaces of the Earth and the lower ionosphere with radii $r = a$ and $r = b$ respectively.

The reasons behind the difference between theoretical and experimental value of SR frequencies are: (a) the inhomogeneities and asymmetry of the ionosphere in day and night time, (b) variations of conductivity of the ionosphere, (c) variation of the spatial distribution of sources of lightning and (d) influence of pollutant particles etc. These were not considered by Schumann in his theory. Parameters of SR amplitude, frequency and Q factor contain information on the world thunderstorm activities as these are the main sources of natural electromagnetic noise in that range 4-40 Hz.

Distribution pattern of global thunderstorm activity is complicated and varies both diurnally and annually, which include: (i) variations in the location of thunderstorm sources, (ii) their intensities, (iii) width and (iv) nature of the regions. All these factors affect the SR parameters, in particular, the intensities and peak frequencies of the electromagnetic field components. Variety of factors influencing the Schumann resonance impedes interpretation of the experimental data.

Different aspects of SR phenomena as well as their observation and measurement techniques have been published by number of workers in the field [4.1-4.7]. The outcome of continuous measurements of SR during August 1999 to March 2005 at the Lehta (Lat. 65° N, Long. 34° E), St. Petersburg by Yatsevich et al, [4.3] is shown in the figures 4.3(a) to 4.3(d). Average diurnal variations in the intensities and peak frequencies of the first three modes of the electric and magnetic field components in winter, spring, summer and autumn is depicted respectively in the following figures.

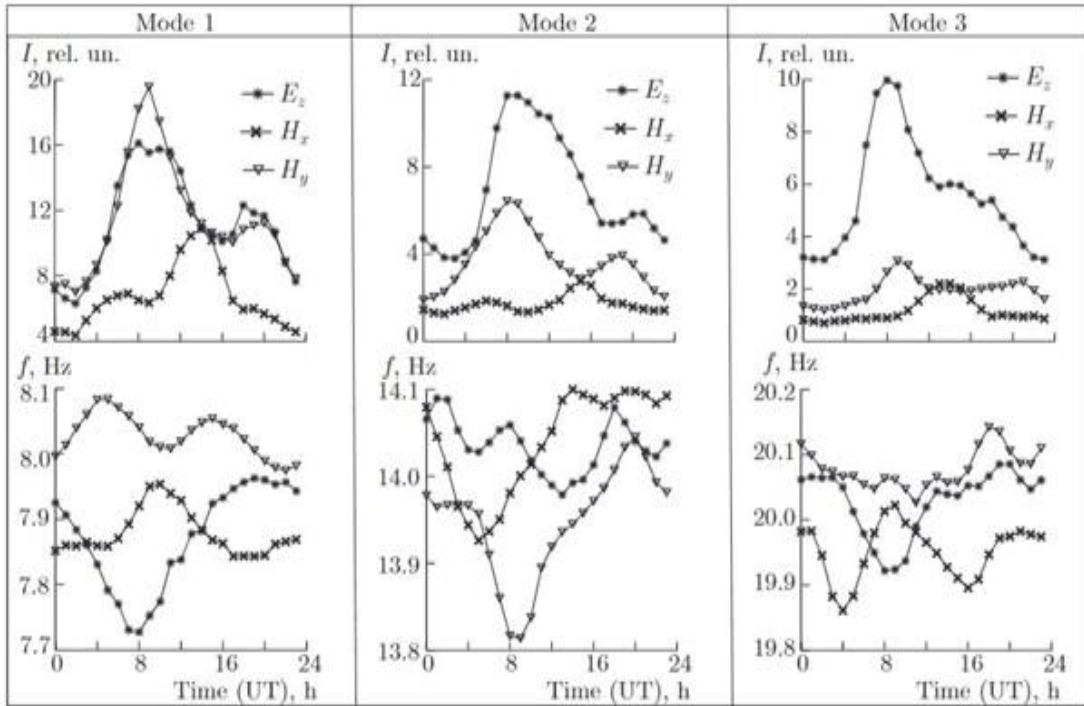


Fig. 4.3(a): Average diurnal variations in the intensities and peak frequencies of the first three modes of the electric and magnetic field components in winter

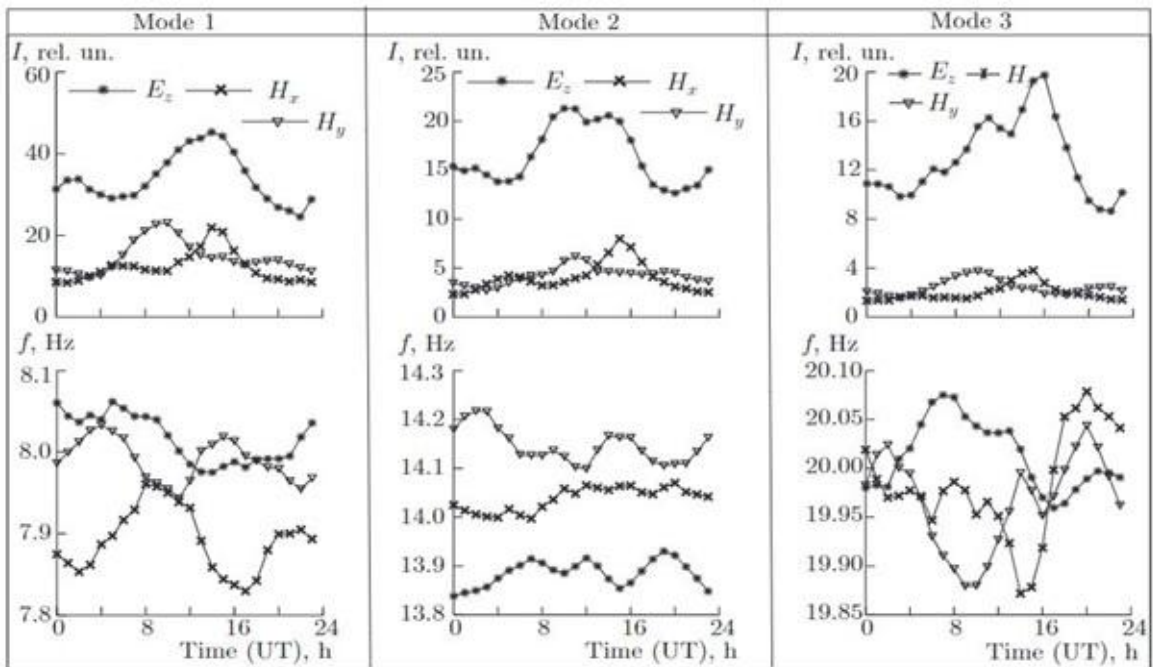


Fig. 4.3(b): Average diurnal variations in the intensities and peak frequencies of the first three modes of the electric and magnetic field components in spring.

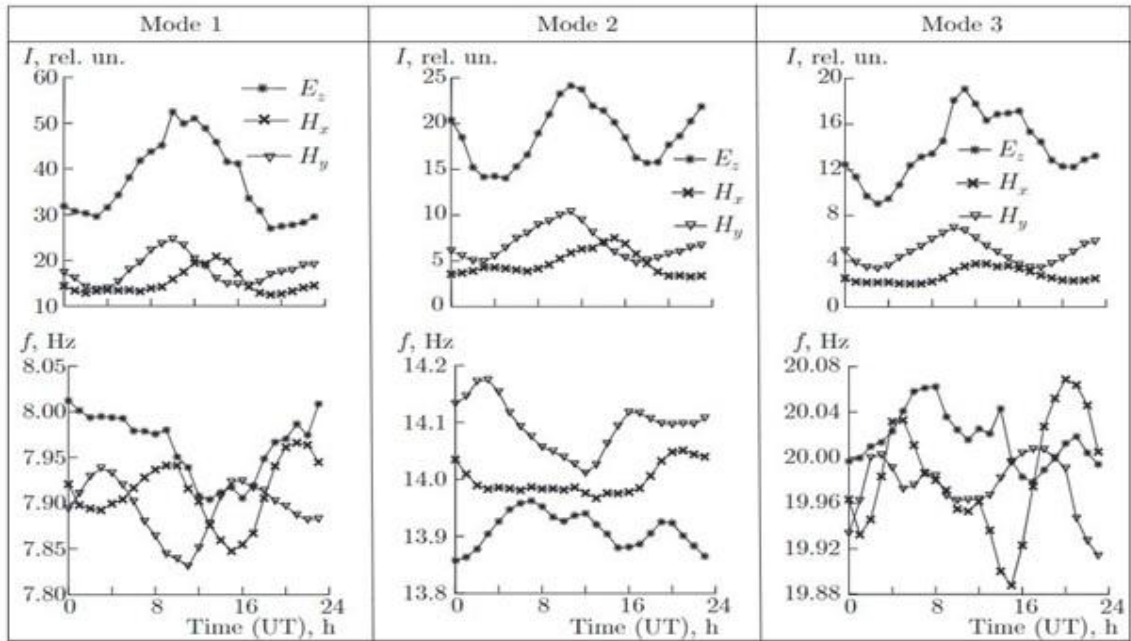


Fig. 4.3(c): Average diurnal variations in the intensities and peak frequencies of the first three modes of the electric and magnetic field components in summer.

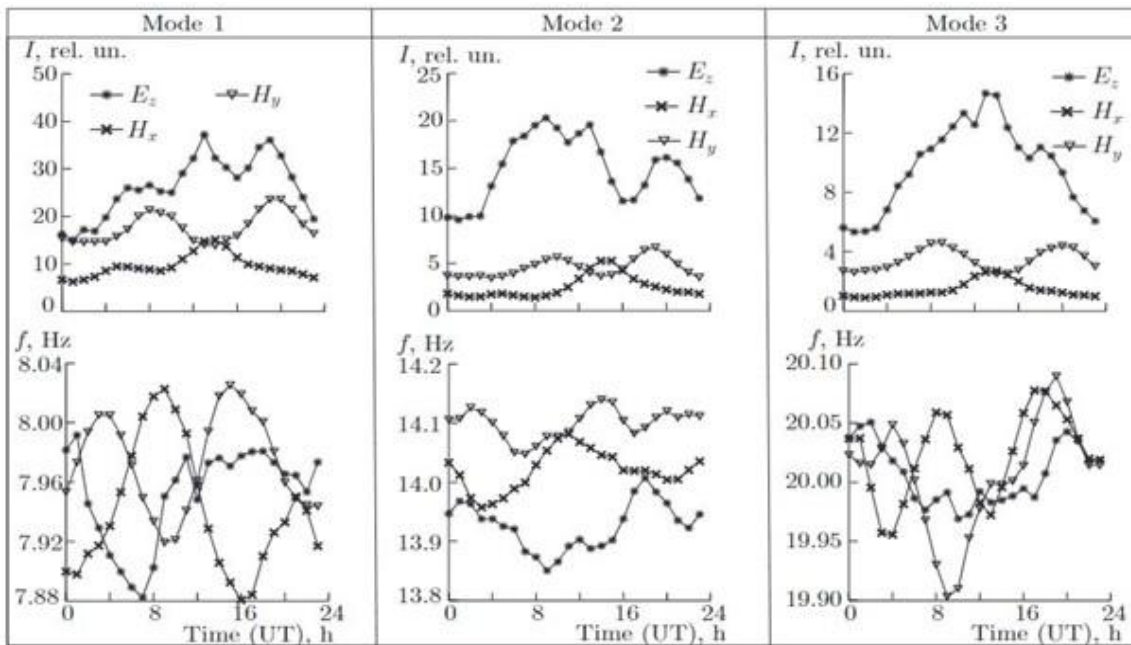


Fig. 4.3(d): Average diurnal variations in the intensities and peak frequencies of the first three modes of the electric and magnetic field components in autumn.

4.4 Different aspects of SR

Diurnal variation of peak frequencies and amplitudes of different modes were utilized to know the characteristics of global thunderstorm activities and the electron number density of the ionosphere. During 1990s and later, the scenario with these sub-ionospheric ELF SR waves changed and several new aspects emerged. Some of those are discussed in this chapter.

4.4.1 Global thunderstorm activity and SR

Schumann resonance intensity records are used to estimate the level of global thunderstorm activities. We developed a calibrated wide-band ELF measurement technique at the Institute of Radio Physics and Electronics, University of Calcutta, India. Observations of signals on SR spectra have been made during the period 1997 to 2003 regularly and after 2004 measurement are carried out as and when required. The records were taken from different noise free regions as far as practicable. In Fig. 4.4 the monthly variation of the global thunderstorm activities deduced from SR amplitude is shown through bar graphs [4.4]. Observational period was of 15 months from January 2000 till March 2001 [4.10].

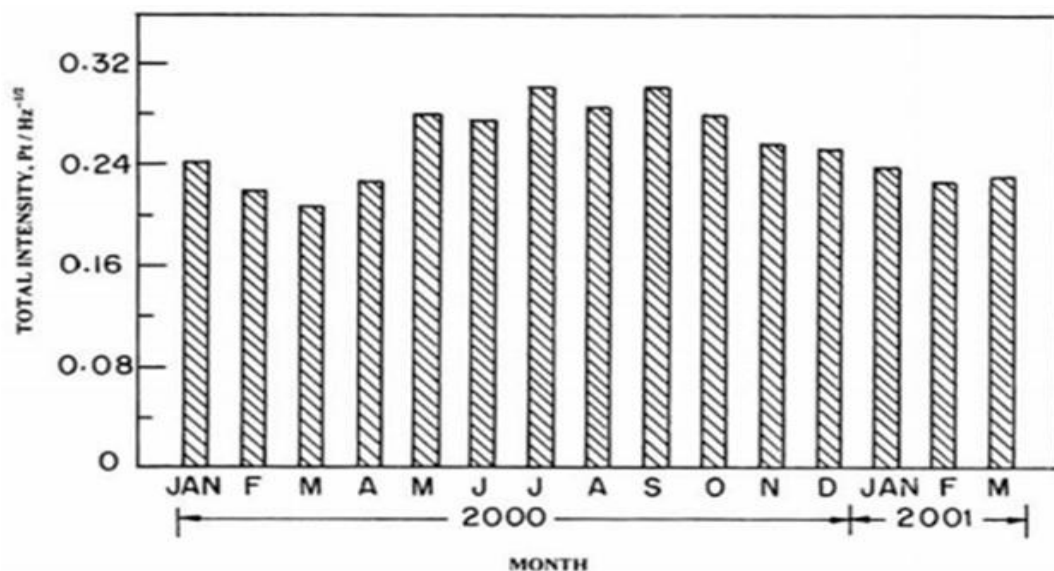


Fig. 4.4: Variation of global thunderstorm activities over Kolkata for a period of 15 months (January 2000- March 2001).

4.4.2 Tropical surface temperature of the Earth and SR

Specific link between SR peak power in the lowest mode (8 Hz) and global, regional temperatures are well established [4.5-4.6]. Relation between SR amplitude and variations in global tropical surface temperature can serve as the (i) Diagnostic of temperature and (ii) Deep convection in the tropical atmosphere. Intensity of SR signals is found to be linked through the logical chain to the tropical surface temperature of the Earth [4.7]. Thus, SR behaves as a sensitive global tropical thermometer on diurnal and seasonal time scales [4.5]. The SR amplitude follows the temperature variation quite closely. Warmer and cooler periods of the entire tropical belt are due to the enhanced and suppressed magnetic field amplitudes of SR.

4.4.3 Global Electric Circuit and SR

It is a current system circuit where the current flows upward through the troposphere into the ionosphere and magnetosphere along the magnetic field lines to the opposite hemisphere. In course of time, it returns to the Earth's surface as the fair-weather air-earth current, thus closing the circuit. Sources of electromotive force driving the global circuit are, e.g., (i) thunderstorms, (ii) dynamo-interaction between the solar wind and the magnetosphere and (iii) dynamo effect of atmospheric tides in the thermosphere as stated earlier. The first one, thunderstorms, is considered to be the most powerful. All these are quasi-DC sources. Cloud-to-ground lightning strokes return the charge to the thunderstorm and close the global circuit. The SRs are caused by electromagnetic emissions from lightning activities which can be considered as a state of excitations of global AC circuit. Here, lightning activity is the energy source, global electrical circuit is the receiver of energy and SR is the vibration mode.

4.4.4 Solar terminator effect on SR at Kolkata

Solar terminator is the zone of the upper atmosphere where severe changes in temperature, electron and ion density, and chemical composition are found during sunrise and sunset hours. These changes are found in this region at all heights of the atmosphere. The height of the lower ionosphere drastically reduced at sunrise and reverse changes are found during sunset. Changes in the structure of the lower ionosphere produce variation in SR parameters during its propagation across such regions.

4.4.5 SR as precursor of earthquake

Significant enhancement in amplitude of the fourth mode of Schumann resonance spectra and the increase in its peak frequency are obtained during the period of earthquakes of Andaman Island, India and Honshu, Japan earthquakes on August 11, 2009 [4.10]. The results of analyses of the recorded data of the day of occurrence of earthquakes, along with the regular normal day data are shown in Fig. 4.5 where magnitude of Fourier transform results in arbitrary unit has been plotted against frequency. Thin continuous lines represent the Schumann resonance spectra within the undisturbed Earth-ionosphere waveguide and the bold line indicates the variations when the disturbance over the earthquake zone sets in.

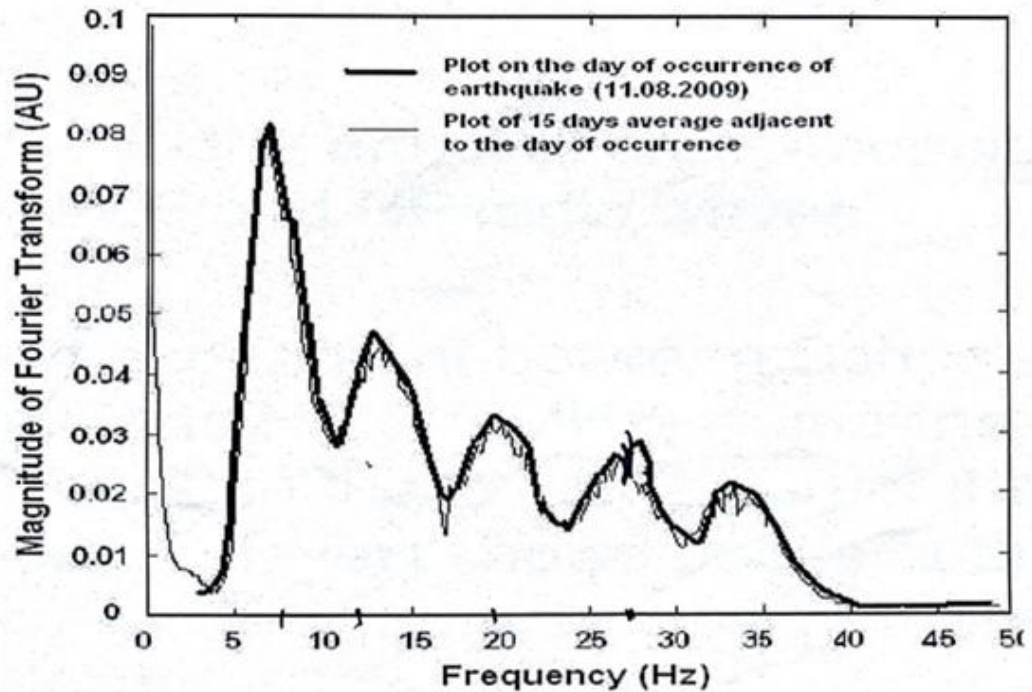


Fig. 4.5: Frequency spectrum of Schumann resonance on the day of occurrence of Andaman Island, India and Honshu, Japan earthquakes on August 11, 2009 (bold line curve) along with the 15 days average plot adjacent to the day of occurrence (thin line curve).

4.5 Results of some observations from Kolkata

Frequency response of received signal recorded on April 2, 2000:

Observations, presented in Fig. 4.6 at different times showed amplitude and frequency fluctuations which are due to the fluctuations of the causes producing such signals spectra from the middle ionosphere [4.9,4.10].

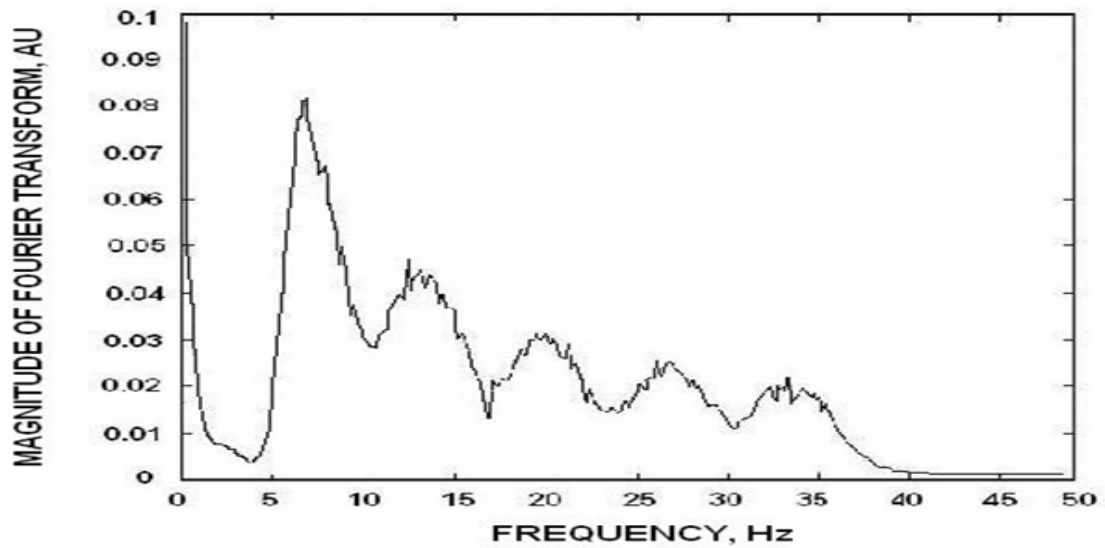


Fig. 4.6.: Frequency response of different peaks of SR in the received signals recorded at Kolkata on April 2, 2000.

Variations of resonance frequencies:

The recorded Schumann resonance spectra over Kolkata on April 12, 2000 [4.9] experience variations in Schumann frequencies which is shown in Fig. 4.7.

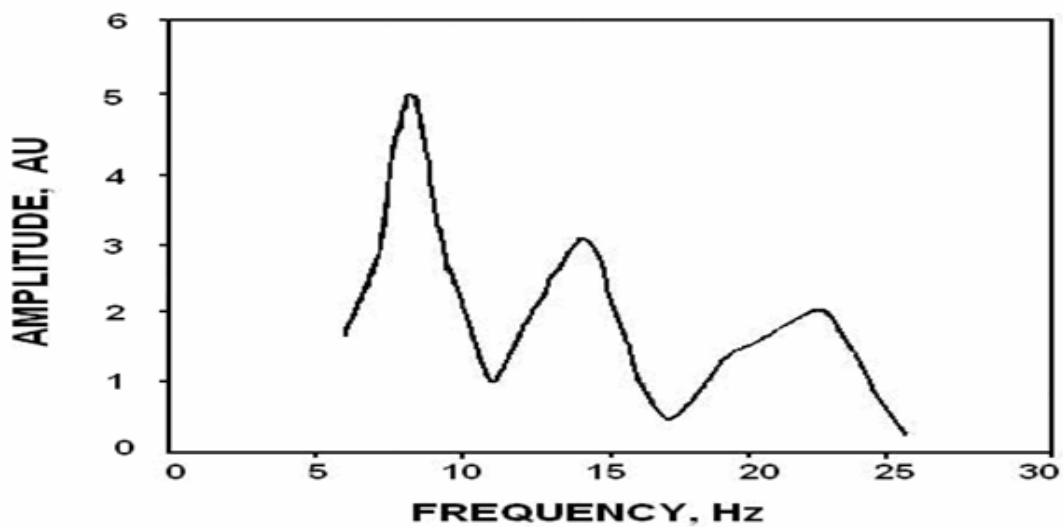


Fig. 4.7: The recorded Schumann Resonance spectra at Kolkata on April 12, 2000, which depicts amplitude and frequency changes in all the three modes.

Variation of resultant intensity of SR modes:

The black colored bar graphs in Fig. 4.8 show the results recorded at Kolkata and the half-tone bar graphs depict the results from the data of Geophysical Observatory at Slovakia (Lat. 48.61° N, Long. 17.31° E). Intensity fluctuations are directly connected to thunderstorm activities [4.9,4.11].

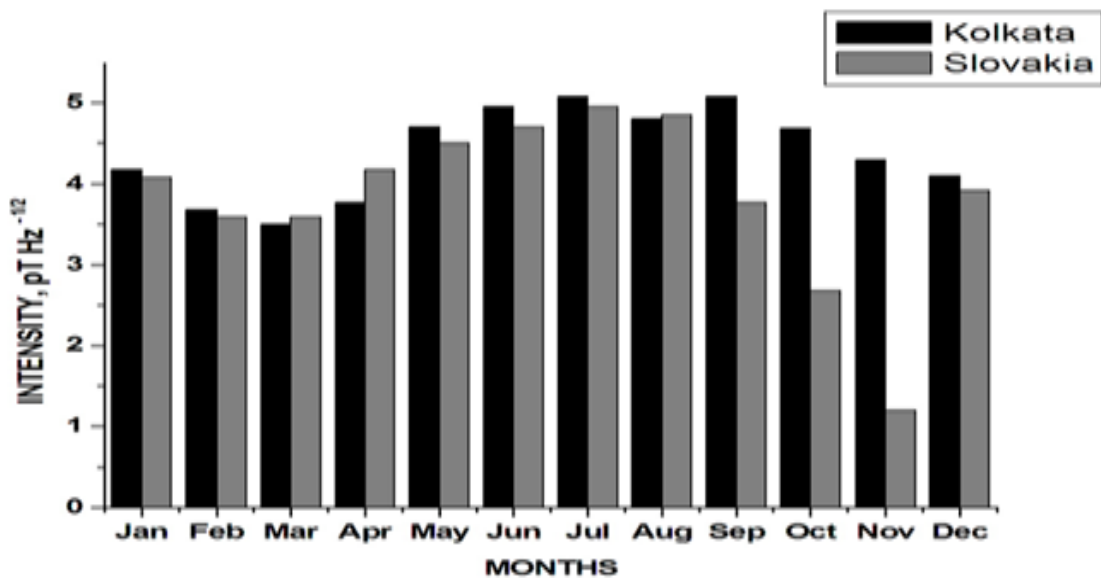


Fig. 4.8: Variation of resultant intensity of SR modes at Kolkata and Slovakia.

Intensity reaches maximum value during summer, which agrees with the results of earlier works [4.12,4.13]. Because of different locations of these two recording centers, the influences of global thunderstorm activity zones for the three modes of SR are also different, for which the annual intensity variations at these two latitudes are different. Kolkata is nearer to Himalayan and Asia-Australia lightning centers compared to Slovakia. This may be the reason for the observed variation of intensity of SR modes. The global variations of thunderstorm activity centers change the source-receiver distance which are believed to be the reason for the seasonal and temporal variations in frequency shift.

Variation of resultant intensity of SR modes:

Fluctuations of resultant intensity of SR modes recorded from four different latitudes during the whole year 2000 are shown in Fig. 4.9; [4.9,4.14].

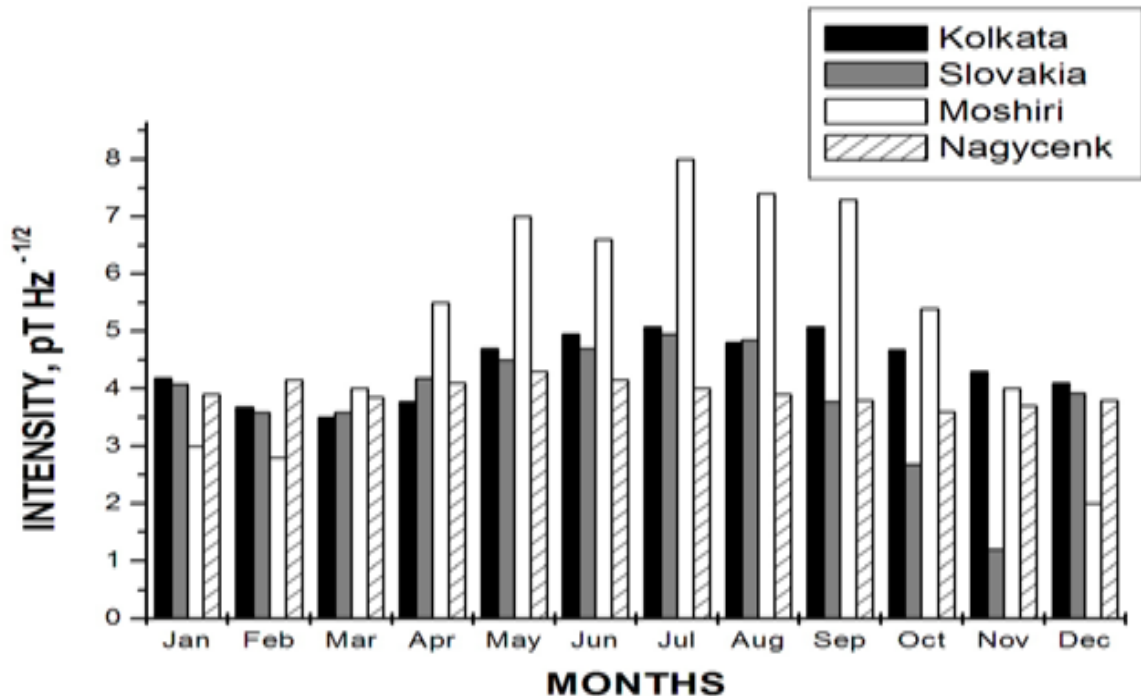


Fig. 4.9. Fluctuations of resultant intensity of SR modes recorded at four different places – Kolkata; Slovakia; Moshiri and Nagycenk.

The black colored and half-tone bar graphs indicates the results recorded from Kolkata and Slovakia, whereas the black bar graphs and the bar graphs filled by slanting hatched lines are due to Moshiri (Lat. 44.29° N, Long. 142.2° W); and Nagycenk (Lat. 47.6° N, Long. 16.7° E). Moshiri is very close to Asia-Australia violent thunderstorm centre than the location of Nagycenk. Because of geographical location of the lightning centers, the magnitude of intensity of SR at Nagycenk may be more dependent on African and European sources than the American sources. The graphical location of Nagycenk is nearer to African sources of thunderstorm centre.

Comparison of peak frequency variations from two different stations:

Variations of the peak frequency of the first SR mode for the spring season (March to May) recorded at Kolkata in the year 2000 are compared with the variations over the same season of the year 2006 at Moshiri, Japan [4.9,4.14] are presented in Fig. 4.10; In the recorded data, the influence of Asia lightning activity center is more in Kolkata and Slovakia than African and American centers. The intensity fluctuation of SR modes due to the main influence of Asian lightning centre can be understood from this figure.

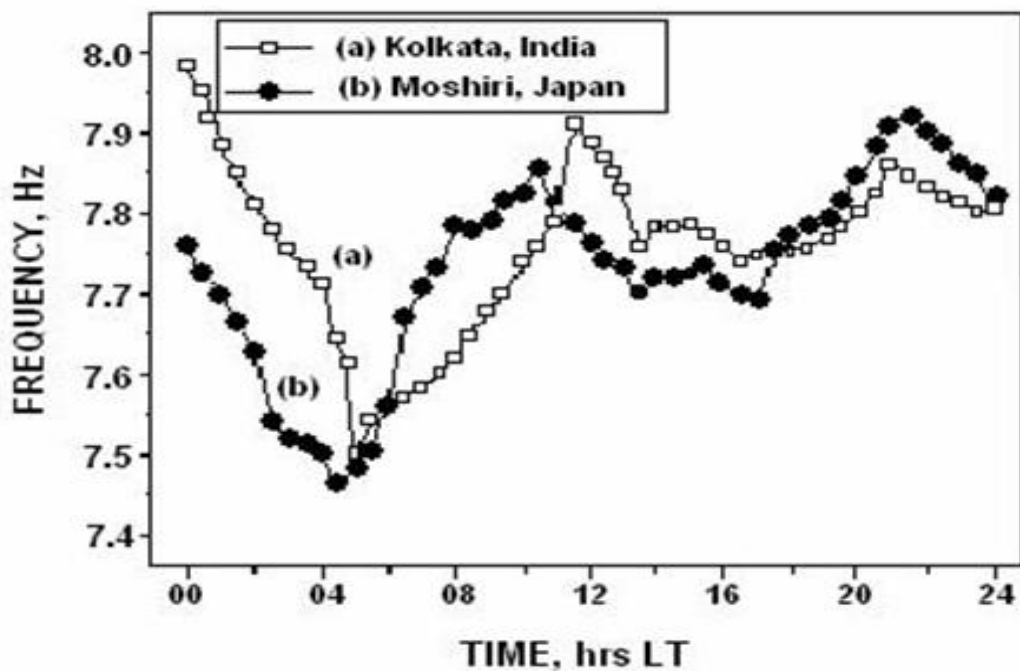


Fig. 4.10: Diurnal and seasonal variations of the peak frequency of the first mode of SR: (a) for the spring season (March to May) recorded at Kolkata; (b) superposed on the results of Moshiri, Japan for the same variations.

Thunderstorm occurrences are high during July-August (rainy season) and low during November-December (winter season) for which SR intensity is high in rainy season than in winter season. The thunderstorm centre of Asia in the rainy season remains at Lat. 15° N, Long. 105° E and it is near to both the centers. For this reason,

SR intensity bears almost the same value during this season. But the Asian thunderstorm center during winter season remains at Lat. 15° S and Long. 130° E and for this, its influence on Slovakia center is less in comparison to Kolkata center. Hence large variation in SR intensities at these centers during winter season is found. Thus Schumann resonance frequencies may be considered as the indicator of the thunderstorm distribution in global lightning activity level. The growth of the global lightning activity is generated by the thunderstorm spreading.

Electromagnetic waves are generated due to excitation energy from lightning. Different records from Kolkata exhibit sub-peaks surrounding the three modes. The occurrences of these unequal sub-peaks are due to the uneven influences of the global thunderstorm activity centers towards the interaction within the Earth-ionosphere cavity generating the modes.

Within the cavity, disturbances like random fluctuations of irregularities are occurring regularly along with other disturbances, like Polar-cap absorption, X-ray bursts, etc. Solar proton precipitation introduces an abrupt frequency variation. Modification of frequency is enhanced by the interaction between the polar ionosphere and precipitation particles. It causes the whole polar ionosphere to shift downward causing the frequency of the first SR mode globally to move to lower values [4.15,4.16].

Protons with energy up to 100 MeV are most often emitted from the sun in conjunction with solar flares which can penetrate deep into the D-region and cause additional ionization leading to conductivity changes thereby modifying SR parameters. High energy solar proton flux of July 14, 2000 was detected by GOES 8 satellite at 10:35 UT which showed maxima at 11:45 UT [4.8] in Fig. 4.11. It was preceded by the

solar X-ray bursts. Its onset occurred at 10:10 UT and the maximum took place at 10:35 UT. The variation of proton flux at energy (E) $510 < E < 700$ MeV and X-ray at wavelength (λ) $0.05 < \lambda < 0.4$ nm are shown by continuous line curve and dashed line curve, respectively. The changes of the first SR frequency on July 14, 2000 over Kolkata are shown by the continuous line graph joining the square blocks. It is superposed on the curves for solar X-ray bursts (continuous line curve) and SPE (dashed line curve).

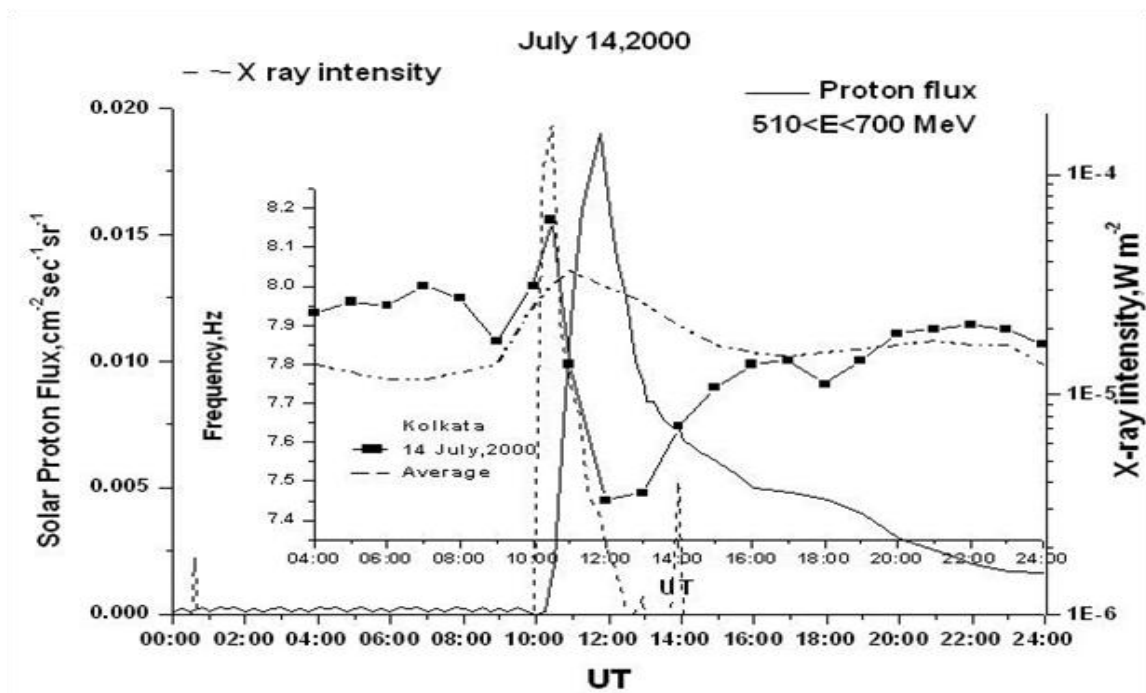


Fig. 4.11: The variation of frequency of the first mode of SR spectra during solar proton events on July 14, 2000 is shown here from the observed data recorded over Kolkata. The result shows the decrease in frequency during the period of occurrence. The severe solar X-ray bursts occur just before the proton event shows enhancement of the first mode frequency.

The values of the first SR frequency averaged over other three days adjacent to the day of occurrence of these two events are plotted by dot-dashed curve. The SR frequency starts enhancing from 09:00 UT and reaches the highest value ~ 8.15 Hz at 10:35 UT during solar bursts. Immediately after, during solar proton flare, its value

approaches towards lower value showing the minima at ~ 7.45 Hz because of the instantaneous occurrence of high energy SPE. The decrease in the first mode SR frequency continued up to around 12:00 UT and returned to its normal value at 16:00 UT.

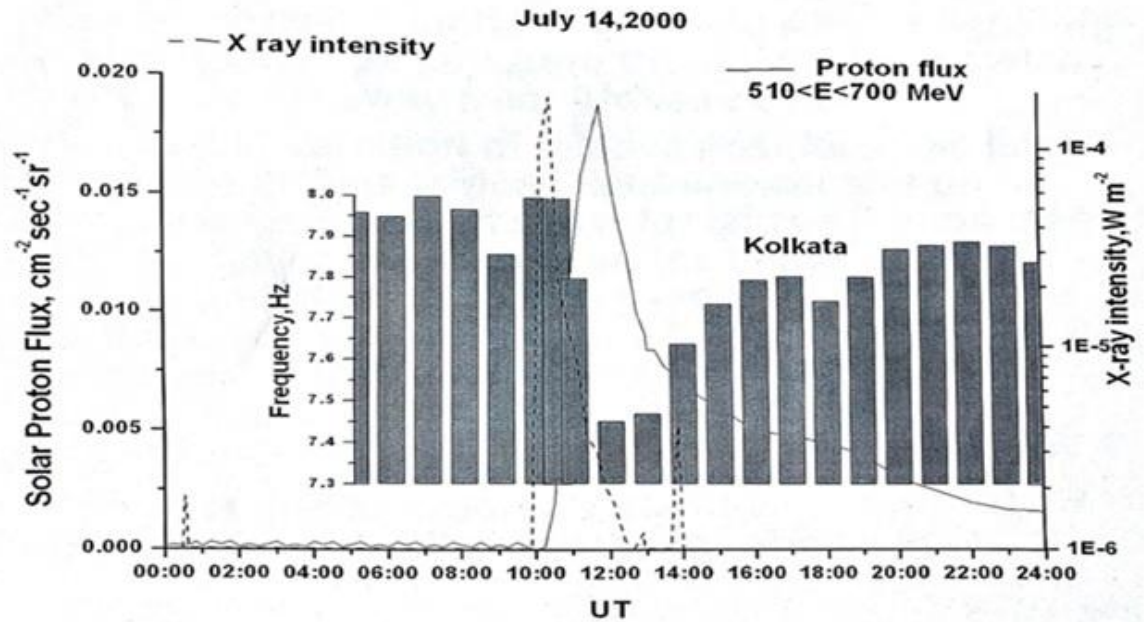


Fig. 4.12: The histogram of the changes of the first mode of SR frequency during X ray flare and solar proton events on the day of occurrence over Kolkata.

During solar activity, along with the exponential variation of conductivity in the vertical direction, there may be two kinds of changes: (i) increase in ionization level at the normal D-region reflection heights, and (ii) the variation of D-region lower edge. The variation of the first can change due to both electron density variations in the ionospheric D-region and the change of height of the lower boundary of the D-region. Growth of X-ray flux enhances electron density without a significant change in ionospheric altitude. So the first SR frequency increases. Solar protons penetrating deep into the atmosphere cause a decrease of altitude of D-region. This gives rise to decrease of the first SR frequency. This could be supported by Fig. 4.12 where histogram of the changes of 1st mode SR frequency is presented during the two events. But, SPE can also affect ionization. So the two terms compete with each other and their relative

magnitudes are the decisive factors. If two terms are comparable, no change in the first SR frequency may be obtained. Later on, two characteristic layers were identified within the lower ionosphere responsible for height variation of vertical electric field and horizontal magnetic field components. Another kind of inhomogeneity can arise during enhancement of solar X-ray or proton flux [4.17].

Seasonal and monthly variation of the first SR frequency over different stations:

Seasonal variation of the first mode SR frequency over different observatories on July 14, 2000 is shown in Fig. 4.13; The amplitude of SR frequency is determined by the temporal and spatial distribution of global lightning. Lightning activity moves from northern to southern hemisphere as the winter sets in northern hemisphere. SR characteristics are therefore, expected to be different on location and seasonal conditions. SR properties are, strongly affected by the global lightning activity and the distance of the SR receiver to the source regions [4.18].

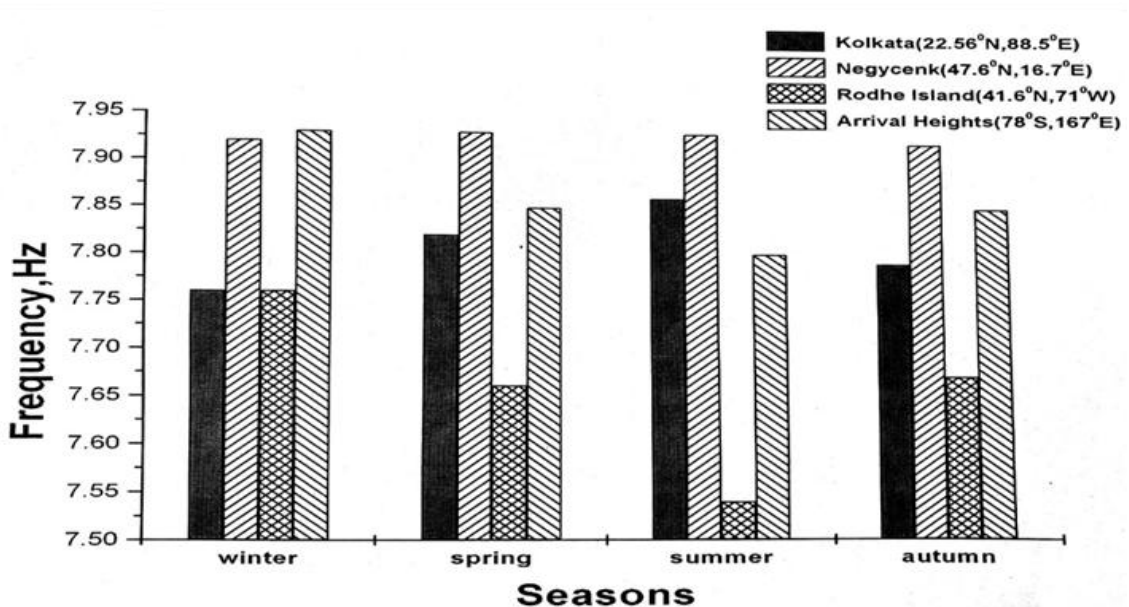


Fig. 4.13: Seasonal variation of the first mode SR frequency over different Observatories on July 14, 2000.

Locations of global thunderstorm regions are at Asia (Lat. 15° N, Long. 105° E), Africa (Lat. 10° N, Long. 10° E) and America (Lat. 30° N, Long. 80° W) [4.19]. Mitzpe Ramon is nearer to both the Asia and African lightning centers, whereas Lovozero is though nearer to Asian center but far away from African center. Due to this variation of relative positions, the joint influence of Asia-African lightning centers on SR frequency is much stronger for Mitzpe Ramon than that for Lovozero. Moreover, the influence of American lightning center is more towards Mitzpe Ramon than Lovozero due to their geographical positions.

Upper Tropospheric Water Vapour (UTWV) and SR:

Schumann Resonances can provide continuous and long-term monitoring of global climate change parameter like UTWV. Both lightning and UTWV are well correlated to the strength of the convection in the tropics. The retrieval of UTWV concentration may be achieved through the continuous magnetic intensity measurements of SR spectra. During the existence of water-vapour, there will be a more charge separation followed by instantaneous recombination processes with the generation of EM radiation at the cost of thermal energy during recombinations. This excess EM energy on the surface of the tropospheric zone would influence the SR magnetic records in a varying manner depending upon the intensity of charge separation process. As said earlier, there being a good correlation between tropospheric water content and SR field, the field could be explored using long term data. After developing a model, climate can be forecasted using SR data with the following sequence:

SR data => Water vapour content => climate forecasting

Monitoring and predicting global climate change require understanding the factors that determine atmospheric concentrations of greenhouse gases. Continental

deep convective thunderstorms transport large amount of water vapour into the troposphere, dominating the variation of UTWV. Tropospheric water vapour is a key element of the Earth's climate, which has direct effects as a greenhouse gas, as well as indirect effect through interaction with clouds, aerosols and tropospheric chemistry. UTWV has a much greater impact on the greenhouse effect than water vapour in the lower atmosphere. The main work in addressing this question is the difficulty in monitoring UTWV globally over long time scale. The changes in the UTWV can be derived from the records of SR. Fig. 4.14 shows the connection between daily SR amplitudes and upper tropospheric water vapour [4.20].

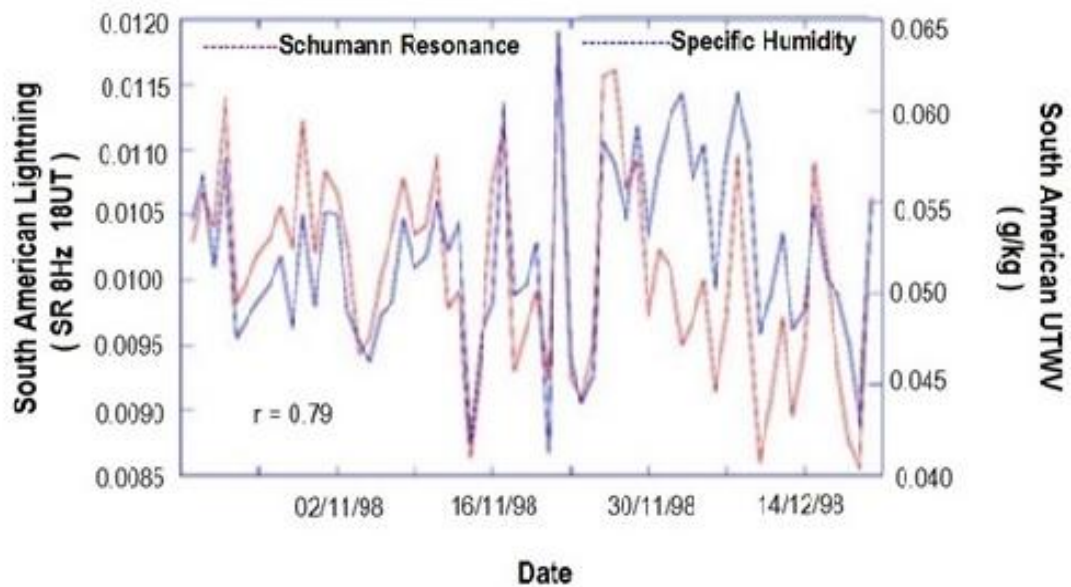


Fig. 4.14: Daily SR 8 Hz magnetic field records and upper tropospheric water vapour.

Thus, the most important parameters of global climate change are surface temperature and UTWV, which can be monitored with SR, utilizing its relation to worldwide thunderstorm activity. The method demands the availability of long-term calibrated data that can provide past and future records of global climate variation on Earth.

4.6 Recent scenario about Schumann Resonance:

Variations in temperature between the ocean and the atmosphere in the east-central Equatorial Pacific is characterised by El Niño-Southern Oscillation (ENSO). The affected area is mostly between 180° and 120° West, roughly 60° of longitude with the appearance of unexpected warm water in the Pacific Ocean. La Niña is exactly opposite phenomenon to El Niño. The variations between El Niño and La Niña normally exist 9 to 12 months. El Niño generally starts from June to August and reaches its peak in December to April period and finally ceases during May to July of the next year. The periodicity of El Niño and La Niña events is not regular and may repeat every three to seven years.

The influence of El Niño on the zonal (East-West) circulation (Walker Circulation) over the tropics is found to be responsible for the periodic weakening of monsoon westerlies for which high summer sea surface temperature is experienced in the West Indian Ocean. High pressure in the East and low in West drive the trade winds in the Pacific area. The trade wind circulation is completed by winds blowing from West to East in the upper part of the atmosphere while the Walker circulation is due to differences in the heat distribution between ocean and land. The tropopause height is correlated to surface temperature and 1 °C increase in sea surface temperature causes the tropopause temperature to rise by roughly 7.5 °C [4.21]. The phenomenon that water in the Indian Ocean towards Africa is unusually warm and that towards Indonesia are extremely cool is described as positive Indian Ocean Dipole (JAMSTEC). The reverse phenomenon, a negative dipole coupled with El Niño gives high probability of drought in India [4.22]. A draught situation in India is more likely in the case of CP El Niño rather than EP El Niño. Central Pacific anomalous warming is found to dominate since late 1990 which are also known as CP or Modoki El Niño [4.23].

The Earth-Ionosphere spherical cavity resonates with standing electromagnetic waves due to excitation energy from the lightning discharges in the equatorial thunderstorm active regions. The SR frequency mode intensity variation with southward shift in global position of lightning activity during El Niño and northward shift during La Niña in longitudinal range is reported from the study of frequency and intensity variation of Schumann Resonance modes. The SR power varies with universal / local time and the receiver position with respect to the lightning centres. Both electric and magnetic components of the Schumann Resonance intensity vary with the spatial shifts of the thunderstorm region under El Niño and La Niña conditions. Due to different spatial distributions of SR electric and magnetic components in the Earth-Ionosphere cavity, different power variation patterns are clearly observed in the electric and magnetic components with the motion of the thunderstorm centres.

Both the intensity and position of lightning activity vary on the ENSO time scale. More lightning is observed in the tropical-extra-tropical land regions during warm, El Niño episodes, especially in Southeast Asia. Oceanic lightning activity is a minor contributor to global lightning. The annual distribution of global lightning is slightly offset from the equator into the Northern Hemisphere due to the North-South asymmetry of the land / ocean area ratio. Schumann resonance intensity variations suggest a southward (equator-ward) shift and satellite observations support this and showed in addition an eastward shift in the global position during warm, El Niño episodes.

The diurnal, seasonal and solar cycle variations of the wave patterns using the global ionospheric maps revealed the existence of the wavenumber-4 (WN-4) patterns which are intense and well developed in boreal summer and early boreal autumn. This seasonal variation is consistent with that of the zonal wind of the non-migrating tidal

mode DE3. The WN-4 patterns shift eastward with a shifting speed that is smaller in day-time than at night [4.24].

Changing distributions of latent heat tidal forcing are thought to induce changes in the strength of the upward and eastward propagating diurnal tide with zonal wave number DE3 which subsequently produces the observed changes in the amplitude of the WN-4 longitudinal structure through modulation of the electric fields generated by the dynamo mechanism in the ionospheric E region. Our results demonstrate that there is a significant inter-annual variability in the ionospheric WN-4 longitudinal structure and further indicates that the ENSO phenomenon represents a source of ionospheric variability which has previously not been considered [4.25].

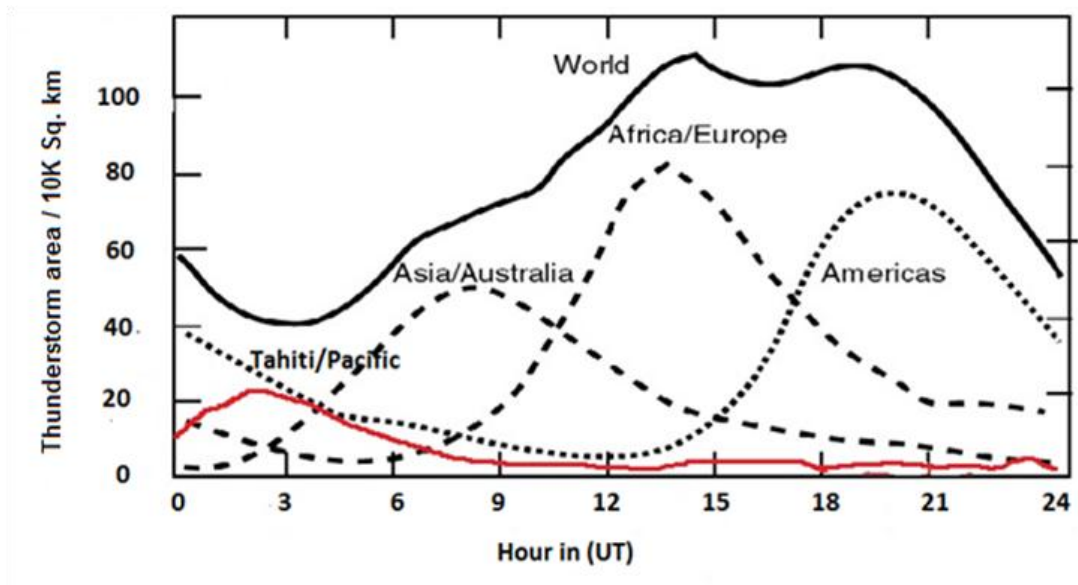


Fig. 4.15: Thunderstorms due to fourth chimney in the dateline area Tahiti / Pacific has a peak around 03:00 Hour UT.

The WN-4 structure appears both in the thermospheric (neutral) and ionospheric parameters observed around the Earth above the near-equatorial zone. It is attributed to latent heat release in deep tropospheric convection in the equatorial region where the three main tropical lightning chimneys are found. In addition to the three known chimneys (Africa, America, Maritime Continent), a smaller fourth chimney has been

identified near Tahiti, in the Pacific Ocean (Fig. 4.15). Some general features between the thermospheric / ionospheric WN-4 structure and the global tropical lightning characteristics are identified through SR [4.26].

4.7 Conclusions

Schumann Resonances have numerous applications in lightning research and this is one of the few tools, which during variations in global lightning activity can provide continuous and long-term monitoring of important global climate change parameters, eg., surface temperature and UTWV. Now, it is clear that in order to make a systematic study regarding UTWV variability and other meteorological parameters affecting the global climatic change via SR, the experimental records of SR signals through ball antenna and induction coil antenna are necessary.

Significant progress is achieved during the past decades in the areas of Schumann resonance research, lightning and thunderstorm related to global electric circuit using ground and satellite based equipments. But, the temporal and spatial variability of lightning and thunderstorms are not available by satellite looking down on the Earth continuously. Still there are many open challenges in this field to tackle, viz., to know in detail how the global atmospheric electric circuit could be used as a useful tool to study and monitor the Earth's changing climate by continuously measuring SR signals, to investigate the possibility that the global electric circuit and, global and regional lightning frequency might be an indicator of climate change, to determine mechanisms responsible for charge generation and separation in UTWV. Very recently, few relations between the thermospheric / ionospheric WN-4 structure and the global tropical lightning characteristics are identified through SR. These are detected from all the four chimneys with different magnitude and intensity. Further information about the fourth chimney are yet to be explored.

4.8 References

- [4.1] Balser, M. and Wagner, C.A., 188 (1960), 638.
- [4.2] Nickolaenko, A.P. and Hayakawa, M., *Resonances in the Earth-ionosphere cavity*, Vol. **19**, Springer Science & Business Media (2002).
- [4.3] Yatsevich, E.I., Nickolaenko, A.P., Pechonaya, B.O., *Radiophysics and Quantum Electronics*, 51, (2008) 528.
- [4.4] De, S.S., Saha, A.K. and De, M., *Indian J. Radio Space Phys.*, **33**, (2004) 32.
- [4.5] Williams, E.R., *Science*, **256** (1992), 1184.
- [4.6] Balling Jr, R.C. and Hildebrandt, M., *Climate Research*, **16** (1), (2000) 31.
- [4.7] Nickolaenko, A.P., Sátori, G., Zieger, B., Rabinowicz, L.M., Kudintseva, I.G., *Journal of Atmospheric and Solar-Terrestrial Physics*, 60 (3), (1998) 387.
- [4.8] De, S.S., De, B.K., Bandyopadhyay, B., Paul, S., Haldar, D.K. and Barui, S., *Journal of Atmospheric and Solar-Terrestrial Physics*, **72** (11-12), (2010) 829.
- [4.9] De, S.S., De, B.K., Sarkar, B.K., Bandyopadhyay, B., Haldar, D.K., Paul, S. and Barui, S., 2009, Analyses of Schumann resonance spectra from Kolkata and their possible interpretations, *Indian J. Radio Space Phys.*, 38, 208.
- [4.10] De, S.S., 2007, Schumann Resonance - Its different aspects and latest wonders, *Indian J. Radio Space Phys.*, 36 (5), 359.
- [4.11] https://www.stuba.sk/english.html?page_id=132).
- [4.12] Nickolaenko, A.P., Hayakawa, M., Hobara, Y., *Journal of Geophysical Research: Atmospheres*, **104** (D22), (1999) 27585.
- [4.13] Nickolaenko, A.P. and Rabinowicz, L.M., *Journal of Atmospheric and Terrestrial Physics*, **57** (11), (1995) 1345.
- [4.14] Sekiguchi, M., Hobara, Y. and Hayakawa, M., *Journal of atmospheric electricity*, **28** (1), (2008) 1.

- [4.15] Schlegel, K. and Füllekrug, M., *Journal of Geophysical Research: Space Physics*, **104 (A5)**, (1999) 10111.
- [4.16] Roldugin, V.C., Maltsev, Y.P., Vasiljev, A.N., Shvets, A.V. and Nikolaenko, A.P., 2003, *Advance in Earth and Space Science*, **108**, (2003) 1103.
- [4.17] Greifinger, C., and Greifinger, P., *Radio Science*, **13(5)**, (1978) 831.
- [4.18] Sentman, D.D., Wescott, E.M., Osborne, D.L., Hampton, D.L. and Heavner, M.J., *Geophysical research letters*, **22(10)**, (1995) 1205.
- [4.19] Barr, R., Jones, D. L., Rodger, C.J., *Journal of Atmospheric and Solar-Terrestrial Physics*, **62(17-18)** (2000) 1689.
- [4.20] Price, C., Pechony, O., Greenberg, E., *Lightning Research*, **1**, (2007) 1.
- [4.21] Farrell, B. F., *Journal of atmospheric Sciences*, **47(24)**, (1990) 2986.
- [4.22] Kumar, K.K., Rajagopalan, B., Hoerling, M., Bates, G., Cane, M., *Science*, **314**, (2006) 315.
- [4.23] Xiang, B., Wang, B. and Li, T., 2013, A new paradigm for the predominance of standing central Pacific warming after the late 1990s, *Climate Dynamics*, **41 (2)**, (2013) 327.
- [4.24] Wan, W., Liu, L., Pi, X., Zhang, M. L., Ning, B., Xiong, J. and Ding, F., *Geophysical Research Letters*, **35**, (2008), 12.
- [4.25] Pedatella, N.M., Lei, J., Larson, K. M. and Forbes, J.M., *Journal of Geophysical Research: Space Physics*, **114** (2009) A12.
- [4.26] Sători, G., Ortega, P., Guha, A. and Williams, E., *2nd TEA-IS Summer School*, June 23rd–June 27th (2014), Collioure, France.

CHAPTER 5

Responses of Meteorological Parameters During August 24, 2016 Myanmar Earthquake

5.1 Introduction

A huge amount of energy is released during an earthquake in the form of thermal, gravitational emissions of radiation. The release of strain through thermal energy and associated latent heat in the case of pressurized fluid are contained in the earthquake zone. The thermodynamic equilibrium of the troposphere is very much connected with the atmospheric pressure, temperature, humidity, rainfall and wind speed. Some anomalies are observed on the surface temperature and other atmospheric parameters during the period. The anomalous surface latent heat increase takes place within a time interval of several days before a strong earthquake in this earthquake preparation zone. The variations in Lithosphere-Ionosphere-Atmosphere (LIA) coupling take place during the occurrence of the earthquake and resulted in anomalous changes in different meteorological parameters. The variations in LIA may be due to enhanced radon and other greenhouse fluid emanations during the pre-and post-earthquake period.

A continental plate movement in the Sunda Trench region resulted into the Myanmar earthquake ($M=6.8$) that took place on 24 August, 2016. The meteorological data analyzed to investigate these observations as well as to invoke responses during the occurrences along with the pre-and post-periods of this earthquake from 1 August, 2016 to 30 August, 2016 are reported in this chapter.

There is strong co-relation between atmosphere-ionosphere disturbances and core structure of the Earth which involves radioactive gas emanations over the micro-fracture region of the earth [5.1, 5.2]. This emitted radon gas ionizes the neutral

particles which cause changes in the conductivity of air thereby modifying the atmospheric electric field. Apart from the radioactive radon, other greenhouse gases are also emanating from the Earth surface during pre- and post-seismic periods which introduce changes in the meteorological parameters. Abnormal enhancements of outgoing IR radiation above the seismo-active regions along the fault system of Earth's crust are observed in the thermal images taken from satellite [5.3-5.5].

Thermal anomalies are detected weeks before earthquake and continued for a week or more with the increase in temperature of a few Kelvin and covering hundreds of km above the fault zone. The area of coverage depends on the magnitude of the earthquake and depth. The air temperature increased around the fault region by 3–4 K about ten days' pre- and post-earthquake. Thermal anomalies are recorded 4–7 days before and continued for a few days after the earthquake $M > 6$ and for distance of the order of 500 km. [5.6, 5.7]. The LAI coupling model involving seismic processes could lead to atmospheric perturbations which could explain the origin of some preseismic electromagnetic effects in the ULF, VLF and HF frequency range [5.6-5.8]. The thermal balance of the boundary layer of the atmosphere gets affected through significant changes in humidity and temperature [5.2].

Thermal anomaly is an indicator for the seismo-atmospheric and seismo-ionospheric coupling [5.5,5.9,5.10]. The abnormality in the meteorological conditions like air humidity, temperature variations and air refractive index have been predominantly noticed in seismically active regions near the coast [5.11]. There exists a close relationship between the abnormal variations in air refractive index and ground-surface temperature [5.11].

Different models of LIA coupling are proposed where the propagation of acoustic-gravity waves through atmosphere have been considered up to the ionospheric

height before strong earthquakes. Some researchers attributed the ionospheric disturbances to the modifications of electric fields and currents in the lithospheric electric process [5.12].

The atmospheric oscillations through acoustic wave (AW or AGW) in the process of LIA coupling cause perturbations in surface temperature, humidity and pressure in a seismo-active region which finally travel up to the ionosphere enhancing density irregularities [5.13-5.15]. The investigations of the lithosphere-ionosphere-atmosphere thermal balance are connected with the observed density changes of the charged particles through satellites [5.16-5.19].

Data Source: The data regarding the air temperature and relative humidity for the earthquake which are dealt in the present chapter are taken from the website: <http://www.worldweatheronline.com/chauk-weather-history/>.

5.2 Observations and Analyses

The fault between the Indian plate and Sunda Trench is known as Sagaing fault which is built at an intermediate depth of Indian plate and Sunda Trench, in Myanmar Earthquake. This fault cuts the centre of Myanmar in western and eastern half, one is moving towards north with the Indian plate and the other with the Eurasian plate, respectively. The Indian plate moves towards the northeast of Sunda Trench with a velocity of 44-49 mm/year. It is conjectured that the Himalayan Mountains are formed due to the uplift of the Tibetan plateau in the past of about 50 million years [5.20].

As sensitive plate boundary traverses towards Myanmar, large earthquakes were seen to initiate significant hazards. During the movements of the Indian plates into Eurasian plate [5.21], the eastern part of this plate slides obliquely sideways past south

eastern Asia along a complex and diffused plate boundary (Fig. 5.1) beneath Myanmar [5.22].



Fig. 5.1 — Image shows Myanmar as a south-east Asian country.

The slanting motion is ripped into two components— (i) East-directed plate convergence that uplifts in the Indo-Myanmar mountain ranges and (ii) Strike-slip motion where India moves towards the north relative to the south eastern Asia [5.23]. Strike-slip is the sub-vertical slip between the plates (Fig. 5.2), which links these two different tectonic domains [5.24 - 5.25]. These two tectonic domains are equally active and divided into a number of structures with the Sagaing Fault, as the significant one.

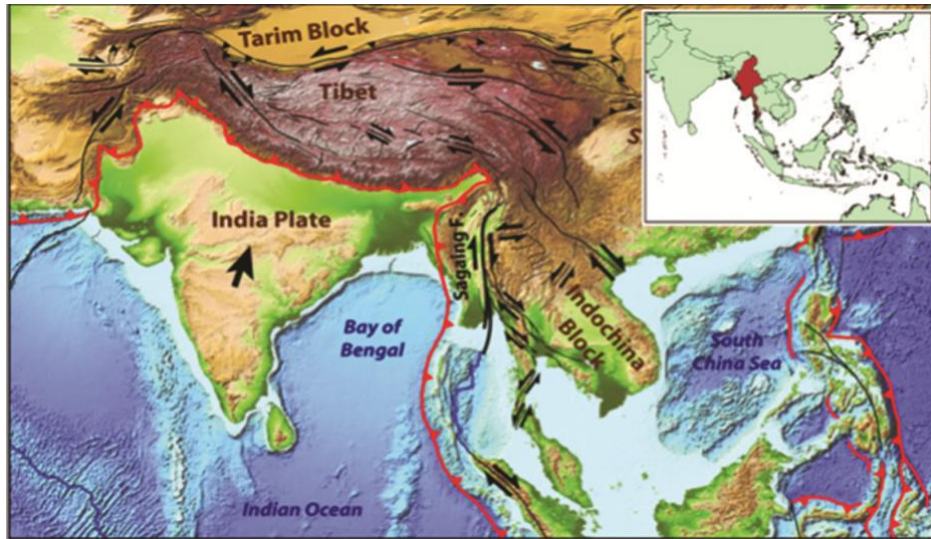


Fig. 5.2: Tectonic map of Myanmar and its surroundings.

In Myanmar, approximately 1500 km long tectonic fault passes through cities like Bago, Nay Pyi, Sagaing and Mandalay (Fig. 5.3). The other type of strike-slip fault on Earth is the San Andreas Fault in the western USA. Both these faults are passing through highly populated and rapidly developing cities. These two faults are almost similar except the average slip rate per year. The sagaing Fault slips at an average rate of 18-20 mm/year [5.22], while the San Andreas Fault at San Franciscoslips at a rate about 24 ± 3 mm/year [5.26].

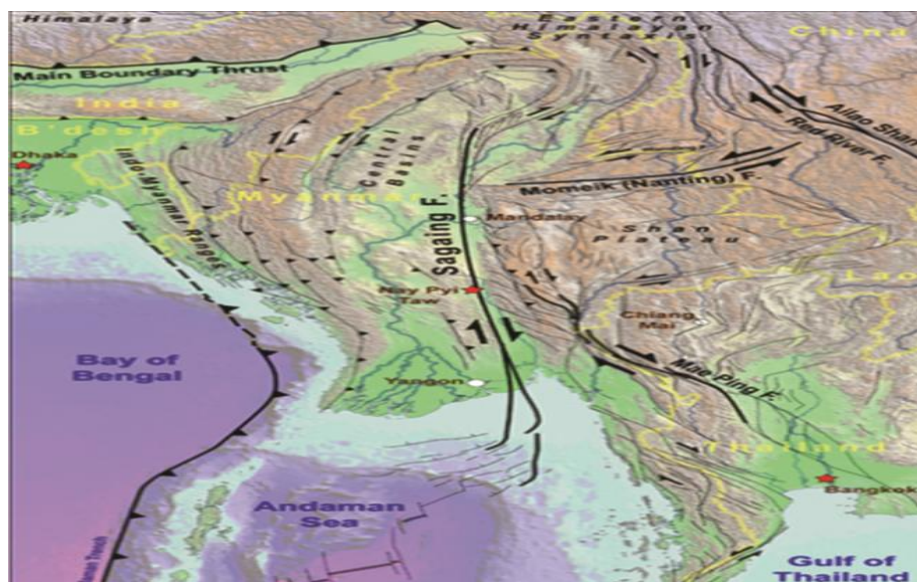


Fig. 5.3: Nearly 1500 km long tectonic fault in Myanmar and surrounding areas.

These faults remain locked for many years until enough stress is built to overcome friction on the fault. An earthquake releases all these stresses, and the sides of the fault slide a few decimeters to meters past each other, depending on how much time has elapsed since the last earthquake (stick-slip behaviour). There are two conspicuous seismic gaps along the Sagaing fault where there were no historical earthquake greater than $M=7$ [5.27].

Thermal anomalies have a greater impact on the atmosphere a few days before the earthquake. The changes due to the thermal anomalies can be observed on the surface temperature and upon other atmospheric parameters like relative humidity, air pressure etc. The troposphere in thermodynamic equilibrium is a complex system of interrelated atmospheric temperature and humidity. Another important parameter is the latent heat which is closely related with the water content in the air and the processes of water evaporation. In the earthquake preparation zone, the anomalous surface latent heat increase takes place within a time interval of several days before a strong earthquake.

The thermodynamics of the lower atmospheric layers are manifested by the action of the ionization source and strong electric fields which are supposed to be the most probable sources of observed thermal and surface latent heat flux anomalies before strong earthquakes [5.2].

The coupling processes among Lithosphere-Ionosphere-Atmosphere layers through the electromagnetic channel and the acoustic channel during the Myanmar earthquake with $M=6.8$ on 24 August, 2016 is depicted through the variations of different meteorological parameters like temperature, humidity, pressure that may be

caused by the enhanced radon emanations along with some other diffused inputs due to the venting of carrier gases from the sub-surface (Fig.5.4, a–h).

Here the satellite data were analyzed to investigate the variations of temperature, humidity and other atmospheric parameters and ionospheric responses during the Myanmar earthquakes. The data of ionospheric variability, air temperature and relative humidity were taken from Chauk Historical Weather, Myanmar ground stations (<http://www.worldweatheronline.com/chauk-weather-history/>). The daily temperature as well as humidity variations during the pre-and post-periods of this earthquake from 1August, 2016 to 30August, 2016 is shown in figure 5.4 at Chauk recording stations at Myanmar. Relative humidity variations to minimum and maximum value of the order of 15% and temperature were between 24 °C -31 °C during this period.

The relation of air temperature and pressure was inversely related although contradicting with their nature (Fig. 5.5). The maximum temperature and pressure variation was started to follow the same pattern 3-4 days before.

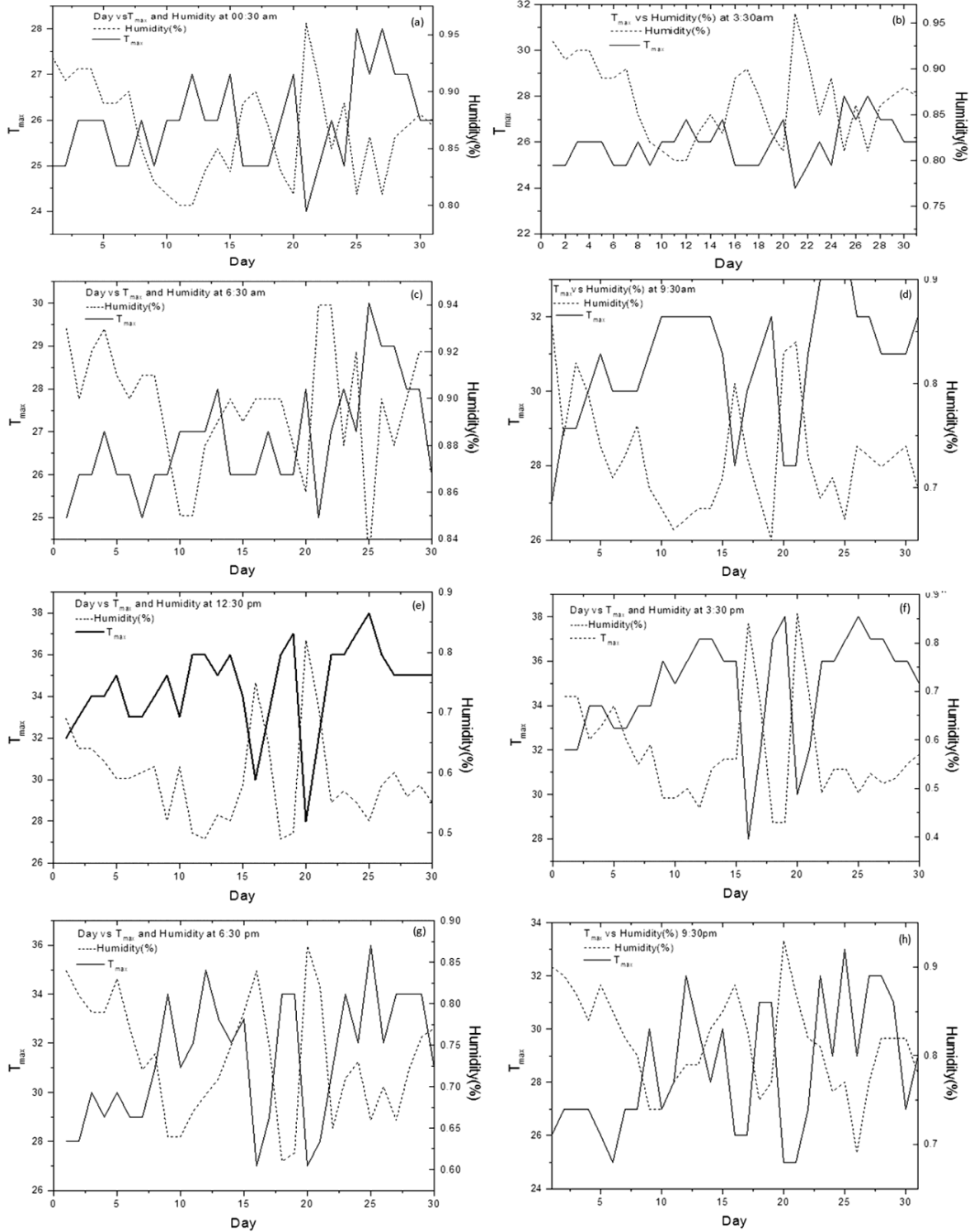


Fig. 5.4: Thirty days daily maximum temperature and relative humidity range variations registered for the Myanmar earthquake; Figures (a) to (h) depict the inverse relation of these two meteorological parameters which becomes significant 4-5 days before the main shock.

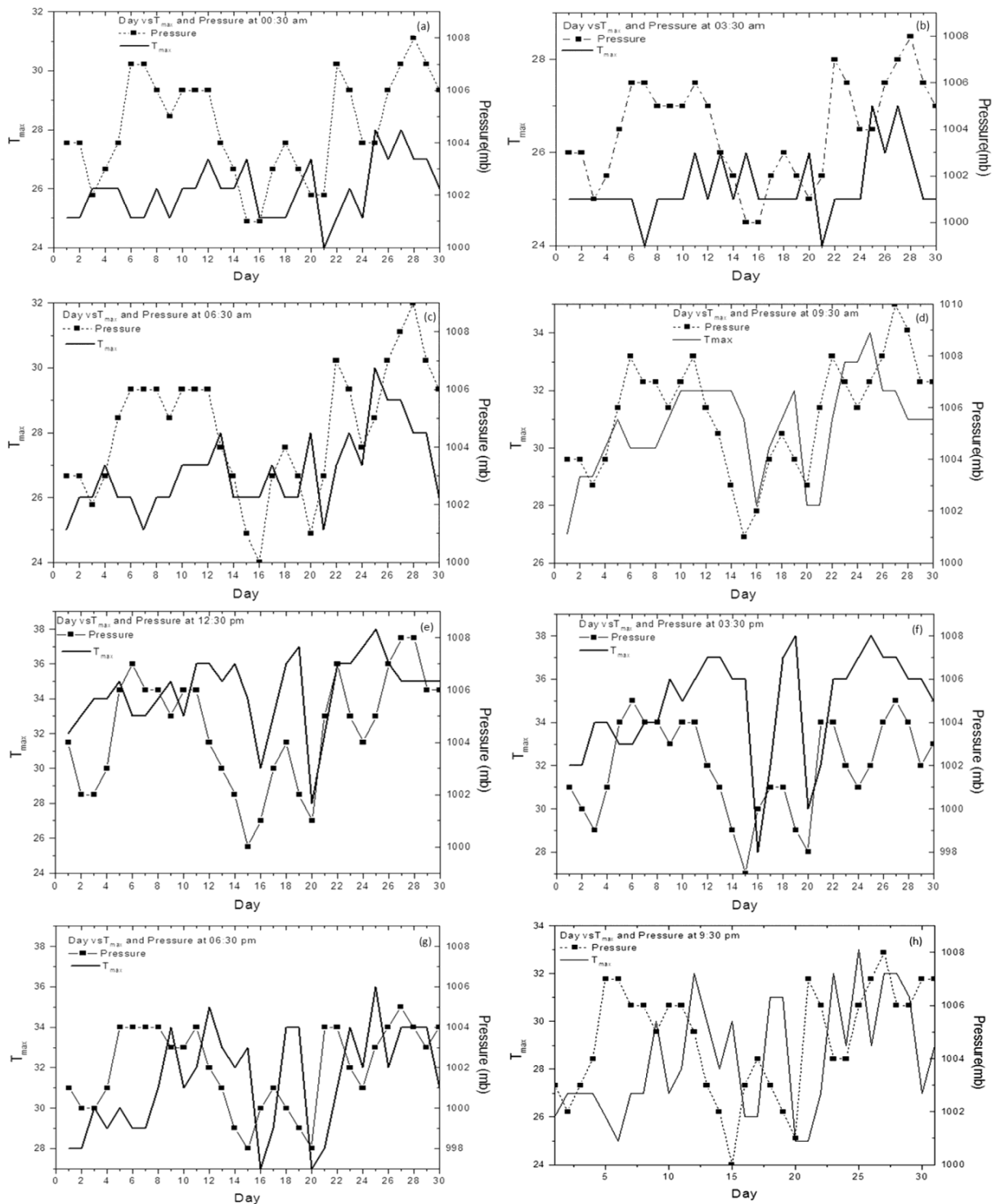


Fig. 5.5: Variations of air pressure and maximum temperature for a period of 30 days before and after the Myanmar earthquake are depicted for different times of the day through figures (a) to (h). These show the extent of maximum air pressure about 1008 mb, which is reasonably higher than the normal value.

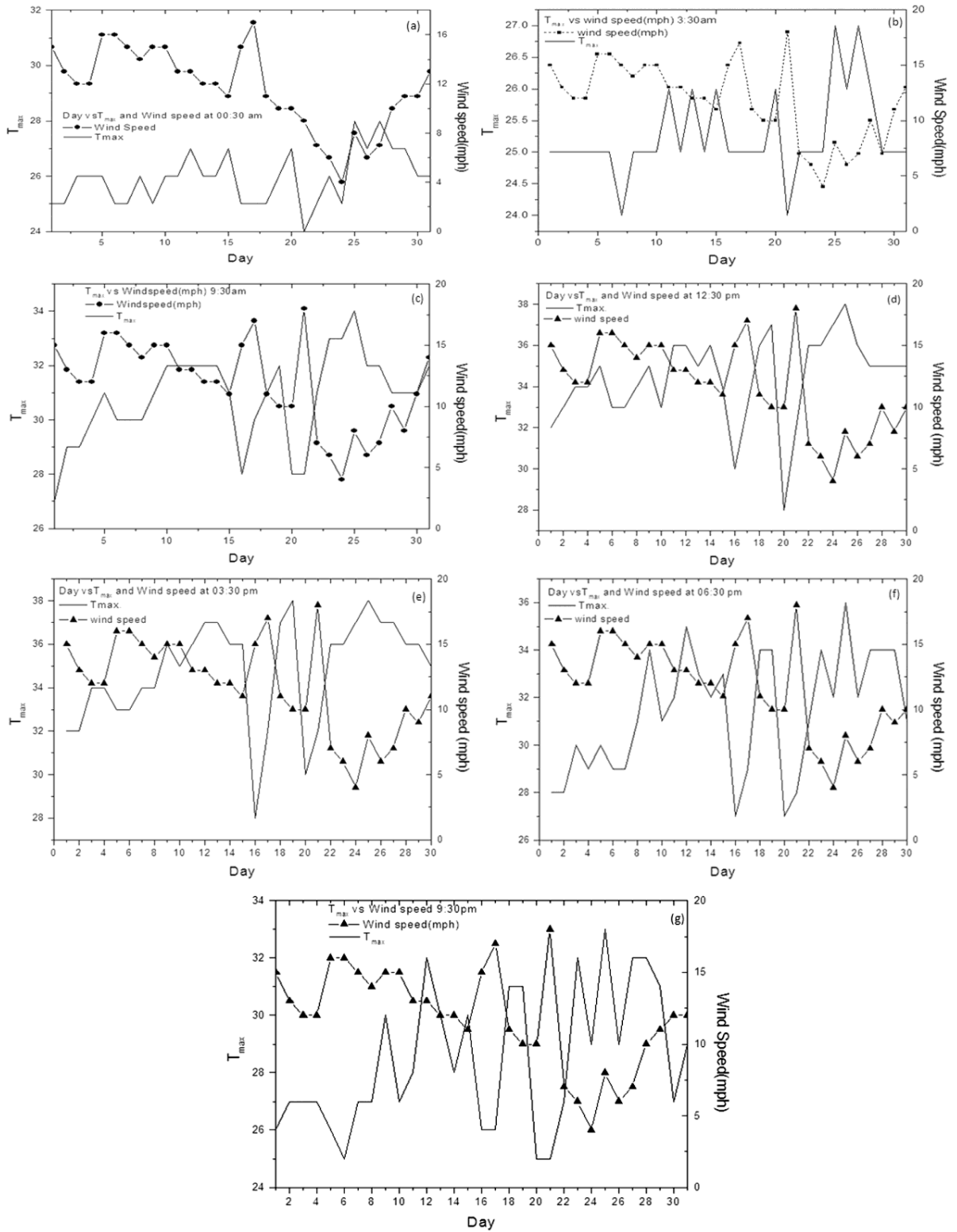


Fig. 5.6: Wind speed started to decrease 2-3 days before the earthquake and approached the minimum on the day of earthquake as depicted through figures (a) to (h).

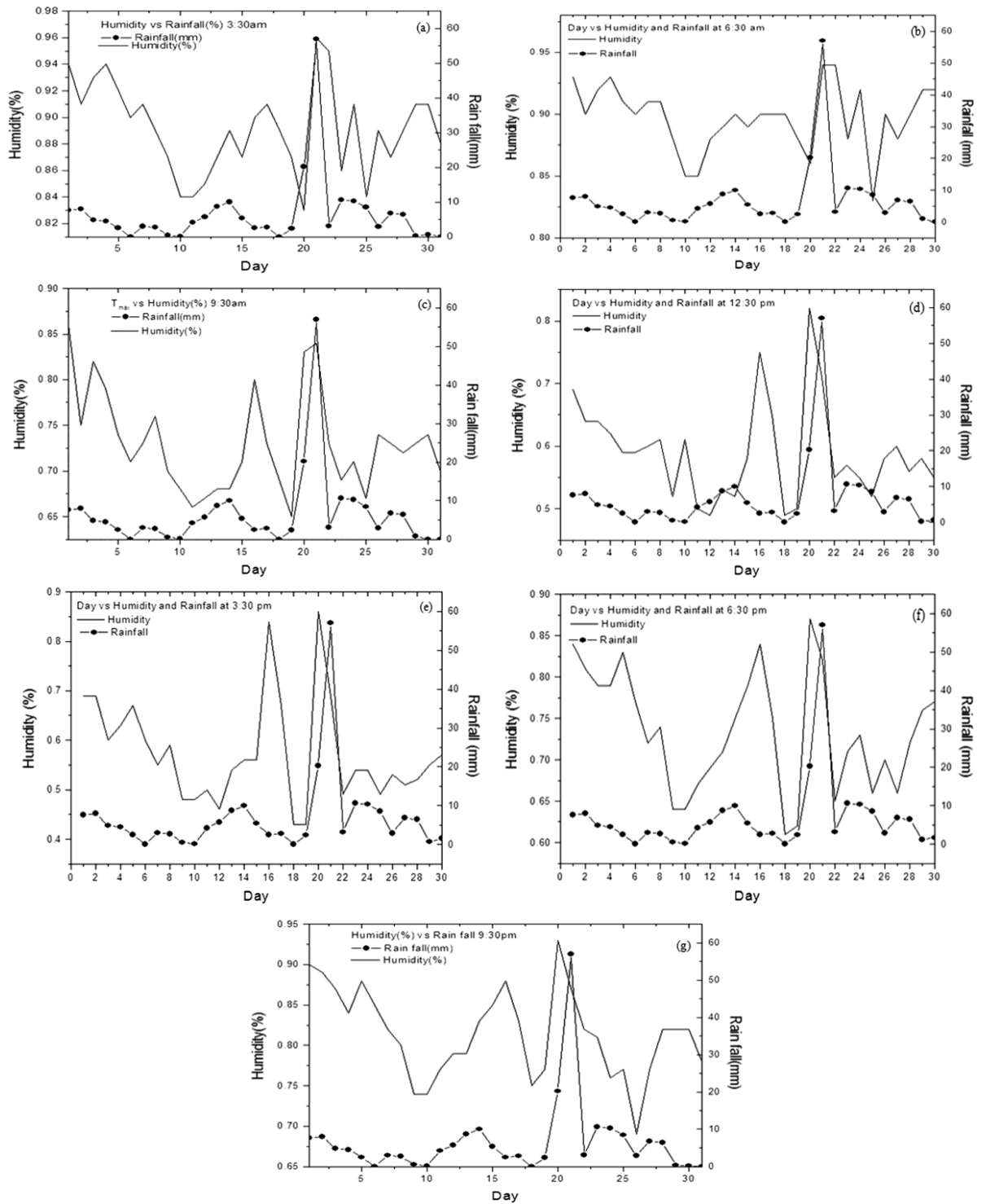


Fig. 5.7: The figures presented here are indicating the meteorological parameter variations of rainfall & relative humidity both of which reaches the highest value almost 2 days before the earthquake. The variations of meteorological parameters, rainfall & relative humidity almost follow the similar trend.

The variation in wind speed with maximum temperature was found to start 6 days before large earthquakes in Myanmar on 24 August 2016, (fig.5.6). The variations of maximum temperature and wind speed for the region of occurrences of the earthquake station, namely Chauk, Myanmar, showed ample variation, but during the earthquake it followed some common trend. The noticeable correlation of humidity and rainfall with the occurrence of the earthquake is depicted in Fig. 5.7 on the earthquake day.

5.3 Conclusion

The responses upon some meteorological parameters of Myanmar Earthquake of 24 August 2016 are presented in this chapter. The data from the Chauk Historical Weather, Myanmar ground stations (<http://www.worldweatheronline.com/chauk-weather-history/>) are used in the study. The responses are caused by the co-ordinated interactions in the geophysical processes within the Lithosphere-Inosphere-Atmosphere system. The anomalies in the meteorological conditions- humidity, temperature, pressure and wind speed predominantly were noticed near the Myanmar Earthquake Zone. The changes are also attributed to the anomalous surface latent heat increase several days before the earthquake. The observed variations may be attributed to the enhancement of radon and other greenhouse fluids during the occurrence of this earthquake. Our results of the observed thermal effects surrounding the tectonic plates are also in line with the observations made by other researchers in this field.

5.4 References

- [5.1] Shaftan VA, Zlotnikov MF, Vinogradov JI & Tchigin EP, *Magnetospheric Investigations*, **8** (1986), 126.
- [5.2] Pulinets S A & Dunajevka M A, *Tectonophys* , **431** (2007) 221
- [5.3] Tronin A A, Terra Scientific Publishing Company, (1999), 717.
- [5.4] Tramutoli V, Belio D, Pergola G N & Piscitelli S, *Annali di Geofisica*, **44** (2001) 295.
- [5.5] Tronin A A, Hayakawa M & Molchanov O A, *J Geodyn*, **33** (2002) 519
- [5.6] Tronin A A, Biagi P F, Molchanov O A, Khatkevich Y M & Gordeev E I, *Phys Chem Earth*, **29** (2004a) 501.
- [5.7] Tronin A A, Molchanov O A & Biagi P F, *Int J Rem Sens*, **25** (2004b) 2649.
- [5.8] Ouzounov D, Pulinets S, Tramutoli V, Liu T, Hattori K, Parrot M, Namgaladze A & Solomentsev D, *URSI GASS*, (2014) 1.
- [5.9] Hayakawa M & Molchanov O A, TERRAPUB, (2002).
- [5.10] Dey S & Singh R P, *Nat Hazards Earth Syst Sci*, **3** (2003) 749.
- [5.11] Hayakawa M, VLF, *Sensors*, **7** (2007) 1141.
- [5.12] Liperovsky V A, Pokhotelov O A, Meister C V & Liperovskaya E V, *Geomag Aeron*, **48** (2007) 795.
- [5.13] Molchanov O A, Hayakawa M & Miyaki K, *Adv Polar Upper Atmos Res*, **15** (2001) 146.
- [5.14] Miyaki K, Hayakawa M & Molchanov O A, TERRAPUB (2002), 229.
- [5.15] Hayakawa M, Raulin J P, Kasahara Y, Bertoni F C P, Hobara Y & Guevara-Day W, *Nat Hazards Earth Syst Sci*, **11** (2011) 513.
- [5.16] Gokhberg M B, Pilipenko V A & Pokhotelov O A, *Doklady AN SSSR*, **268** (1982) 56.

- [5.17] Gokhberg M B, Pilipenko V A & Pokhotelov O A, *Izv. AN SSSR, Fizika Zemli*, **10** (1983) 17.
- [5.18] Migulin V V, Larkina V I, Liperovsky V A, Molchanov O A, Nalivaiko A V, Gokhberg M B, Pilipenko V A, Pokhotelov O A & Shalimov S L, *IZMIRAN AS USSR*, Preprint No. **25a** (1982).
- [5.19] Larkina V I, Nalivaiko A V, Gershenson N I, Liperovsky V A, Gokhberg M B & Shalimov S L, *Geomag Aeron*, **23** (1983) 842.
- [5.20] Yin A, Dubey C S, Kelty T K, Gehrels G E, Chou C Y, Grove M & Lovera O, *Curr Sci*, **90** (2006) 195.
- [5.21] Socquet A, Vigny C, Chamot-Rooke N, Simons W, Rangin C & Ambrosius B, *J Geophys Res*, **111** (2006) 1.
- [5.22] Vigny C, Socquet A, Rangin C, Chamot-Rooke N, Pubellier M, Marie-Noe, Bouin L, Bertrand G & Becker M, *J Geophys Res*, **8** (2003) 2533.
- [5.23] Nielsen C, Chamot-Rooke N, Rangin C & the ANDAMAN Cruise Team, *Marine Geol*, **209** (2004) 303.
- [5.24] Curray J R, *J Asian Earth Sci*, **25** (2005) 187.
- [5.25] Searle M P & Morley C K, *Tectonic and Thermal Evolution of Thailand*, (2011) 539.
- [5.26] Niemi T M & Hall N T, *Geol*, **20** (1992) 195.
- [5.27] HuruKawa N & Maung P M, *Geophys Res Lett*, **38** (2011) 1.

CHAPTER 6

Precursor of Earthquake - Mathematical Analysis and Experimental Observations

6.1 Irregularities in the plasma of ionosphere in presence of precursory signals from earthquake

6.1.1 Introduction

Some effects on the upper atmosphere of the electromagnetic fields from earthquakes have been investigated in this work through some model calculations. The expressions of the variation of electron concentration and electron temperature as the ionospheric precursors of the earthquake have been deduced. The production of periodic inhomogeneities and their decay at different heights due to precursors at the active regions of the upper atmosphere as a whole have been considered through quasi-hydrodynamic formulations. There are models for seismic waves and seismo-associated electromagnetic phenomena on the occurrence of any earthquake [6.1–6.3]. The electromagnetic emissions are observed prior to the occurrence of any earthquake. Both precursory and post-seismic variations in ELF-VLF amplitude and in the ionospheric parameters have been reported from satellite based observations surrounding earthquakes [6.4–6.8]. The study of seismic related phenomena shows enhancement of DC electric field accompanied with the generation of periodic inhomogeneities in the electrical conductivity of the lower ionosphere and formation of geomagnetic field-aligned plasma layer in the upper atmosphere [6.9–6.11]. The lower ionosphere disturbances produced by the electromagnetic field are due to large scale current systems in the terrestrial core at the final stage of earthquake generation [6.12,6.13].

Preceding an earthquake, a strong variation in the electric field is observed which changes the direction of the field near the surface. As a result, significant changes in the electric field amplitude would be expected in the lower atmosphere that initiates the changes in the lower atmospheric parameters [6.14–6.16].

The results of model calculations have been presented in this chapter to estimate the changes in the electron concentration and the electron temperature through energy balance equation, continuity equation and ionization balance equation for the ionospheric regions. The system of equations is solved for temperature and density irregularities in the stated situation. Ion-collision energy losses are more than those of electrons and the ion conductivity is less than those of electrons. For this, the ion heating is relatively small. The electron-neutral molecule collision frequency and the electron energy loss per collision with molecule depend on temperature. As a result, the equation for electron temperature variation becomes non-linear. The equations for fluctuations of electron temperature and electron density are derived under the stated circumstances.

6.1.2 Mathematical Formulation

The model here deals with the following momentum transport equation, energy balance equation and continuity equations to investigate the effects of electromagnetic field due to earthquake on the variation of ionospheric parameters:

$$N \frac{\partial \vec{v}}{\partial t} + N(\vec{v} \cdot \nabla) \vec{v} = \frac{e}{m} N \vec{E}(t) - N \nu_e(T_e) \vec{v} - \frac{\nabla p}{m} - \eta \nabla^2 \vec{v} - \frac{eN}{m} (\vec{v} \times \vec{H}) \quad (1)$$

$$\frac{3}{2} \frac{\partial}{\partial t} (NkT_e) + eN\vec{v} \cdot \vec{E} + \frac{3}{2} \delta \nu_e(T_e) Nk(T_e - T) - \nabla \cdot \vec{W} + Q_i \frac{\partial N}{\partial t} = 0 \quad (2)$$

$$\frac{\partial N}{\partial t} = q_i + v_{de} \lambda N - v_\alpha N - \alpha_r N^2 (1 + \lambda) + \frac{\partial}{\partial z} \left\{ (D_t + D_\alpha) \frac{\partial N}{\partial z} \right\} \quad (3)$$

$$\frac{\partial N^+}{\partial t} = q_i - \alpha_r N^2 (1 + \lambda) - \alpha_i N^2 \lambda (1 + \lambda) + \frac{\partial}{\partial z} \{ (D_t + D_\alpha) \frac{\partial N^+}{\partial z} \} \quad (4)$$

Where, $N^+ = N + N^-$

Here, $\vec{E}(t)$ is external seismo-electric field;

\vec{H} is the geomagnetic field;

q_i is the ionization rate;

ν_{de} is the effective electron detachment rate from the ions;

ν_α is the rate of electron attachment to neutrals;

D_t is the eddy diffusion coefficient;

D_α is the molecular diffusion coefficient;

α_r is the effective coefficient of the dissociative recombination of electrons and positive ions;

Z is the altitude;

α_i is the ion-ion recombination coefficient;

K is the Boltzmann constant;

ν_e is the effective electron collision frequency;

Q_i is the ionization energy of the plasma medium;

\bar{v} is the average electron velocity;

N is electron number density;

$\delta = \frac{2m}{m'}$; where, m' is the mass of the heavy particle;

T is the equilibrium temperature;

η is the coefficient of viscosity;

\vec{W} is the heat flow vector;

The heat flow vector is expressed as:

$$\vec{W} = -\chi(T_e)\nabla T_e$$

Where $\chi(T_e)$ is the effective coefficient of electron energy conduction,

$$\lambda = k_T(1 - \mu\tau' / \sigma_0 k_T)$$

k_T is the coefficient of electron energy conduction at constant electron velocity;

M is the coefficient of electron energy conduction due to dc electric field;

τ' is the current flow coefficient due to thermal gradients at constant pressure,

$$p = NkT_e$$

σ_0 is the dc electrical conductivity.

The other symbols have their usual significance.

6.1.3 Results and discussions

In the presence of external electric field due to earthquake, the expression for fluctuation of electron temperature within the upper atmosphere has been deduced in the approximation of small perturbation. It is given by

$$\begin{aligned} & \frac{\partial \Delta T_e}{\partial t} + \frac{1}{\delta v_e T_e} \left[q_i + \Delta N (v_{dc} \chi - v_\alpha) + N_0 \delta v_e (T_e) - \alpha_r (i + \chi) N_0^2 \right] \Delta T_e \\ & = \Delta N \delta v_e (T_e) - \frac{2Q_i}{3kT \delta v_e (T_e)} \left[q_i + (v_{dc} \chi - v_\alpha) N_0 + (D_t + D_\alpha) \frac{\partial^2 N}{\partial z^2} - \alpha_r (1 + \chi) N_0^2 \right] + \\ & + \frac{2e^2 \Delta N}{3mkT \delta v_e (T_e)} \vec{E} \cdot \left[\exp \left\{ (-A) + \frac{e}{m} \int_{t'}^t X dt'' \right\} \right] \left[\int_0^t \vec{E}(t') \exp \left\{ 1 + \frac{e}{m} \int_{t'}^t X dt'' \right\} dt' \right] \end{aligned}$$

(5)

Where, $\tau = \delta v_e (T_e) t$,

$$N = N_0 + \Delta N,$$

$$\text{and } T_e = T_{e0} + \Delta T_e$$

The expression for density fluctuation under this situation is obtained as

$$\begin{aligned} & \frac{N_0 k (T_e - T)}{m} \frac{\partial^2 (\Delta N)}{\partial z^2} + \frac{2Q_i}{3kT_e} [(D_t + D_\alpha) v_e (T_e)] \frac{\partial (\Delta N)}{\partial z} = \frac{\partial^2 (\Delta N)}{\partial t^2} - 2\alpha_r N_0 (1 + \chi) \Delta N - \\ & - \frac{3}{2} \frac{N_0 k}{m} v_{de} \frac{\partial^2}{\partial z^2} (T_e - T) + 2v_{de} \chi \frac{\delta (\Delta N)}{\partial t} \end{aligned} \quad (6)$$

From the equations (5) and (6), the expected changes in the temperature and number density at different heights due to precursors at the active regions of the ionosphere can be estimated numerically.

6.2 Statistical analyses on three sub-ionospheric transmitted signals recorded at Kolkata during 18 earthquakes

6.2.1 Introduction

Some significant effects of 18 large earthquakes of different magnitudes upon the VLF (Very Low Frequency) transmitted sub-ionospheric signals at 16.4 kHz from Novik, Norway (Lat: 66.97° S; Long: 13.9° E), 19.8 kHz from North West Cape, Australia (Lat: 21.82° S; Long: 114.16° E) and 25 kHz from Petropavlovsk-Kamchatski, Russia (Lat: 53° N; Long: 158° E) are recorded at Kolkata (Lat: 22.56° N, Long: 88.5° E) have been investigated during the period April 3, 2013 to April 24, 2013 when there occurred 18 large earthquakes having $M \geq 5.0$. VLF transient variations of significant magnitude in the form of spikes on the amplitude at these frequencies are observed few days prior to the day of occurrence of each earthquake. The variations are investigated statistically at most there are $\pm 2\sigma$ variations from mean or not during, pre- and post-

seismic periods of earthquakes. Significant variations ($> \pm 2\sigma$) are obtained for different earthquakes on particular frequency. These observations are supposed to be very much connected with the fracture of rocks producing radiation that migrate into upper atmospheric region.

6.2.2 Recording of the VLF transmitted signals

The transmitted signal at frequencies 16.4 kHz 19.8 kHz and 25 kHz have regularly been recorded from Kolkata over the last several years. The ELF-VLF receiving system has been presented in Section 2.2.4 of Chapter 2.

6.2.3 Analyses of recorded data

Fig. 6.1 shows the location of the VLF transmitters and receivers, as well the earthquakes with $7.8 \geq M \geq 5.0$ (depth below 10 km) which occurred in the network. The data regarding the location and magnitudes of these significant global earthquakes dealt in here are collected from <http://www.imd.gov.in/section/seismo/dynamic/last-monthApr13.htm>. Distance between two points is calculated using “haversine” formula available at <http://www.movable-type.co.uk/scripts/latlong.html>. The Dst and Kp indices for the month of April, 2013 has been taken respectively from <http://wdc.kugi.kyoto-u.ac.jp/dstae/index.html> and <http://wdc.kugi.kyoto-u.ac.jp/kp/index.html>.

The date-wise occurrence of 18 earthquakes with magnitude (M), depth and Indian Standard Time (I.S.T.) along with their Earthquake Zone to Receiver distances (D) are presented in Table 6.1.

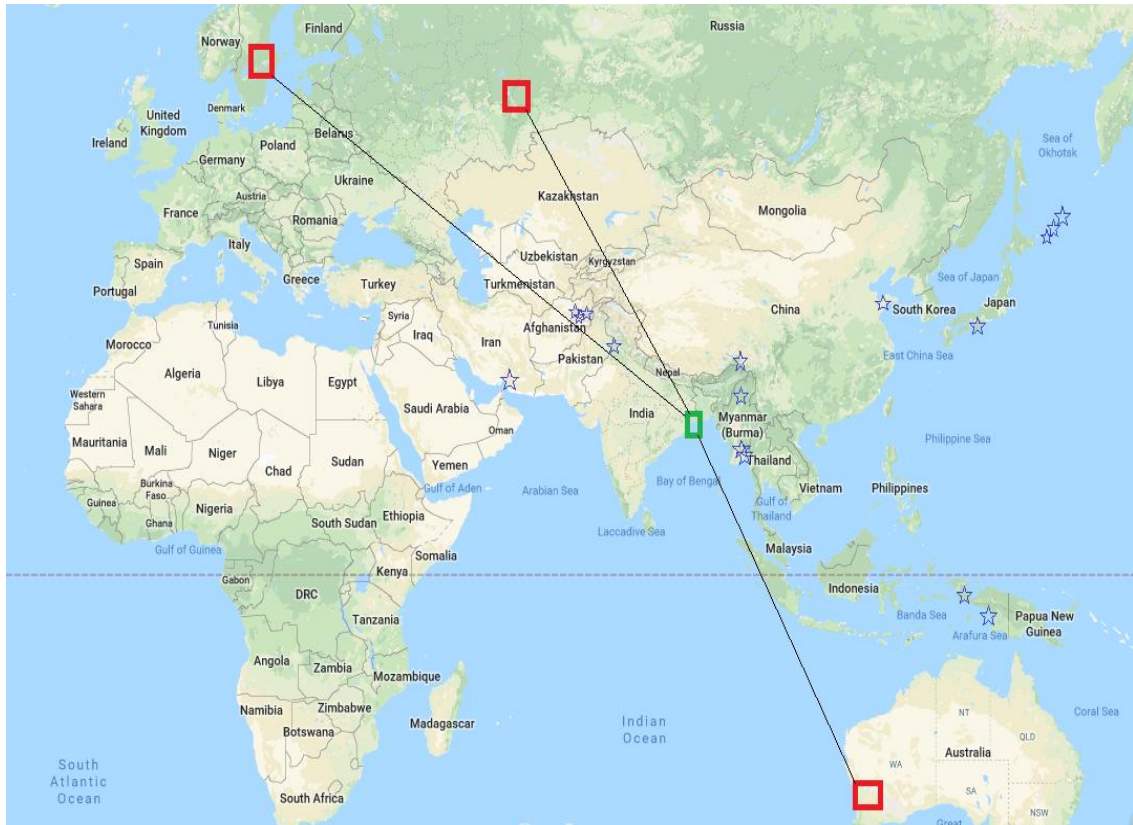


Fig.6.1 Map showing the location of the receiver (by green rectangle) and the transmitters (by red rectangles). The transmitters are at Norway, Russia and Australia; the receiver is located at Kolkata, respectively. The three VLF radio paths are indicated by black lines. The blue stars display the $M > 5$.

Table 6.1 Date-wise occurrence of several earthquakes along with the descriptions of different connecting parameters

Date	Time (I.S.T.)	Depth (km)	Magnitude (M)	Region	Distance from Kolkata (22.56° N, 88.5° E), D (km)
03.04.2013	22:05:48	10	5.5	Myanmar (19.3° N, 95.2° E)	784
04.04.2013	12:01:37	237	5.8	Hindu Kush, Afghanistan (36.1° N, 71.6° E)	2218
04.04.2013	20:46:26	40	5.4	Myanmar (19.3° N, 95.7° E)	831
05.04.2013	18:30:02	570	6.3	N.E. China Border (42.8° N, 131.0° E)	4505
06.04.2013	04:25:00	80	5.4	Hindu Kush, Afghanistan (36.4° N, 71.5° E)	2246
06.04.2013	10:12:40	90	7.1	Papua Indonesia (3.6° S, 138.1° E)	6118
09.04.2013	17:22:55	42	6.2	Southern Iran (28.5° N, 51.6° E)	3746
11.04.2013	09:17:03	12	5.4	Myanmar (19.3° N, 95.7° E)	831
14.04.2013	07:02:24	41	6.5	Papua New Guinea (6.4° S, 154.5° E)	7862
16.04.2013	14:04:09	10	5.0	India(Arunachal Pradesh) (29.0° N, 95.0° E)	967
16.04.2013	16:14:11	46	7.8	Pakistan-Iran Border (28.0° N, 62.1° E)	2717
17.04.2013	04:25:26	10	6.8	Papua New Guinea (3.2° S, 142.5° E)	6519
19.04.2013	08:35:51	97	7.3	Kuril Islands (46.2° N, 150.8° E)	6112
20.04.2013	01:28:40	10	6.1	Kuril Islands (50.0° N, 157.5° E)	6623
20.04.2013	05:32:48	29	6.6	Sichuan, China (30.2° N, 103.0° E)	1673
20.04.2013	18:42:47	10	6.1	Kuril Islands (50.4° N, 157.3° E)	6609
21.04.2013	08:52:16	422	6.2	Izu Islands, Japan (29.9° N, 138.9° E)	5054
24.04.2013	14:55:29	66	5.7	Hindu Kush, Afghanistan (34.5° N, 70.2° E)	2221

The analyses of the spiky variations for 18 earthquakes, from the total number for brevity, 13 days recorded data have been considered as the stated time interval. Fig.6.3(a)-(m) represent the time-series graphs of 16.4, 19.8 and 25 kHz signals at different dates of occurrence of the earthquakes having $M \geq 5.0$.

We have investigated the observed variations in the VLF amplitude statistically whether at most there are $\pm 2\sigma$ variations from mean or not during, pre and post seismic periods of earthquakes. In this process, we have taken all 86400 data for each signal to

compute standard deviation and mean through graphing software. Then $\pm 2\sigma$ lines are drawn along with the mean line for each signal for all the 13 days except April 9, 14, 17 and 21, 2013. Mean lines are indicated by black straight lines while $+2\sigma$ and -2σ lines are by red and magenta colours respectively. On the above said four days no variations for any signals beyond $\pm 2\sigma$ from the mean are obtained. For other days, significant variations, i.e, $\pm 2\sigma$ from mean are obtained for different earthquakes on particular frequencies and the deviations that are plotted. Only for April 24, 2013 variations are obtained beyond $\pm 2\sigma$ from mean for two frequencies 16.4 and 25 kHz, and hence both are plotted.

As discussed earlier, Fig.6.2 shows the variations of the Dst and Kp indices. The Dst index is a measure of the variations in geomagnetic field due to the equatorial ring current [6.17].

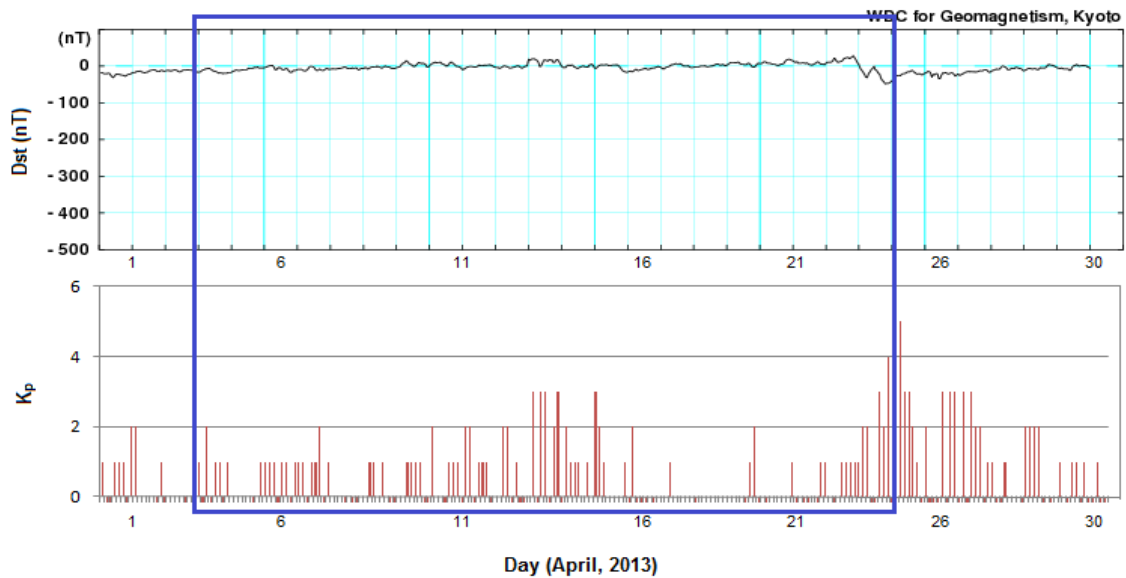
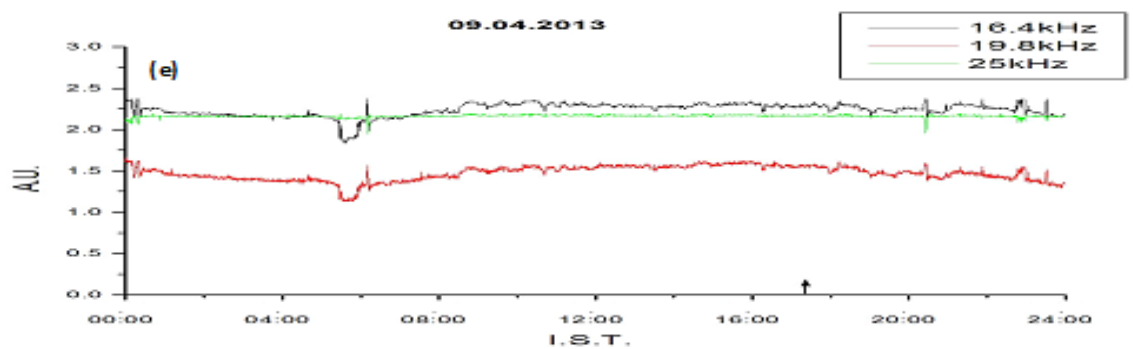
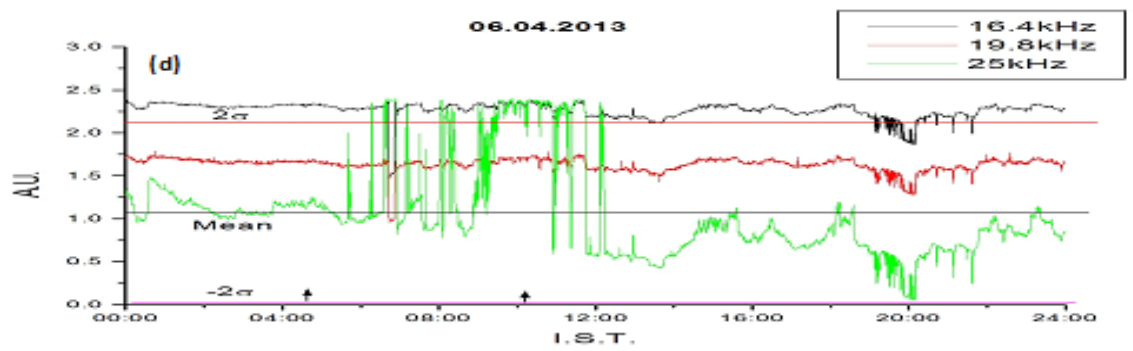
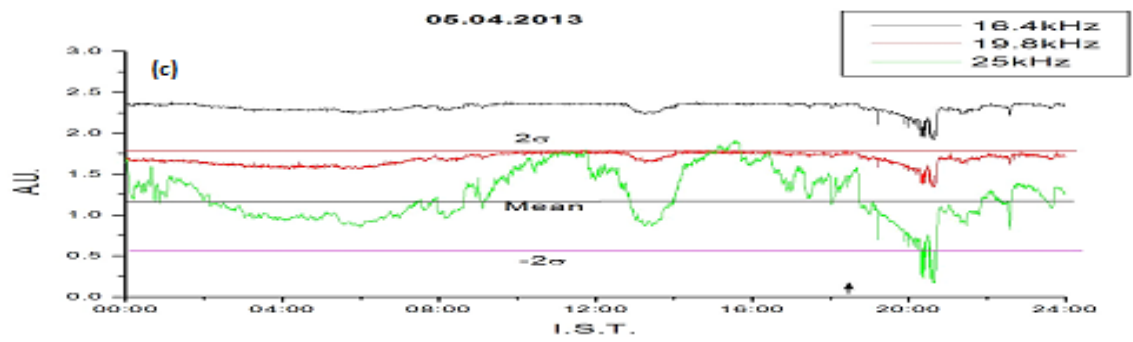
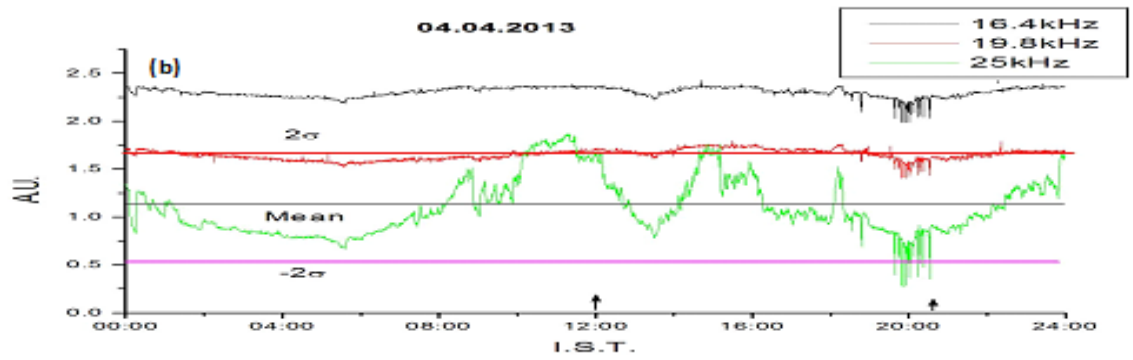
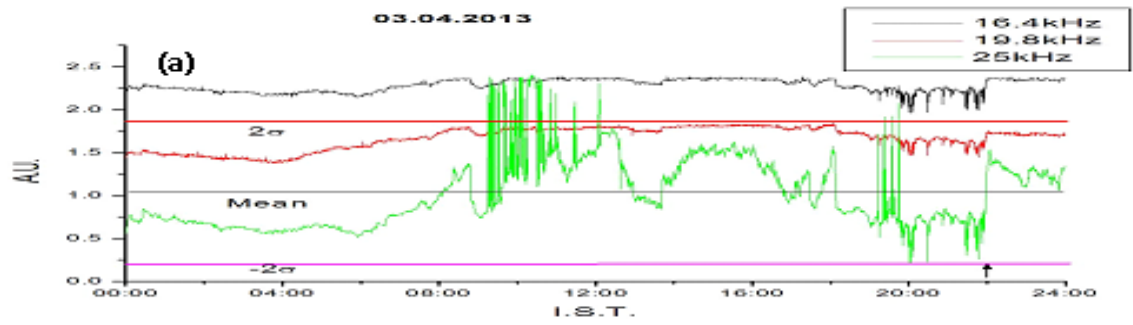
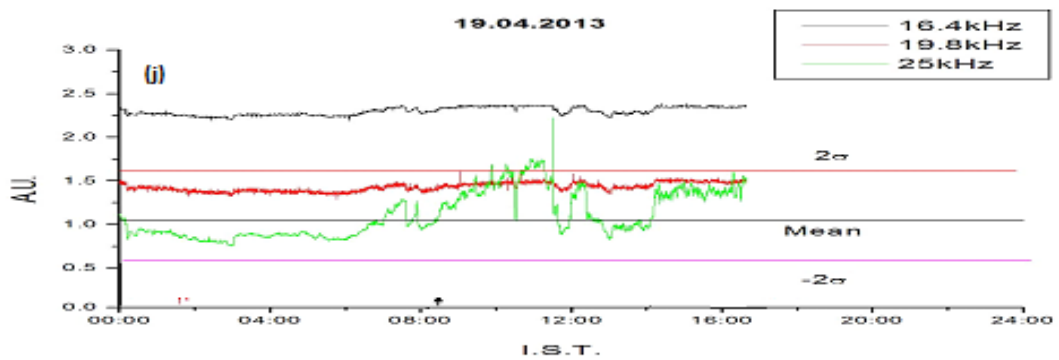
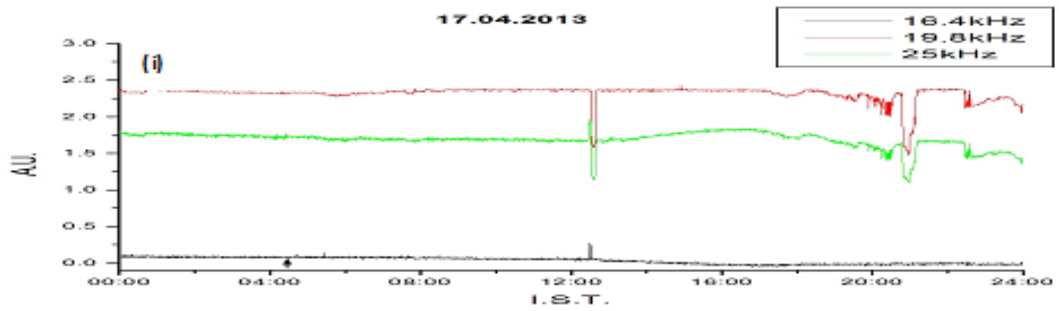
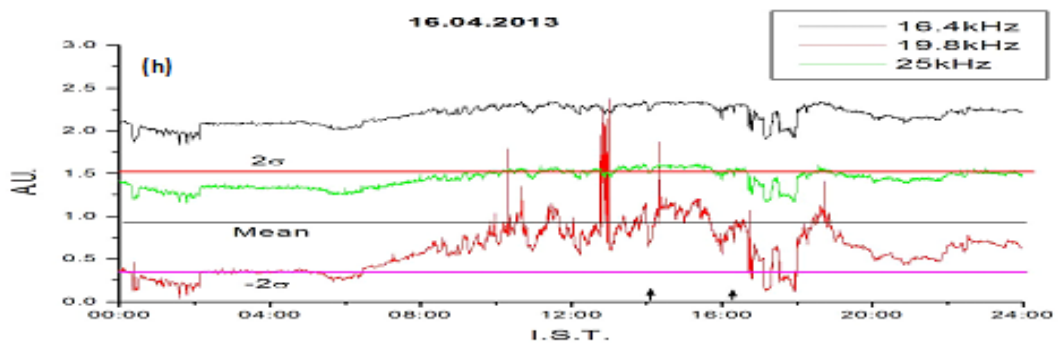
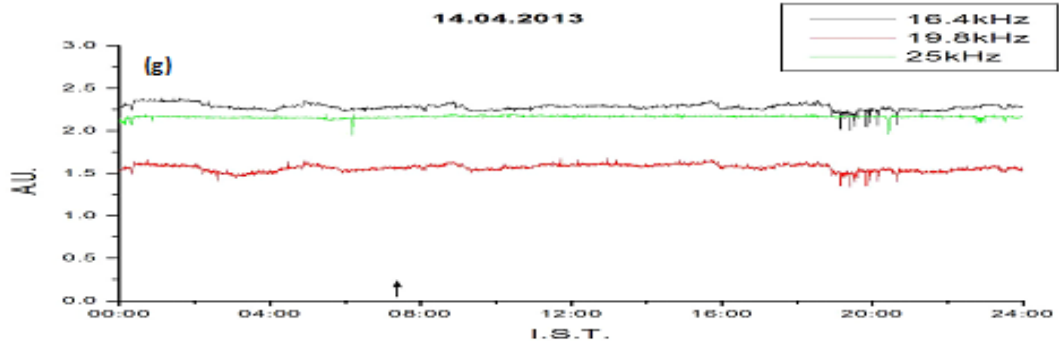
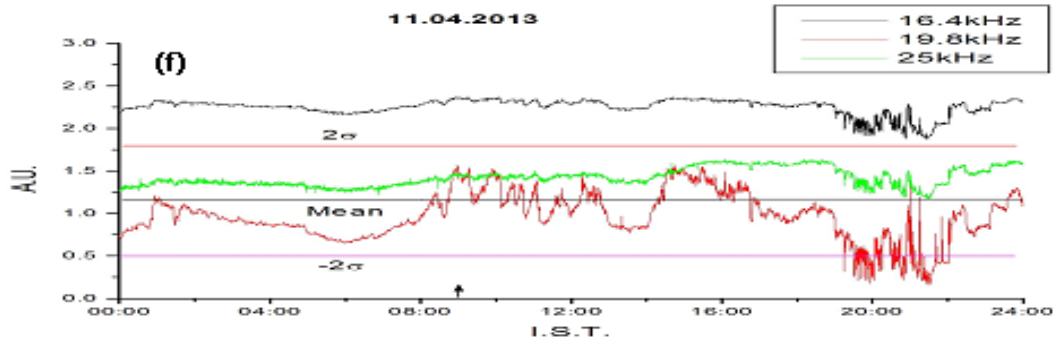


Fig.6.2 The variations of Dst and Kp indices for the month of April, 2013. Blue rectangular area indicates the dates of occurrences of earthquakes.





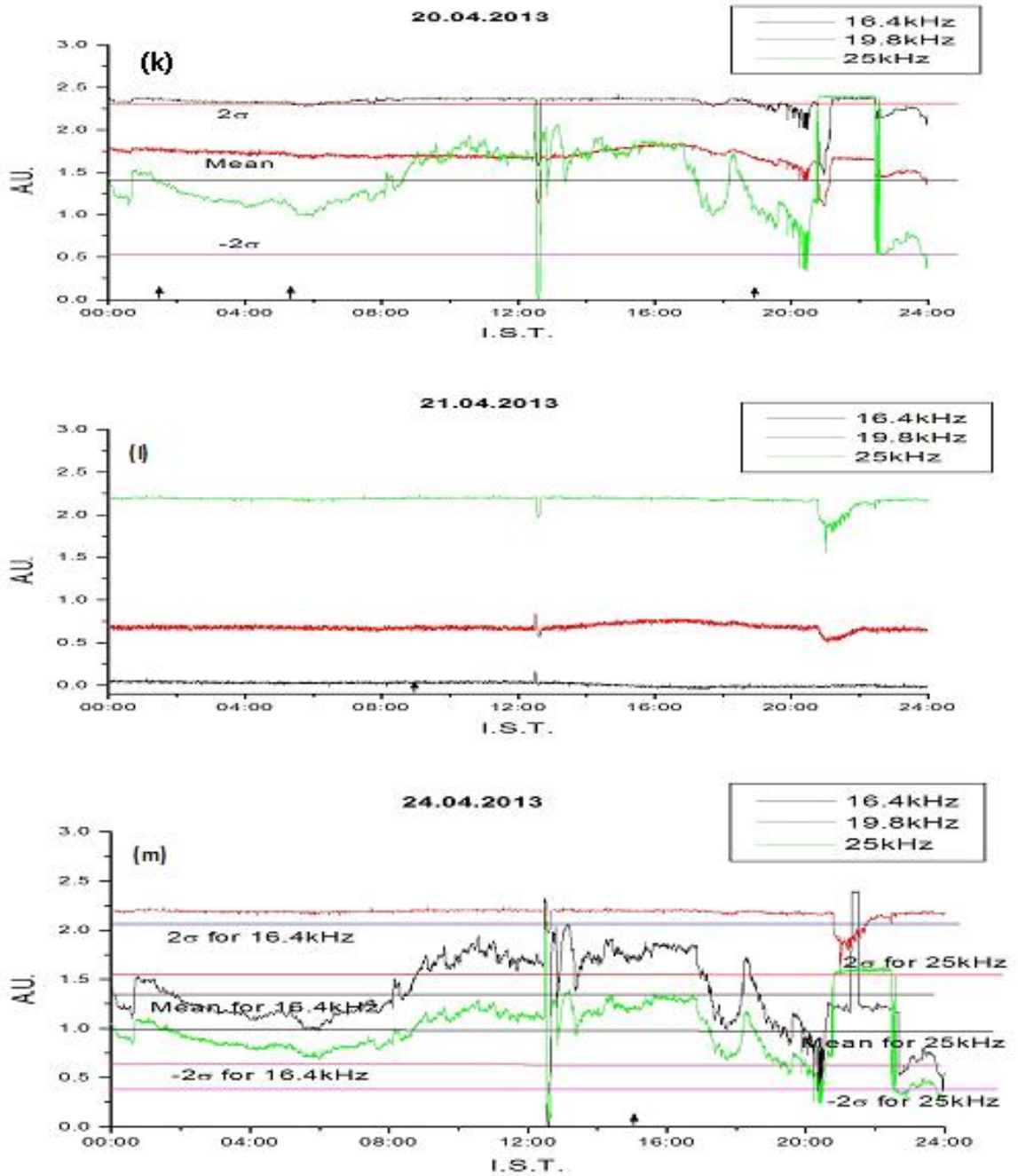


Fig.6.3 Diurnal variations of 16.4, 19.8 and 25 kHz sub-ionospheric transmitted signals observed at Kolkata during April 03, 04, 05, 06, 09, 11, 14, 16, 17, 19, 20, 21, 24, 2013 [Panels (a)-(m)]. Arrow marks are for denoting the commencement time of earthquakes. Three signals are represented by black, red and green colours respectively.

6.2.4 Results and consequences

The VLF signal waves are trapped between the ground and the lower ionosphere. Any variations of the earth ionosphere waveguide, especially the variations on the ionospheric D/E region, can lead to the changes in VLF propagation conditions [6.18, 6.19, 6.20-6.22]. There are some specific sources which can affect the earth-ionosphere waveguide, e.g., solar activities, and corresponding geomagnetic activities [6.23,6.24]. This work describes some important observations that are related to atmospheric disturbances in the time before earthquakes.

Most of the data analysed here are for the earthquakes occurred in the region of North-East quadrant with respect to the experimental site (Fig. 6.1). During earthquakes, the spiky VLF excitation in the presence of an anomalous electric field had also been reported and assessed [6.25]. The present observation is confined to three particular frequencies at 16.4 kHz from Norway, 19.8 kHz from Australia and 25 kHz from Russia (Fig.6.3).

Fig.6.2 showing the variations of the Dst and Kp indices indicates that the geomagnetic activity were relatively quiet around time of these earthquakes. So, it can be said that the observed $\pm 2\sigma$ perturbations might be attributed to seismic activity, and independent of geomagnetic field disturbances. Also, the Dst and Kp values confirm that the variations were devoid of any real event such as magnetic disturbances or solar proton events, etc.

6.3 References

- [6.1] M. Hayakawa and Molchanov, O. A., *Terr. Atmos. Oceanic Sci.*, **15**, (2004) 311.
- [6.2] S. A. Pulinets, A. D. Legenka, T. V Gaivoronskaya, V. K. Depuev, *J. Atmos. Solar-Terr. Phys.*, **65**, (2003b) 1337.
- [6.3] S. A Pulinets, V. V. Khagai, K., A. Boyarchuk and A. M. Lomonosov, *Phys.-Uspekhi*, **41**, (1998a) 515.
- [6.4] S. A. Pulinets, “*Adv. Space Res.*” **22**, (1998b) 903.
- [6.5] A. V. Shvets, M. Hayakaawa, and O. A. Molchanov, “*J. Atmos. Electricity*”, **22** (2002) 87.
- [6.6] O. A. Molchanov, and M. Hayakawa, “*J. Geophys. Res.*”, **103**, (1998) 17489.
- [6.7] O. A Molchanov, and M. Hayakawa, T. Ondoh, and E. Kawai, “*Phys. Earth Planet. Inter.*”, **105**, ((1998) 239.
- [6.8] V. M. Chemirev, N. V Isaev, O. N. Serebryakova, V. M. Sorokin, and , Y, P. Sobolev, “*J. Atmos. Solar-Terr. Phys.*”, **59**, (1997) 967.
- [6.9] S. I. Martynenko, I. M. Fuks, and R. S. Shubova, “*Geomag. Aeronomy*” , **34**, (1994) 223.
- [6.10] V. V. Belikovich, E. A. Benediktov, P. N. goncharovand A. V. Tolmacheva, *J. Atmos. Sol.-Terr. Phys.*, **59**, (1997) 2447.
- [6.11] S. I. Matrynenko, *J. Atmos. Elec.*, **19**, (1999) 1.
- [6.12] S. I. Matrynenko, *Ann. Geophys.,Part III, Space Planetary Science suppl. III*, Vol. **16**, 1998.
- [6.13] V. M. Sorokin, V. M. Chmyrev, and A. K. Yaschenko, *J. Atmos. Sol. Terr. Phys.*, **67**, (2005) 1259.
- [6.14] S. A. Pulinets, *Adv. Space Res.*, **22**, (1998) 903.

- [6.15] J. Y. Liu, Y. I. Chen, Y. J. Chuo and C. S. Chen, *J. Geophys. Res.*, **111**, (2006) A05304.
- [6.16] Y. Hobara and M. Parrot, *J. Atmos. Sol.-Terr. Phys.*, **67**, (2005) 677.
- [6.17] De, S. S., Paul, S., Barui, S., Haldar, D. K., and Guha, G., *Terr. Atmos. and Oceanic Sci.* **26**, (2014) 135.
- [6.18] De, S. S., De, B. K., Bandyopadhyay, B., Paul, S., Haldar, D. K., Bhowmick, A., & Ali, R, *Natural Hazards and Earth System Sciences*, **10(4)**, (2010) 843.
- [6.19] Hayakawa, M., Kasahara, Y., Nakamura, T., Muto, F., Horie, T., Maekawa, S., Hobara, Y., Rozhnoi, A. A., Solovieva, M., and Molchanov, O. A., *Journal of Geophys. Res.* **115**, (2010).
- [6.20] Hazra, P., Barui, S., De, S. S., and Paul, S. (2015). *Rom J Phys*, **60(7-8)**, (2015) 1218.
- [6.21] Hayakawa, M., Y. Hobara, A. Rozhnoi, M. Solovieva, K. Ohta, J. Izutsu, T. Nakamura, and Y. Kasahara, *Terr. Atmos. & Oceanic Sci.*, **24**, (2013), 3.
- [6.22] Molchanov O., Hayakawa M., Miyaki K. *Advances in polar upper atmosphere research*, 2001, 146-158.
- [6.23] Hayakawa, M., Y. Hobara, Y. Yasuda, H. Yamaguchi, K. Ohta, J. Izutsu, and T. Nakamura, *Annals of Geophysics*, **55(1)**, (2012)
- [6.24] Molchanov, O., M. Hayakawa, T. Oudoh, and E. Kawai, *Physics of the Earth and Planetary Interiors*, 105(3), (**1998**), 239.
- [6.25] Bardakov, V. M., Vugmeister, B. O., Petrov, A. V., and Chramtsov, A., *Annual Report of Irkutsk State Techni-cal University, Irkutsk*, 2004.

CHAPTER 7

Summary and Conclusions

7.1 Summary

The investigations presented in this thesis, concerned on the studies of different responses of the upper atmospheric electricity parameters like, thunderstorm, lightning, solar eclipse, earthquake, VLF / LF sferics signals as well as transmitted VLF signals. It embodies mainly the investigations of lightning generated electric field upon some parameters of the lower atmosphere. Theoretical modelling is addressed on some of these aspects that led to the solution of different problems closely related to certain geophysical and extra-terrestrial phenomena. Different experimental data are recorded in the laboratory which have been analysed and the outcome are published in different referred journals of national and international repute.

The analyses of some characteristics of Schumann resonance phenomena recorded over Kolkata and some atmospheric electricity parameters based on the effects of different geophysical and extra-terrestrial events like, Earthquake, thunderstorm, lightning, solar eclipse, solar flare, Leonid meteor showers, etc., upon the transmitted subionospheric VLF signals. Spectral characteristics of VLF atmospherics recorded from Calcutta showed some connectivity between atmospheric and ionospheric parameters. The outcome of the theoretical analyses of problems at different area as well as experimental observations have been presented in the thesis. We tried to study in detail the different characteristics of several earthquakes and few geophysical and extra terrestrial events like thunderstorm, lightning, solar eclipse, solar flare, meteor shower etc. through the study of their effects on some electricity parameters e.g.

atmospheric potential gradient and point discharge current, and upon VLF sferics signals and VLF sub-ionospheric transmitted signals. Most of the events have been recorded over Kolkata and some are from Tripura University site at Agartala, India. The analyses of the data-set for different events have been presented in various chapters of the thesis.

At the onset, in chapter 1, a general background about the contents of the thesis is narrated along with the outline of the chapters following.

An overview of the rudimentary concepts, measurement setup and techniques used in this work regarding the description of antenna systems, buffer electronic circuits and system calibration is presented in chapter 2.

In chapter 3, the diurnal and seasonal variations of atmospheric potential gradient are analysed. The results of measurement of the atmospheric vertical potential gradient (PG) in Kolkata (Lat: 22.56° N) on the ground surface for 90 fair weather days during 2006–2009. The results are compared with those reported by others at various stations. The observed records of point discharge current (PDC), conductivity and PG during the stated period are analysed. Also, the correlations studies are carried out among PG and PDC.

Analyses of recorded data on SR spectra and some aspects of SR phenomena have been presented in chapter 4. During 1990s and later, the scenario with these sub-ionospheric ELF SR waves changed and several new aspects emerged. The measurements of Schumann resonance spectra from Kolkata have been recorded since 1998. The variation of amplitude and frequency in the recorded data of SR from Kolkata, for the period January 2000 to December 2000 are investigated. The variation of global thunderstorm activity as inferred from monthly intensity fluctuations of global

SR signals over Kolkata and Modra (Lat. 48.61° N, Long: 17.27° E) have been presented and the observed difference is interpreted. The enhancements of the amplitude and frequency of the fourth mode of SR spectra which had been detected during the occurrence of earthquakes. It includes the impact of SR in the study of precursors of earthquake.

The most important parameters of global climate change are surface temperature and upper tropospheric water vapour (UTWV). It can be monitored with SR, utilizing its relation to worldwide thunderstorm activity. The method demands the availability of long-term calibrated data that can provide past and future records of global climate variation on Earth.

More lightning is observed in the tropical-extra-tropical land regions during warm, El Niño episodes, especially in Southeast Asia. Oceanic lightning activity is a minor contributor to global lightning, an opposite behaviour is observed in the Pacific and other oceanic regions. Schumann resonance intensity variations suggest a southward (equator-ward) shift and satellite observations support this and showed in addition an eastward shift in the global position during warm, El Niño episodes. The intensity and position of lightning activity vary on the ENSO time scale.

In chapter 5, some typical variations of maximum temperature, relative humidity, air pressure, wind speed and rainfall are presented for a large earthquake occurred in Myanmar during August 24, 2016. During the occurrences, abrupt increase in greenhouse gases (like CO₂, CH₄, H₂ etc.) and enhancement of radon emanations are found which introduced anomaly in the fluid expulsion from seismically active faults and produce air ionization before the large earthquake. Anomalous increase in surface

latent heat introduces changes in the observed meteorological parameters in the region of earthquake.

In chapter 6, a model calculation is set up to estimate the changes in the electron concentration and the electron temperature through energy balance equation, continuity equation and ionization balance equation for the ionospheric regions are derived in section 6.1. The system of equations is solved for temperature and density irregularities in the stated situation. In section 6.2, the statistical analyses are pictured on three sub-ionospheric transmitted signals at Kolkata during 18 earthquakes. The recorded data of VLF transmitted sub-ionospheric signals at 16.4, 19.8, and 25 kHz at Kolkata have been investigated during the period April 3, 2013 to April 24, 2013 when there occurred 18 large earthquakes having $M \geq 5.0$. The variations are investigated statistically. There are $\pm 2\sigma$ variations from the mean value in most cases during, pre- and post- seismic periods of the earthquakes. Significant variations ($> \pm 2\sigma$) are obtained for different earthquakes on the particular frequency. These observations are supposed to be very much connected with the fracture of rocks producing radiation that migrate towards the upper atmospheric region.

The work presented in different chapters of this thesis is summarized in chapter 7. The possible extensional works in different fields, covered in this thesis, have been planned.

7.2 Conclusions

The investigations presented in this thesis, concern mainly on the studies of responses of atmospheric electricity during geophysical and extra-terrestrial events. Both experimental and theoretical investigations are initiated that led to solution of different

problems closely related to the stated fields. Results of numerical computations have also been presented in the concerned areas of researches. In some of the stated areas, further explorations would be necessary to explain aspects of the physical processes involved other than what have been considered. There are ample scopes to extend the analysis of the various problems presented in different chapters in this thesis. The parametric measurements of SR occurrences can be used to study the inter-annual variability of global thunderstorm activity centers in the three different continental regions. Because of the geomagnetic field, the conductivity of the cavity becomes tensorial in nature which influences the wave propagation in the earth-ionosphere cavity. The inhomogeneity and anisotropy of the cavity introduce line splitting of SR spectra which is due mainly to geomagnetic field. Solar eclipse, solar flare, geomagnetic event are mostly responsible for the observed changes in the sub-ionospheric transmitted signals as well as VLF-LF spheric signals.

Further works may be initiated to investigate how ionospheric parameters during solar eclipse had been affected. The recording of different characteristics of several earthquakes and few geophysical events has been made which are analyzed and the results are presented in the thesis. From the study of several large seismic events it can be concluded that variations of air temperature and humidity before and after earthquake due to latent heat release are occurred during water vapour condensation. These are also supposed to be associated with the variations of radon (^{222}Rn) during the period of tectonic activity. In the thesis, different problems are studied in the areas of nonlinear phenomena of earth's atmospheric electricity parameters during geophysical and extra-terrestrial events. Further works are suggested which are expected to cover in future research works.

7.3 Further scope

During the last few decades, the stated investigations resulted in opening up a new dimension towards the study of various physical processes and different parameters along with their variations within the upper atmosphere. However, there are various areas where further studies are necessary to gather more information and to reconcile, where possible, with the results of other researchers for predicting new features.

Although several topics in this context are explored in the work conducted and explored through theoretical analyses and experimental observations, yet modeling of the problems in different topics still needs to be explored. Some of these will be contemplated in our future work.